INVESTIGATING CHAOS IN OCEAN ACOUSTICS
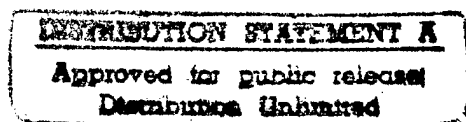
PREPARED UNDER THE GRANT (N00014-95-10443) FROM THE OFFICE OF NAVAL RESEARCH

Kang K. Yen, Jianguo Yan

January 1997

19970218 112

REPORT DOCUMENTATION PAGE

Public reporting burden for this collection of information is estimated to average 1 hour per response, including the time for reviewing instructions, searching existing data sources gathering and maintaining the data needed, and completing and reviewing the collection of information. Send comments regarding this burden estimate or any other aspect of this collection of information, including suggestions for reducing this burden to Washington Headquarters Services, Directorate for Information Operations and Reports, 1215 Jefferson Davis Highway, Suite 1204, Arlington, VA 22202-4302, and to the Office of Management and Budget, Paperwork Reduction Project (0704-0188), Washington, DC 20503.

1. AGENCY USE ONLY (Leave blank)	2. REPORT DATE January 30, 1997	3. REPORT TYPE AND DATES COVERED

4. TITLE AND SUBTITLE

Investigating Chaos in Ocean Acoustics

5. FUNDING NUMBERS

N00014-95-10443

6. AUTHOR(S)

Kang, K. Yen, Jianguo Yan

7. PERFORMING ORGANIZATION NAME(S) AND ADDRESS(ES)

Florida International University
   Department of Electrical and Computer Engineering
Miami, FL 33199

8. PERFORMING ORGANIZATION REPORT NUMBER

9. SPONSORING / MONITORING AGENCY NAME(S) AND ADDRESS(ES)

Office of Naval Research
800 North Quincy Street, Ballston Tower One
Arlington, VA 22217-5660

10. SPONSORING / MONITORING AGENCY REPORT NUMBER

11. SUPPLEMENTARY NOTES

12a. DISTRIBUTION / AVAILABILITY STATEMENT

Approved for public release; distribution unlimited.

12b. DISTRIBUTION CODE

13. ABSTRACT (Maximum 200 words)

Chaos is a term assigned to a class of motions in deterministic systems whose time history has a sensitive dependence on initial conditions. Such phenomenon has previously been shown to exhibit in ocean acoustics' ray tracing, and called "ray chaos" by the ocean acoustics community. Since 1995, we have made a further investigation on the ray chaos, as a basic research sponsored by the Office of Naval Research (Grant No. N00014-95-10443). The results of this investigation are presented in this report.

Two new topics are addressed. The first is the chaos in three-dimensional (3-D) ray tracing. We study the chaos in Heard-to-Ascension (HA) propagation, and California-to-Hawaii (CH) propagation. Chaos appeared in both cases. Loss of predictability occurred in HA case. However, CH problem was predicted with high accuracy even in the presence of chaos. Comparison between the HA and the CH case leads to a hypothesis on overcoming ray chaos. The signature of chaos in the received signals is discussed.

The second topic is the chaos in double-channel propagation. We use the 2-D equations and a double-channel model to study the effects of internal waves on chaos. Then we use the 3-D ray equations and measured sound speed data to conduct a further investigation. Numerical results show that chaos in a double-channel is likely to be induced by internal waves. Much larger chaoticity was observed when measured sound speed data were used.

14. SUBJECT TERMS		15. NUMBER OF PAGES
Chaos Underwater Sound Acoustics		87
		16. PRICE CODE

17. SECURITY CLASSIFICATION OF REPORT	18. SECURITY CLASSIFICATION OF THIS PAGE	19. SECURITY CLASSIFICATION OF ABSTRACT	20. LIMITATION OF ABSTRACT
Unclassified	Unclassified	Unclassified	UL

Summary

Chaos is a term assigned to a class of motions in deterministic systems whose time history has a sensitive dependence on initial conditions. Such phenomenon has previously been shown to exhibit in ocean acoustics' ray tracing, and thus called "ray chaos" by the ocean acoustics community. Since 1995, we have made further investigations on the ray chaos, as a basic research project sponsored by the Office of Naval Research (Grant No. N00014-95-10443). The results of these investigations are presented in this report.

Two topics are addressed. The first is the chaos in three-dimensional (3-D) ray tracing. All of the previous studies have a common shortcoming: They all used two-dimensional (2-D) ray equations. The 2-D equations are not valid for long-range transmissions, while chaos is well known as a long-range problem. This means that the 2-D equations may lose validity before chaos is manifest. To overcome this shortcoming, we use the 3-D equations. We also use measured sound speed data for our study to be more realistic. First, we study the chaos in Heard-to-Ascension (HA) propagation, and then California-to-Hawaii (CH) propagation. Chaos appeared in both cases. Loss of predictability occurred in HA case. However, CH problem was predicted with high accuracy even in the presence of chaos. Comparison between the HA and the CH case leads to a hypothesis on overcoming ray chaos. The signature of chaos in the received signals at Ascension Island is discussed.

The second topic we address in this report is the chaos in double-channel propagation. First we use the 2-D equations and a double-channel model to study the effects of internal waves on chaos. Then we use the 3-D ray equations and measured sound speed data to conduct a further investigation. Numerical results show that chaos in a double-channel is likely to be induced by internal waves. In addition, much larger chaoticity was observed when the measured sound speed data were used. This suggests that in a real ocean environment the double-channel chaos might have larger chaoticity than that in our model experiments.

Table of Contents

I. INTRODUCTION

A. *Scientific background*

Chaos is a term assigned to a class of motions in deterministic systems whose time history has a sensitive dependence on initial conditions[1]. In ocean acoustics, Palmer et al. [2] have shown that acoustic ray paths in a weakly range-dependent deterministic ocean model exhibit such chaotic behavior. This implies that even if the sound speed structure were known with infinite precision, a limitation is imposed on one's ability to make deterministic predictions using ray theory, because small errors in initial conditions (source depth and launch angle) grow exponentially in range. The Palmer et al.'s pioneering work created a new field of ocean acoustics: Acoustic ray chaos. Further studies in this field have been conducted by Abdullaev and Zaslavskii[3], Tappert et al.[4], Brown et al.[5,6], Smith et al.[7,8], Yan[9], Collins and Kuperman[10], and Tappert and Tang[11].

These previous studies have provided some new insights. However, all of the previous studies have a common shortcoming: They all have used two-dimensional (2-D) ray equations. The 2-D equations apply only to short range transmissions, while chaos is well known as a long-range problem. This implies that the ray equations may lose validity before chaos is manifest. Hence, some conclusions of the previous studies might be controversy. To conduct a more realistic investigation, we started a research project sponsored by The Office of Naval Research (Grant No. N00014-95-10443). The project started on February 1, 1995, and ended on January 30, 1997. The results of this investigation are presented in this report.

B.   *About this report*

Two studies are made in this report. The first is the study of ray chaos using a

newly developed three-dimensional (3-D) ray equations[12]. As mentioned above, all of the

previous studies have a common shortcoming: The ray equations used in the studies are

two-dimensional (2-D) equations. These equations are valid for at most 100 km range,

but they were integrated to thousands of kilometers (far beyond their range limitation) to

construct Poincare sections and estimate Lyapunov exponents. This leads to some

unreasonable result. For example, a predictability horizon of 1000 to 2000 km has been

estimated in reference 8 using Lyapunov exponents, but the ray equations used in that

work are only valid for about 100 km. This suggests that the predictability of ray

acoustics is determined by ray equations, rather than the chaos. Hence, that predictability

horizon is to be questioned. To overcome the shortcoming of the previous studies, we

use the 3-D ray equations in this project, as well as measured sound speed data rather than

models. These two improvements allow our study to be more realistic.

The second topic we address in this report is the chaos in double-channel

propagation. In the previous work, Yan[9], one of us, has discovered that in an oceanic

double-channel, sound propagation is more likely to exhibit chaotic behavior. This

phenomenon is further investigated in this project, by using a measured sound speed data

base and taking into account the earth curvature in ray tracing.

3

The remainder of this report is organized as follows. In section II, we study the ray chaos using the 3-D ray equations and measured sound speed data. Two propagation problems are studied. The first is the Heard Island to Ascension Island sound transmission, which is a part of the Heard Island Feasibility Test (HIFT) conducted in January 1991. The second is the California to Hawaii sound transmission, which is a part of the project of Acoustic Thermometry of Ocean Climate (ATOC). The first problem (with propagation range of 9200 km) is very difficult to predict due to chaos. The second problem (with propagation range of 3300 km), however, is predicted with very high precision even in the presence of chaos. Comparison between the two cases leads to a hypothesis in overcoming ray chaos. Predictability of ray acoustics is also discussed in this section. In section III, we study the chaos of underwater sound in double-channel propagation. First, we use two-dimensional ray equations and a double-channel model to perform numerical simulations. Further investigations are then carried out by using three-dimensional ray equations and measured sound speed data. Chaos is shown to exhibit in double-channel propagation. Section IV deals with the discussions on the signature of chaos in acoustic measurements. A concluding remark is presented in Section V. There are also three appendixes, i.e., Sections VI, VII, and VIII, concerning, respectively, the derivation of the range equation used in 3-D ray tracing, more numerical results, and finally, an article entitled "Lyapunov exponent does not quantify predictability." This article shows that Lyapunov exponent cannot be used to quantify the predictability horizon while it has been used by the ocean acoustics community.

II.   CHAOS IN 3-D RAY TRACING

In the previous studies, [2 to 11] used are 2-D ray equations, which are valid only for short range transmissions. Since chaos is well known as a long-range problem, why don't we use long-range ray equations to study the ray chaos? Currently, there are two sets of long-range ray equations we can use. The first is Munk et al.'s[13] horizontal ray equations, constructing ray path on the latitude-longitude plane. The second is our new 3-D ray equations[12] that construct a ray path in the dimensions of latitude, longitude and ocean depth. Both take into account the curvature of an ellipsoid earth and 3-D refraction, so that they do not have range limitation. We have already applied the Munk et al.'s equations to the study of chaos in horizontal ray tracing, and presented the results in a previous paper.[14] In this section, we present the results of chaos in 3-D ray tracing.

Two propagation problems are studied here. The first is the Heard Island to Ascension Island sound propagation, and the second is the California to Hawaii propagation. The first problem is very difficult to predict due to chaos. However, the second problem is predicted with high precision in the presence of chaos. Predictability of ray acoustics is discussed.

A. Heard Island to Ascension Island sound propagation

1. Problem statement

During January 1991, the Heard Island Feasibility Test (HIFT) was carried out to determine the feasibility of acoustically measuring the rate of ocean warming. Underwater acoustic signals were transmitted from a ship in the southern Indian Ocean and monitored at listening stations throughout the world[15,16]. This experiment provides us with a good opportunity to study the ray chaos, considering that the propagation paths in this case are long enough for the ray chaos to exhibit. In this section, we perform 3-D ray tracing for the sound propagation from Heard Island to Ascension Island to investigate if ray chaos exists in this case.

For our investigation to be as realistic as possible, we use the 3-D ray equations[12] that do not have range limitation. In addition, we use a measured sound speed data base provided by the National Oceanographic Data Center (NODC). The data are for the seasonal period, December through March. This seasonal period covers that during which HIFT was performed.

Ascension Island (7°57'S, 14°24'W) is located in the Atlantic Ocean. From the source ship (53°33'S, 74°30'E) to Ascension Island, the distance along the geodesic is approximately 9200 km[17], about one quarter of the distance around the earth. Table 1 shows the parameters of the source and the receiver used in this calculation. The

receiver's parameters in Table 1 are those of the hydrophone 23 that is located south of

the Ascension Island [17].

Table 1 Parameters of source and receiver

	Source	Receiver
Latitude (Deg)	53°22'S	8°4.2'S
Longitude (Deg)	74°30'E	14°25.2'W
Depth (km)	0.175	0.832

2.   Methods

a)   New 3-D ray equations

As mentioned in the first section, a common shortcoming of previous studies is

the use of 2-D ray equations that apply only to short range transmissions while chaos is a

long-range problem. To overcome this shortcoming, we use the new 3-D ray equations

that do not have range limitation. The new 3-D ray equations we [12] have previously

derived are

$$\frac{d\phi}{ds} = \frac{\cos\theta\cos\alpha}{\mu - r} \tag{1}$$

$$\frac{d\lambda}{ds} = \frac{\cos\theta\sin\alpha}{(v - r)\cos\phi} \tag{2}$$

$$\frac{dr}{ds} = \sin\theta \tag{3}$$

7

$$\frac{d\alpha}{ds} = \frac{\cos\theta\tan\phi\sin\alpha}{\nu-r} + \sin\theta\sin\alpha\cos\alpha\left(\frac{1}{\nu-r} - \frac{1}{\mu-r}\right)$$
$$+ \left(-\frac{\sin\alpha}{\mu-r}\frac{\partial}{\partial\phi} + \frac{\cos\alpha}{(\nu-r)\cos\phi}\frac{\partial}{\partial\lambda}\right)\frac{\ln N}{\cos\theta} \tag{4}$$

and

$$\frac{d\theta}{ds} = -\cos\theta\left(\frac{\sin^2\alpha}{\nu-r} + \frac{\cos^2\alpha}{\mu-r}\right)$$
$$+ \left(-\frac{\sin\theta\cos\alpha}{\mu-r}\frac{\partial}{\partial\phi} - \frac{\sin\theta\sin\alpha}{(\nu-r)\cos\phi}\frac{\partial}{\partial\lambda} + \cos\theta\frac{\partial}{\partial r}\right)\ln N \tag{5}$$

where

$$\mu = \frac{a(1-e^2)}{(1-e^2\sin^2\phi)^{3/2}} \tag{6}$$

and

$$\nu = \frac{a}{(1-e^2\sin^2\phi)^{1/2}} \tag{7}$$

are the radius of curvature and the radius of curvature in prime vertical, respectively[18]. In Eqs. (1) through (7), ϕ is geographic latitude; λ is longitude, east of Greenwich being positive; r is ocean depth, downward positive; α is azimuth, measured clockwise from north; θ is grazing angle; a is the semimajor radius of the reference ellipsoid; and e is the eccentricity of the ellipsoid. These ray equations account for the curvature of an ellipsoid earth and 3-D refraction, and thus, should not have range limitation. Apart from these ray

equations we have previously derived, we also use the following equations to compute

travel time

$$\frac{dt}{ds} = \frac{1}{C} \tag{8}$$

and the propagation range

$$\frac{dR}{ds} = \cos\theta \sqrt{\left(\frac{\mu}{\mu-r}\cos\alpha\right)^2 + \left(\frac{v}{v-r}\sin\alpha\right)^2} \tag{9}$$

The derivation of equation (9) is presented in Appendix 1.

b)   Numerical calculations

Before ray tracing, we sort the NODC sound speed data sets into numerical orders

of latitude and longitude, respectively. Meanwhile, we index each data set. The straight

insertion method[19] is used for sorting the data. The index of a data set is to be used for

finding a particular sound speed data set during the 3-D sound speed interpolation as

described in the following paragraph.

We integrate the ray equations (1) through (5) using the fourth-order Runger-

Kutta method with adaptive step size control.[19] The calculation accuracy is controlled by

specifying a maximum fractional error (10^{-6}) in any single integration step. For a given

location (ϕ_0,λ_0,r_0), the sound speed is estimated through the interpolation of the pre-sorted NODC 3-D sound speed data base. In the 3-D interpolation, we first find the grid square in which the point (ϕ_0,λ_0) falls. Then we find the sound speed data sets on the grid square through the index we give to each data set during the sorting process described in the previous paragraph. We estimate the sound speed at depth r_0 for the grid points using Cubic Spline method.[19] Finally we obtain the sound speed at (ϕ_0,λ_0,r_0) by performing Bilinear Interpolation[19] on the $\phi\lambda$-plane.

The following method is used to find eigenrays -- rays connecting the source and the receiver. First, we search for the launch azimuth with which the ray passes within a given error tolerance for both the latitude and the longitude of the receiver. Successive Shooting method[20] is used for the searching process. Then we adjust launch grazing angle and again the launch azimuth through trial-and-error to continue searching. A ray is determined as an eigenray, if it passes within given error tolerances of the receiver's coordinates (ϕ_r,λ_r,r_r). This is a very difficult task due to ray chaos, as will be described in Section A 3.

c) Diagnosis of chaos

Two methods are used to diagnose chaos. The first is the Lyapunov exponent method. The ith one-dimensional Lyapunov exponent is defined as[21]

$$\lambda_i = \lim_{t \to \infty} \frac{1}{t} \log_2 \frac{p_i(t)}{p_i(0)}, \tag{10}$$

where p is the length of the ellipsoidal principle axis, and λ_i are ordered from the largest to the smallest. Lyapunov exponents are the average exponential rates of divergence or convergence of nearby orbits in the phase space. Any system containing at least one positive Lyapunov exponent is defined to be chaotic. To estimate the Lyapunov exponents, Wolf et al.'s [21] method is used, and their published FORTRAN code is adapted for this calculation.

For calculating $p_i(t)$, we use the following variational equations:

$$\frac{d\delta\phi}{ds} = -\frac{\cos\theta\cos\alpha}{(\mu-r)^2}\frac{\partial\mu}{\partial\phi}\delta\phi + \frac{\cos\theta\cos\alpha}{(\mu-r)^2}\delta r - \frac{\cos\theta\sin\alpha}{\mu-r}\delta\alpha - \frac{\cos\alpha\sin\theta}{\mu-r}\delta\theta \tag{11}$$

$$\frac{d\delta\lambda}{ds} = -\frac{\cos\theta\sin\alpha}{[(v-r)\cos\phi]^2}\left[\frac{\partial v}{\partial\phi}\cos\phi - (v-r)\sin\phi\right]\delta\phi + \frac{\cos\theta\sin\alpha\cos\phi}{[(v-r)\cos\phi]^2}\delta r$$
$$+ \frac{\cos\theta\cos\alpha}{(v-r)\cos\phi}\delta\alpha - \frac{\sin\theta\sin\alpha}{(v-r)\cos\phi}\delta\theta \tag{12}$$

$$\frac{d\delta r}{ds} = \cos\theta\delta\theta \tag{13}$$

$$\frac{d\delta\alpha}{ds} = \{\cos\theta\sin\alpha\frac{(\nu-r)/\cos^2\phi - \tan\phi\,\partial\nu/\partial\phi}{(\nu-r)^2}$$

$$\sin\theta\sin\alpha\cos\alpha\left[\frac{\partial\mu/\partial\phi}{(\mu-r)^2} - \frac{\partial\nu/\partial\phi}{(\nu-r)^2}\right]$$

$$-\frac{\sin\alpha}{\cos\theta}\left[\frac{(\mu-r)\partial^2\ln N/\partial\phi^2 - (\partial\ln N/\partial\phi)(\partial\mu/\partial\phi)}{(\mu-r)^2}\right]$$

$$+\frac{\cos\alpha}{\cos\theta}\left[\frac{(\partial^2\ln N/\partial\phi\partial\lambda)(\nu-r)\cos\phi - \frac{\partial\ln N}{\partial\lambda}\left[\frac{\partial\nu}{\partial\phi}\cos\phi - (\nu-r)\sin\phi\right]}{[(\nu-r)\cos\phi]^2}\right]\}\delta\phi$$

$$+\frac{1}{\cos\theta}\left[-\frac{\sin\alpha}{\mu-r}\frac{\partial^2\ln N}{\partial\phi\partial\lambda} + \frac{\cos\alpha}{(\nu-r)\cos\phi}\frac{\partial^2\ln N}{\partial\lambda^2}\right]\delta\lambda$$

$$+\{\frac{\cos\theta\tan\phi\sin\alpha}{(\nu-r)^2} + \sin\theta\sin\alpha\cos\alpha\left[\frac{1}{(\nu-r)^2} - \frac{1}{(\mu-r)^2}\right]$$

$$-\frac{\sin\alpha}{\cos\theta}\frac{\frac{\partial^2\ln N}{\partial\phi\partial r}(\mu-r) + \frac{\partial\ln N}{\partial\phi}}{(\mu-r)^2}$$

$$+\frac{\cos\alpha}{\cos\theta}\frac{\frac{\partial^2\ln N}{\partial\lambda\partial r}(\mu-r)\cos\phi + \frac{\partial\ln N}{\partial\lambda}\cos\phi}{[(\nu-r)\cos\phi]^2}\}\delta r$$

$$+\{\frac{\cos\theta\tan\phi\cos\alpha}{(\nu-r)} + \sin\theta\left(\frac{1}{\nu-r} - \frac{1}{\mu-r}\right)(\cos^2\alpha - \sin^2\alpha)$$

$$-\frac{1}{\cos\theta}\left[\frac{\cos\alpha}{\mu-r}\frac{\partial\ln N}{\partial\phi} + \frac{\sin\alpha}{(\nu-r)\cos\phi}\frac{\partial\ln N}{\partial\lambda}\right]\}\delta\alpha$$

$$+\{-\frac{\sin\theta\tan\phi\sin\alpha}{\nu-r} + \cos\theta\sin\alpha\cos\alpha\left(\frac{1}{\nu-r} - \frac{1}{\mu-r}\right)$$

$$+\frac{\sin\theta}{\cos^2\theta}\left[-\frac{\sin\alpha}{\mu-r}\frac{\partial\ln N}{\partial\phi} + \frac{\cos\alpha}{(\nu-r)\cos\phi}\frac{\partial\ln N}{\partial\lambda}\right]\}\delta\theta \tag{14}$$

and

$$\frac{d\delta\theta}{ds} = \{\cos\theta\left[\frac{\sin^2\alpha}{(v-r)^2}\frac{\partial v}{\partial\phi}+\frac{\cos^2\alpha}{(\mu-r)^2}\frac{\partial\mu}{\partial\phi}\right]-\frac{\sin\theta\cos\alpha}{(\mu-r)^2}\left[\frac{\partial^2\ln N}{\partial\phi^2}(\mu-r)-\frac{\partial\ln N}{\partial\phi}\frac{\partial\mu}{\partial\phi}\right]$$

$$-\frac{\sin\theta\sin\alpha}{[(v-r)\cos\phi]^2}\left[\frac{\partial^2\ln N}{\partial\phi\partial\lambda}(v-r)\cos\phi+\frac{\partial\ln N}{\partial\lambda}(\mu-r)\sin\phi\right]$$

$$+\cos\theta\frac{\partial^2\ln N}{\partial\phi\partial r}\}\delta\phi$$

$$+\left[-\frac{\sin\theta\cos\alpha}{\mu-r}\frac{\partial^2\ln N}{\partial\phi\partial\lambda}-\frac{\sin\theta\sin\alpha}{(v-r)\cos\phi}\frac{\partial^2\ln N}{\partial\lambda^2}+\cos\theta\frac{\partial^2\ln N}{\partial\lambda\partial r}\right]\delta\lambda$$

$$+\{-\cos\theta\left[\frac{\sin^2\alpha}{(v-r)^2}+\frac{\cos^2\alpha}{(\mu-r)^2}\right]-\frac{\sin\theta\cos\alpha}{(\mu-r)^2}\left[\frac{\partial^2\ln N}{\partial\phi\partial r}(\mu-r)+\frac{\partial\ln N}{\partial\phi}\right]$$

$$-\frac{\sin\theta\sin\alpha}{\cos\phi(v-r)^2}\left[\frac{\partial^2\ln N}{\partial\lambda\partial r}(v-r)+\frac{\partial\ln N}{\partial\lambda}\right]+\cos\theta\frac{\partial^2\ln N}{\partial r^2}\}\delta r$$

$$+\{-2\cos\theta\sin\alpha\cos\alpha\left(\frac{1}{v-r}-\frac{1}{\mu-r}\right)+\frac{\sin\theta\sin\alpha}{\mu-r}\frac{\partial\ln N}{\partial\phi}$$

$$-\frac{\sin\theta\cos\alpha}{(v-r)\cos\phi}\frac{\partial\ln N}{\partial\lambda}\}\delta\alpha$$

$$+\{\sin\theta\left(\frac{\sin^2\alpha}{v-r}+\frac{\cos^2\alpha}{\mu-r}\right)-\frac{\cos\theta\cos\alpha}{\mu-r}\frac{\partial\ln N}{\partial\phi}-\frac{\cos\theta\sin\alpha}{(v-r)\cos\phi}\frac{\partial\ln N}{\partial\lambda} \qquad (15)$$

$$-\sin\theta\frac{\partial\ln N}{\partial r}\}\delta\theta$$

These variational equations are derived from ray equations (1) through (5). They are

numerically integrated along with the integration of the ray equations to estimate

Lyapunov exponents.

The second method we use to identify chaos is the Power Spectrum Method. We

compute the power spectra for each ray path, by using the Fast Fourier Transformation

(FFT) [19] to analyze vertical path data. A chaotic ray path is characterized by broadband,

noisy spectra. The Power Spectra are used together with the Lyapunov exponents to give a conclusive assessment as to whether a ray is chaotic.

3. Numerical results

a) Extremely sensitive dependence on initial conditions

Fig. 1 shows two vertical ray paths between Heard Island and Ascension Island. The upper is an eigenray, which is launched with an azimuth of 266.7258936017752°, and a grazing angle of 0.5000000000000000°; and the lower is the vertical ray path launched with the same azimuth, but a slightly different grazing angle (0.5000000050000000°). By comparing the two ray paths, we can see clearly that a very small difference (0.00000005°) between the launch grazing angles caused substantial change in ray path. This phenomenon -- extremely sensitive dependence on initial conditions -- is just a characteristic of chaos.

The small perturbation to the launch grazing angle not only caused the substantial change in the ray path, but also dramatically changed the ray parameters. This can be seen in Table 2. From this Table we can see that when the small perturbation is imposed to the launch grazing angle, the ray constructed is no longer an eigenray. At the receiver's longitude, the difference in ending longitude is almost 1 degree, and the propagation range is reduced to 9155 km. The latter caused substantial change in travel time.

Table 2   Comparison of ray parameters (The ending latitude is -8.069997° in both cases. The launch angles are given in Fig. 1.)

Parameters at the receiver	Eigenray 1	The perturbed ray	Differences
Longitude (Deg)	-14.420752040715	-13.4235716603278	-0.9972
Depth (km)	0.83525	0.57177	0.26348
Travel time (Sec)	6258.132	6211.618	46.514
Range (km)	9222.607	9155.850	66.757

b)   Positive Lyapunov exponents

We have just shown that the 3-D ray paths we have constructed are extremely sensitive to initial conditions. This phenomenon is the characteristics of chaos. Fig. 2 shows the Lyapunov exponents of the ray in Fig. 1. We can see clearly from Fig. 2 that this ray has positive Lyapunov exponents, suggesting chaos. This is consistent with its behavior of sensitive dependence on initial conditions as shown in Fig. 1. Figure 2 is only a typical result. In fact, we have estimated Lyapunov exponents for all the rays computed in this project. As a matter of fact, all of the rays have positive Lyapunov exponents, indicating chaos.

c) Loss of predictability

The presence of the chaos caused the loss of predictability. This can be seen in Table 3 that gives the last eleven steps of the iteration in shooting the receiver's longitude (-14.42°). In this calculation, for a given launch grazing angle (-3.0°), we successively change the launch azimuth, using bisection method, to drive the ray to the receiver's longitude. We can see clearly from this Table that at the 44-th step, the launch azimuth had already been specified with 16-digit accuracy -- the maximum accuracy in FORTRAN's double precision. However, we still did not arrive at the receiver's longitude. This implies that a limitation due to the ray chaos is imposed on our ability to make predictions. In other words, the loss of predictability occurred in this case.

Table 3 Loss of predictability

Iteration Number	Launch Azimuth (Degree)	Ending Longitude λ_{end} (Degree)	$\|\lambda_{end}-\lambda_{receiver}\|$ (Degree)
35	266.6249999999418	-14.57	0.15
36	266.6249999999709	-14.63	0.21
37	266.6249999999854	-14.65	0.23
38	266.6249999999927	-14.60	0.18
39	266.6249999999964	-14.61	0.19
40	266.6249999999982	-14.55	0.13
41	266.6249999999991	-14.64	0.22
42	266.6249999999995	-14.58	0.16
43	266.6249999999998	-14.60	0.18
44	266.6249999999999	-14.55	0.13
45	266.6249999999999	-14.05	0.37

Mentioned above are only some typical results. In fact, all of the rays computed are chaotic according to their positive Lyapunov exponents. Due to the ray chaos, our

ability to predict is very limited in this case. Until now we have not found an eigenray that satisfies the given accuracy: ±0.000005° for the receiver's latitude and longitude, and ±0.0005 km for the receiver's depth. The best one and also the only one we have found passes within 0.000005° of the receiver's latitude, 0.0008° of the receiver's longitude, and 0.0033 km of the receiver's depth. Its travel time (6258.132 sec) seems in good agreement with the measurements (1 hr, 44 min, 17 sec.,) but we got this result by chance, rather than by any conventional algorithms. This is illustrated in Table 4. The data in this table are taken from a shooting process, with a launch grazing angle of 0.5° and launch azimuths between 266° and 269°. The error tolerances we set for this calculation were within 0.000005° of both the receiver's latitude and the receiver's longitude, and within 0.0005 km of the receiver's depth. We did not get any ray that satisfies this criterion. Instead, we list those which are closest to the receiver in Table 4. We can see that the ray computed at the 45-th step of shooting is not better than that at the 28-th step, since the former has larger errors at the receiver. Obviously, continuing shooting cannot improve the accuracy of prediction. Therefore, we lose predictability in this case due to chaos.

It is interesting to discuss how accurate we can predict in this case. Table 5 lists those rays that are closest to the receiver during a shooting process. In the calculations, the ending longitude is obtained with an error of 0.000005 degree. We wish to get the ending longitude with the same accuracy, but we could not. Instead, we list

Table 4 — Some rays in a shooting process

No. of shooting	Travel time (sec.)	Range (km)	Ending Longitude (Deg)	Ending Depth (km)	Error of Longitude at receiver	Error of Depth at receiver
15	6257.977	9222.457	-14.4186	0.7903	0.0014	0.042
20	6258.247	9222.778	-14.4233	0.8953	0.0033	0.0633
28	6258.132	9222.607	-14.4208	0.8353	0.0008	0.0033
45	6258.206	9222.845	014.4243	0.8849	0.0043	0.0329

Table 5   Errors at the receiver: A typical result (launch azimuth is successfully changed using bisection method, and launch grazing angle is fixed at 0.5°)

	Travel time, Sec	Range, km	Longitude, Deg.	Depth, km
Ray 1	6257.977	9222.5	-14.4186	0.7903
Ray 2	6258.247	9222.8	-14.4233	0.8953
Ray 3	6258.132	9222.6	-14.4208	0.8353
Ray 4	6258.206	9222.8	-14.4243	0.8849
Prediction	6258	9223	-14.42	1

those results that satisfies ±0.005° error tolerance for the receiver's longitude. From this

Table, we can see that at the receiver's longitude (-8.07000°),

- the receiver's longitude we got has an error of 0.005°, corresponding to about 500 m

  error in the longitude direction;

- the travel time we got can be accurate to seconds (in this case, 6258 sec);

- the range predicted can be accurate to ten meters (in this case, 9220 km); and

- The receiver's depth we got may only be accurate to kilometers.

Considering that the propagation range in this case is about 9220 km, the accuracy of the

travel time, the range, and the receiver's longitude appears to be good. However, the

accuracy of the receiver's depth, which can only be accurate to kilometers, cannot be

accepted for a 3-D ray tracing. In addition, the accuracy of travel time may not meet the

needs of ocean acoustic tomography. Table 5 lists a typical result. In our calculation, the

accuracy we predicted varies with the launch grazing angle. More ray data are given in

Appendix 2.

4.   Conclusions

We have shown that in the case of the Heard-to-Ascension sound propagation, chaos occurred in ray tracing. Due to the chaos, our ability to make deterministic prediction is very limited in this case. Consequently, we have not gotten any eigenray that satisfies the given error tolerances at the receiver. The best one and also the only one we have got passed with 0.000005° of the receiver's latitude, 0.0008° of the receiver's longitude, and 0.033 km of the receiver's depth. Its travel time (6258.132 seconds) seems in good agreement with the measurements (1 hr, 44 min, 17 sec.,) but we got this result by chance rather than using any conventional algorithms.

B.   *California to Hawaii sound propagation*

We have just shown that in the case of the Heard-to-Ascension sound propagation, predictability is very limited due to chaos. Now we present a very different result: In the presence of chaos, we predict with very high precision for a 3300 km sound propagation problem – the California to Hawaii sound propagation.

1.   Geophysical settings

As part of the Acoustic Thermometry of Ocean Climate (ATOC) program, an Acoustic Engineering Test (AET) was conducted during November 1994. Broad band acoustic data were obtained at about 3,300 km (from California to Hawaii) and 10,000

20

km (from California to New Zealand). Here we study the California-Hawaii sound propagation. The broad band ATOC source was located at about 300 nm of San Diego, California, near Jasper Seamount (31.03416667°N, 123.5903333°W,) and the receiver was placed at 20.65066666°N and -154.0773333°W, near Hawaii.[22] The source location and the receiver's location are given in Table 6.

Table 6 Parameters of source and receiver for California-to-Hawaii ray tracing

	Source	Receiver
Latitude (Degree)	31.03416667°	20.65066666°
Longitude (Degree)	-123.5903333°	-154.0773333°
Depth (km)	0.650	1.2696

2.   Numerical ray tracing

We still use the ray equations (1) through (5) to construct ray paths. The numerical methods and the computer codes are the same as those that used for the Heard-to-Ascension sound propagation described in Section A2. Different from the Heard-to-Ascension ray tracing, however, is that we now use Levitus sound speed data base, rather than the NODC sound speed data. The Levitus sound speed data base is provided by the ATOC group at the Scripps Institution of Oceanography, University of California at San Diego. Compared with the NODC data, the Levitus data are smoother in horizontal direction.

Before searching for eigenrays, we determine the maximum fractional error for the Runge-Kutta method. This is done by specifying different values of the maximum fractional error in any single integration step. The results are presented in Table 7.

Table 7 Dependence of ray parameters on the maximum fractional error (Eps) specified in Runge-Kutta code..

Eps	Ending ϕ (Degree)	Ending λ (Degree)	Ending r (km)	Travel time (sec)	Range (km)
1D-4	20.344388	-154.077338	0.5782	2206.673	3267.881
1D-5	20.344383	-154.077338	0.5646	2206.673	3267.881
1D-6	20.344387	-154.077338	0.5674	2206.673	3267.881
1D-7	20.344393	-154.077331	0.5675	2206.673	3267.880
1D-8	20.344390	-154.077334	0.5675	2206.673	3267.880

We can see from this table that when it is less than 1D-6, the *Eps* significantly affects the accuracy of the ray parameters. This is due to the rounding-off errors in the numerical calculations. To avoid this rounding error effect, we choose Eps=1D-6 in the

following calculations. We still use the successive shooting method described in section 1 to find eigenrays. Table 8 lists nine eigenrays.

Table 8   *Eigenray parameters and Lyapunov exponents*

No. of Eigenray	Travel Time (sec)	Range (km)	Error of Latitude at receiver	Error of Longitude at receiver	Error of Depth at receiver	Largest Lyapunov Exponents
1	2196.178	3252.383	0.000005°	0.000003°	0.0003km	0.018
2	2195.626	3252.283	0.000001°	0.000001°	0.0003km	0.0090
3	2195.519	3252.383	0.000001°	0.000001°	0.0002km	0.0056
4	2195.387	3252.383	0.000004°	0.000003°	0.0002km	0.0093
5	2194.666	3252.383	0.000003°	0.000000°	0.0001km	0.0025
6	2194.584	3252.383	0.000005°	0.000003°	0.0004km	0.0058
7	2193.085	3252.383	0.000001°	0.000000°	0.0002km	0.0019
8	2192.722	3252.382	0.000003°	0.000002°	0.0004km	0.0022
9	2192.267	3252.383	0.000002°	0.000000°	0.0000km	0.022

3.   Chaos and Predictability

We can see clearly from Table 8 that all of these eigenrays have positive Lyapunov exponents, indicating chaos. Figure 3 is the calculation of the Lyapunov exponents for these eigenrays. Another evidence to show that these rays are chaotic is that all of these rays have broadband noisy power spectra, as are shown in Figure 4. These spectra are obtained by using FFT to analyze the vertical ray paths of the eigenrays. In each calculation, the vertical ray path is sampled at every 0.3 km range step.

Positive Lyapunov exponents and broadband noisy power spectra indicate that all of the rays listed in Table 8 are chaotic. However, these rays, though chaotic, are all predicted with very high accuracy: within 0.000005° of both the receiver's latitude and the receiver's longitude, and within 0.0005 km of the receiver's depth (Please see Table 8). It is worthwhile mentioning that these high accuracy predictions are made even in the presence of chaos.

4.   Conclusions

In this section, we have studied chaos of underwater sound from California to Hawaii. We still use the 3-D ray equations that have been used to study Heard-to-Ascension propagation in the previous section. However, we use Levitus sound speed data in this case, rather than NODC data. Our numerical results show that all of the rays were chaotic, but even in the presence of chaos, we still made predictions with very high accuracy.

C.   Overcoming ray chaos: A hypothesis

We have just presented two cases of chaos in ocean acoustics. The first case, Heard-to-Ascension propagation (HAP), has a very limited predictability due to chaos. However, the second case, California-to-Hawaii propagation (CHP), is predicted with very high accuracy in the presence of chaos. We wonder why in CHP case we can predict with very high accuracy even in the presence of chaos.

To answer this question, let us find the differences between the HAP case and the CAP case. There are apparently two differences. The first is in propagation range. HAP, whose predictability is very limited, has a range of about 9222 km, while CHP has a range of only 3258 km. The second difference is in sound speed data. HAP used NODC data base that has large fluctuations in the upper ocean (for instance, see Fig. 5). However, CHP used Levitus data that is smooth in horizontal (for instance, see Fig. 6). The smoothness of the Levitus data might be a reason why in CHP case we predicted with a very high precision. Both range and the smoothness of sound speed field can affect predictability.

In practice, we cannot change propagation range, but we can change the smoothness of a sound speed data base by using some mathematical methods. From comparisons between HAP and CHP cases, we infer that a smoothed sound speed data base might help overcome the chaos in ocean acoustics, significantly enhancing our

ability in long-range ocean acoustic prediction. To test this hypothesis is one of our future efforts.

D. On predictability horizon

Ray chaos means that very long range forecasting using ray theory is impossible, but there remains an important question: How far from a source can we predict? Smith et al.[8] have given an answer to this question. Using Lyapunov exponent, they defined a predictability horizon within which a ray acoustic problem is predictable. They performed numerical calculations with an ocean model taking into account mesoscale structure, and concluded that the predictability horizon is about 1,000 to 2,000 km.[8]

However, Smith et al. used two-dimensional (2-D) ray equations in their research. Those equations are valid only for short ranges, at most 100 km, which is much shorter than the predictability horizon (1,000 to 2,000 km) they estimated. In other words, the 2-D ray equations lose validity before chaos is manifest. Therefore, the 1,000 to 2,000 km predictability horizon suggested by Smith et al.[8] means that one's ability to make deterministic prediction is not limited by the ray chaos, but rather it is restricted by the accuracy of the 2-D ray equations.

Consequently, to enhance our ability to predict using ray acoustics, first of all, we need to overcome the range limitation of the ray equations. This was the motivation of our previous paper,[12] in which we derived a set of three-dimensional (3-D) ray equations.

The 3-D equations take into account the curvature of an ellipsoidal earth and 3-D refraction, so that they should not have range limitation.

In this report, we have used these 3-D equations to simulate sound propagation with special interest in the study of ray chaos. The propagation range of California-to-Hawaii is about 3,300 km, i.e., far beyond the predictability horizon (1000 km to 2000 km)[8] estimated using the 2-D model. However, the predicted results (receiver's locations, and travel time) are of very high accuracy (within 0.000005° of both the latitude and the longitude of the receiver, and within 0.0005 km of the receiver's depth). It is also worthwhile mentioning that all of the ray paths, which are predicted with such a high accuracy, are chaotic according to their positive Lyapunov exponents and broadband noisy Power Spectra.

This means that even in the presence of chaos, the ray model (3-D equations with Levitus sound speed data base) was still suitable for global ocean acoustic prediction. Although the prediction range of this demonstrated example is 3258 km, we may predict with satisfactory accuracy for much longer ranges. This is because that the error tolerances we currently specified are very harsh and the 16-digit accuracy of FORTRAN's double precision was not used up to specify the initial conditions.. Therefore, the 3-D ray equations (1) through (5) combined with a Levitus sound speed data base may become a powerful and more accurate model for global scale ocean acoustics ray tracing.

However, it is impossible to estimate a predictability horizon according to our current knowledge. There are two difficulties. First, the predictability is case sensitive. It depends on both the range and the smoothness of a sound speed field, as have been discussed in the previous section. Second, we have discovered that Lyapunov exponent, which is used by some researchers to quantify predictability, cannot correctly quantify predictability. This is explained as follows.

Using the largest Lyapunov exponent to quantify predictability is first suggested by Shaw,[23] and followed by some researchers, for instance, in references 5,7,8,21. However, there is not enough evidence to support this concept. In the published references 5,7,8,21, those researchers who believe that Lyapunov exponent quantifies predictability did not provide any numerical result to show it in their specific cases. In fact, the only evidence we have found is the result of the analog computer experiment presented by Shaw.[23] We show, in the Appendix 3 of this report, that Lyapunov exponent does not quantify predictability. Here we emphasize that it is not correct to use Lyapunov exponent to estimate predictability horizon in ocean acoustics, and nor in any other fields.

III. CHAOS IN DOUBLE-CHANNEL PROPAGATION

We have just studied the chaos in three-dimensional, long-range sound propagation in the ocean. Now we further investigate another chaotic behavior in ocean acoustics – chaos in double-channel propagation.

By using Linear Stability Analysis, Yan[9] has found that acoustic ray paths in an oceanic double-channel exhibit chaotic behavior with larger chaoticity than in a deep ocean acoustic channel. This section deals with a more detailed investigation on the double-channel chaos, with special interests in the effects of oceanic internal waves. In the following, we use the ray equations consistent with parabolic equation and a double-channel sound speed model derived from a set of measured data from the North Atlantic Ocean to perform numerical simulations. Poincare sections are constructed to identify chaos. It is found that oceanic internal waves are likely to induce chaos in a double-channel.

A. An investigation using 2-D model

1. 2-D model

The 2-D ray equations, consistent with the parabolic wave equation[24], are used in this study to predict acoustic propagation. The equations are

$$\frac{dz}{dr} = \frac{\partial H}{\partial P} \tag{16}$$

and

$$\frac{dP}{dr} = -\frac{\partial H}{\partial z} \tag{17}$$

where

$$H(z, P, r) = 0.5P^2 + V(z, r) \tag{18}$$

and

$$V(z,r) = 0.5\left(1 - \frac{C_0^{\ 2}}{C(z)^2}\right) + g(z,r) \tag{19}$$

Here, z is the depth, r is the range, P is the tangent of grazing angle, H is the Hamiltonian, V is the potential, C_0 is the reference sound speed, C is the sound speed, and g is the perturbation in the potential function.

The double-channel sound speed profile is given by the following model:

$$C(z) = \begin{cases} 1.49323 - 0.0471063z + 0.147473z^2 \\ \qquad - 0.145517z^3 + 0.0452260z^4, \quad when\ z < 1.5km \\ \\ 1.49170 + 0.0133(z - 1.5), \quad when\ z \geq 1.5km \end{cases} \tag{20}$$

which is obtained in the previous study[9] by fitting the North Atlantic double-channel data in reference [25]. The perturbation used here is the same as that of Palmer *et al.*[2], and also the same as Yan's previous work[9], i.e.,

$$g(z,r) = \sqrt{2}A\exp(-1.5z / B)\sin(2\pi r / R) \tag{21}$$

where R is the perturbation wave length. This perturbation could be interpreted as a highly idealized internal wave or as a single baroclinic mode representing mesoscale structure. The exponential dependence on depth was derived from Brunt-Vaisala frequency; the sinusoidal formulation is similar to what Lee[26], and Baxter and Orr[27] used to investigate the effects of internal wave on sound in the ocean. This perturbation is not realistic. The advantage of using this simplified model is that Poincare section can be used to show chaos graphically. By using this sound speed model, a double-channel profile is depicted in Fig. 7.

2. Numerical calculations

The ray equations (16) and (17) are integrated using the fourth-order Runge-Kutta method with adaptive step size control.[19] The calculation accuracy is controlled by specifying a maximum fractional error (10^{-6}) in any single integration step. Reflections are assumed at the ocean surface and bottom. After each step of integration, a check is made to see if the ray has penetrated the surface and bottom. If it has, then an iterative search is performed to determine the depth (with error less than 1 mm) and the angle of reflection.

Poincare section is used to show chaos. It is depicted in such a way that the ray path is sampled every cycle of the range-dependent perturbation, i.e., 10 km when the perturbation wave length R in Eq. (21) is 10 km.

31

The parameters in Eq. (21) are B=1.0, R=5,10, and 15 km, respectively, which are typical in a fluctuating ocean[28][R=5 km corresponds to the horizontal wavelength of an internal wave (peak of spectrum)]. Two values are used for the parameter A in Eq. (21). The first is A=0.0025 that corresponds approximately to 5m/s of sound speed perturbation, a typical value in the ocean[29], and the second is A=0.001 corresponding to δC= 2.0 m/s in reference[30]. This ocean model, of cause, is not realistic. However, the numerical results produced as follows can provide qualitative information.

3.   Results

Fig. 8 through 13 are Poincare sections with perturbation strength A=0.0025. In these figures, the smooth closed curves are regular trajectories; and the apparently random distribution of points in some bounded region represent the chaos. We can see from these figures that chaos occurred in this case. From Yan's paper[9], we know that this perturbation strength did not induce chaos in a deep ocean acoustic channel, but it did induce chaos in both Yan's paper and this work. This illustrates that ray chaos is more likely to occur in a double-channel than in a deep ocean channel. From Fig. 8, 9, and 10, we can also see that chaotic trajectories vary with the perturbation wave length R, but we still do not know how the parameter R affects chaoticity. The horizontal wave length of an internal wave ranges from 0.5 km to 50 km, and for the peak of spectrum is about 5 km[28]. Here, we only used 5, 10, and 15 km in the calculations, i.e., the values around the peak of spectrum.

Figs. 14 through 19 are the Poincare sections for perturbation strength $A=0.001$. These figures also show that some of the ray trajectories exhibit chaotic behavior. However, in these figures, chaotic trajectories were significantly less than those in Figs. 8 through 13. This is due to the decrease in the perturbation strength. It is difficult to specify a maximum perturbation strength for internal waves. It varies at the different region of the oceans, and varies significantly in published references. The values used here are taken from published references.[29,30]. To have a better understanding, we use measured sound speed data to make a further study.

B.   *Further study using 3-D model with measured sound speed data*

1.   Ray tracing

We have just shown that chaos can be induced by internal waves in a double-channel. In that study, we used 2-D ray equations and a sound speed model. That study has two shortcomings. First, the ray equations are 2-D so that they may lose validity before chaos manifests. Second, the sound speed model may not well represent the real ocean environment. To overcome these shortcomings, we use the ray equations (1) through (5) and the measured sound speed data provided by the National Oceanic Data Center (NODC).

In our original plan, a 3-D ray tracing was to be performed using the NODC data. However, we cannot complete this task because the NODC data we got cannot be used to construct a 3-D sound speed field. The most sound speed data sets we have obtained are

lack of the data corresponding to the depths between 400 to 2000 m, while these data are crucial to constructing a double-channel profile. Fortunately, we found some complete double-channel data at longitude 14°E, as are depicted in Fig. 20. We use these double-channel sound speed profiles (SSP) to perform ray tracing. For each SSP, Cubic Spline Method[19] is used to estimate the sound speed at a given depth. Then the linear interpolation between the two adjacent SSPs gives the sound speed at a given latitude.

We still use the 3-D ray equations (1) through (5). However, we use

$$\frac{\partial C}{\partial \lambda} = 0, \quad and \quad \alpha(0) = 0 \tag{22}$$

to restrict a ray to stay at 14°E, because as mentioned above the double channel sound speed profiles we got are along this longitude direction. In this way, we use the 3-D ray equations and the 2-D sound speed field (Fig. 22) to perform ray tracing. Although horizontal refraction is neglected in this case, earth curvature is taken into account in the ray tracing by using the 3-D ray equations. In addition, we use the measured double-channel profiles. These approaches allow the following numerical results to be more realistic than those in the previous section.

2.   Numerical results

Figure 21 shows the ray paths in the double-channel. In these calculations, the source was placed at the upper channel axis with depth of 0.4 km. Table 9 lists the

largest Lyapunov exponents for these rays. We can see from this table that all of the rays have positive Lyapunov exponents, indicating chaos. We also constructed power spectra for these rays, as are shown in Fig. 22. These power spectra are obtained by using FFT to process the vertical path data sampled at 1 km step in range. We can see clearly that all of the power spectra are broadband, indicating chaos. This is consistent with the positive Lyapunov exponents listed in Table 9.

Table 9   Lyapunov exponents for the acoustic rays in the double-channel

Launch grazing angle (Deg.)	Largest Lyapunov exponent
0	0.057
1	0.076
2	0.067
3	0.015
4	0.076
5	0.011
6	0.012
7	0.027
8	0.036
9	0.035
10	0.029

Recall that in the previous section we used 2-D ray equations and a weakly range-dependent double-channel model to study chaos. Our numerical results of those calculations suggested that only a few rays are chaotic, and that the number of chaotic rays depends on the perturbation strength assigned to the model. The numerical results (Table 9, and Fig. 22), however, provide a different point of view: all of the rays constructed using the measured sound speed data are chaotic. It appears that in a real ocean environment chaoticity (here, we mean the number of chaotic rays) is significantly larger than that we estimated using the ocean model.

IV. DISCUSSIONS: ON THE SIGNATURE OF CHAOS IN ACOUSTIC MEASURMENTS

We have shown in Section II that the rays between Heard Island and Ascension Island are very chaotic. We are now interested in finding the signature of the chaos in the acoustic measurements made at Ascension Island during the Heard Island Feasibility Test. According to the published reference 17, the received signals at Ascension Island are characterized as "An unexpected combination of phase stability and amplitude variability." What is the signature of the chaos?

Ray chaos means that the ray paths are extremely sensitive to launch angles (the launch azimuth and the launch grazing angle in the 3-D case). However, no matter how sensitive to the launch angles they are, some eigenray paths should exist between Heard Island and Ascension Island where the signals were received. In addition, these eigenray

In summary, chaos might enhance the amplitude variability of the received signals at Ascension Island. The discussions presented above appear to explain why the received signals at Ascension Island were characterized as "unexpected combination of phase stability and amplitude variability." For shallow water and a moving source however, chaos might have quite different signature.

ACKNOLEGMENTS

V.   APPENDIX 1: DERIVATION OF RANGE EQUATION

The derivation of the range equation is as follows. At the sea level, we have

$$dR = \sqrt{(\mu\, d\phi)^2 + (v\cos\phi\, d\lambda)^2} \tag{23}$$

according to Geodesy[18]. Using Eq. (23), we can write

$$\frac{dR}{ds} = \sqrt{\left(\mu\frac{d\phi}{ds}\right)^2 + \left(v\cos\phi\frac{d\lambda}{ds}\right)^2}$$

$$= \cos\theta\sqrt{\left(\frac{\mu}{\mu-r}\cos\alpha\right)^2 + \left(\frac{v}{v-r}\sin\alpha\right)^2} \qquad (24)$$

where use was made of Eqs. (1) and (2). Now we complete the derivation. We can see from this equation that when $r=\theta=0$ (i.e., a ray is restricted at the sea surface,) $dR=ds$. This means that the range equals to the path length in this particular case.

VI. APPENDIX 2: PARAMETERS OF HEARD-TO-ASCENSION RAYS

Listed as follows are all the rays that satisfied the error tolerance: 0.000005° for the latitude at the receiver, and 0.005° for the longitude at the receiver. In all of our shooting processes, the error tolerance for the ending longitude is also set to 0.000005°, but none of the rays satisfied this error tolerance, due to chaos. Instead, we list those rays that are closest to eigenrays. In the following, LA represents launch grazing angle. Ray number in the first column means the number of shooting in searching for an eigenray.

Table 10 Rays between Heard Island and Ascension Island

LA=0

	Time, sec	Range,km	Longitude	Depth	Error L	Error D
Ray 1	6258.395	9222.779	-14.42369	0.8735	0.0037	0.0415
Ray 2	6258.037	9222.246	-14.4158	0.9369	0.0042	0.1049

LA=0.25

	Time, sec	Range,km	Longitude	Depth	Error L	Error D
Ray 1	6257.977	9222.315	-14.4168	0.7847	0.0032	0.0473
Ray 2	6258.009	9222.362	-14.4175	0.71613	0.0025	0.1159
Ray 3	6257.943	9222.273	-14.4162	0.87732	0.0038	0.0453
Ray 4	6258.237	9222.73	-14.423	0.88307	0.003	0.051
Ray 5	6257.937	9222.288	-14.4164	0.91303	0.0036	0.081
Ray 6	6257.933	9222.333	-14.41704	1.003	0.003	0.171

	Time, sec	Range,km	Longitude	Depth	Error L	Error D
Ray 7	6258.134	9222.579	-14.4207	0.7939	0.0007	0.0381
Ray 8	6258.295	9222.81	-14.42416	0.8364	0.0042	0.0044

LA=0.5

	Time, sec	Range,km	Longitude	Depth	Error L	Error D
Ray 1	6257.977	9222.457	-14.4186	0.7903	0.0014	0.042
Ray 2	6258.247	9222.778	-14.4233	0.8953	0.0033	0.0633
Ray 3	6258.132	9222.607	-14.4208	0.8353	0.0008	0.0033
Ray 4	6258.206	9222.845	-14.4243	0.8849	0.0043	0.0329

LA=0.75

	Time, sec	Range,km	Longitude	Depth	Error L	Error D
Ray 1	6258.253	9222.9	-14.42496	0.7156	0.005	0.117

LA=1.0

	Time, sec	Range,km	Longitude	Depth	Error L	Error D
Ray 1	None					

LA=1.25

	Time, sec	Range,km	Longitude	Depth	Error L	Error D
Ray 1	None					

LA=1.5

	Time, sec	Range,km	Longitude	Depth	Error L	Error D
Ray 1	6258.049	9222.572	-14.42036	0.73701	0.0004	0.095
Ray 2	6257.886	9222.454	-14.41854	0.9512	0.0015	0.119

LA=1.75

	Time, sec	Range,km	Longitude	Depth	Error L	Error D
Ray 1	6258.167	9222.704	-14.42228	0.78168	0.0023	0.05

LA=2.0

	Time, sec	Range,km	Longitude	Depth	Error L	Error D
Ray 1	6256.658	9222.659	-14.42382	0.9905	0.0038	0.158

LA=2.25

	Time, sec	Range,km	Longitude	Depth	Error L	Error D
Ray 1	6258.186	9222.722	-14.4228	0.76028	0.0028	0.072
Ray 2	6258. 103	9222.659	-14.42199	0.63804	0.002	0.194
Ray 3	6258.133	9222.745	-14.4232	0.74994	0.0032	0.082

LA=2.5

	Time, sec	Range,km	Longitude	Depth	Error L	Error D
Ray 1	6258.229	9222.732	-14.42369	0.87021	0.0037	0.068
Ray 2	6258.112	9222.578	-14.42142	0.97489	0.0014	0.142
Ray 3	6258.207	9222.655	-14.42257	0.95438	0.0026	0.122
Ray 4	6258.134	9222.548	-14.4209	0.91541	0.0009	0.083

LA=2.75

	Time, sec	Range,km	Longitude	Depth	Error L	Error D
Ray 1	None					

LA=3

	Time, sec	Range,km	Longitude	Depth	Error L	Error D
Ray 1	6257.617	9222.487	-14.41976	1.0447	0.0002	0.213
Ray 2	6257.47	9222.271	-14.41661	0.68636	0.0034	0.146
Ray 3	6257.422	9222.258	-14.41636	0.88974	0.0036	0.058
Ray 4	6257.751	9222.751	-14.42381	0.95369	0.0038	0.121

LA=3.25

	Time, sec	Range,km	Longitude	Depth	Error L	Error D
Ray 1	6257.677	9222.538	-14.4209	0.78817	0.0009	0.044

LA=3.5

	Time, sec	Range,km	Longitude	Depth	Error L	Error D
Ray 1	6257.29	9222.512	-14.42021	0.7316	0.0002	0.1

LA=3.75

	Time, sec	Range,km	Longitude	Depth	Error L	Error D
Ray 1	6257.188	9222.652	-14.42245	1.04295	0.0025	0.211
Ray 2	6257.161	9222.576	-14.42111	0.77277	0.0011	0.0592
Ray 3	6256.941	9222.322	-14.41738	1.01895	0.0026	0.187
Ray 4	6256.944	9222.278	-14.41665	0.847133	0.0033	0.015
Ray 5	6257.181	9222.633	-14.4219	0.78541	0.0019	0.0466
Ray 6	6256.957	9222.297	-14.41696	1.0246	0.003	0.192
Ray 7	6256.39	9222.235	-14.4159	1.0387	0.0041	0.206

LA=4.0

	Time, sec	Range,km	Longitude	Depth	Error L	Error D
Ray 1	6256.422	9222.495	-14.4198	1.17785	0.0002	0.345
Ray 2	6257.001	9222.795	-14.42438	0.79234	0.0044	0.0397
Ray 3	6256.943	9222.635	-14.42194	0.909162	0.0019	0.077
Ray 4	6257.036	9222.799	-14.42423	0.93649	0.0042	0.104
Ray 5	6256.694	9222.661	-14.42233	1.121903	0.0023	0.289
Ray 6	6257.053	9222.758	-14.42383	0.86011	0.0038	0.028
Ray 7	6256.991	9222.77	-14.42402	0.998634	0.004	0.166
Ray 8	6257.064	9222.833	-14.42487	0.85878	0.0049	0.026
Ray 9	6256.634	9222.229	-14.41592	0.58457	0.0041	0.2474

LA=4.25

	Time, sec	Range,km	Longitude	Depth	Error L	Error D
Ray 1	6256.681	9222.634	-14.42275	0.60981	0.0028	0.2222
Ray 2	6256.689	9222.694	-14.42352	0.64245	0.0035	0.1895
Ray 3	6256.326	9222.191	-14.41615	1.056633	0.0037	0.255
Ray 4	6256.656	9222.596	-14.42209	1.02702	0.0021	0.195
Ray 5	6256.644	9222.647	-14.42282	1.051741	0.0028	0.22
Ray 6	6256.45	9222.293	-14.41775	0.737135	0.0022	0.095

LA=4.5

	Time, sec	Range,km	Longitude	Depth	Error L	Error D
Ray 1	6256.187	9222.309	-14.41754	1.08604	0.0025	0.254
Ray 2	6256.319	9222.363	-14.41834	0.70026	0.0017	0.132
Ray 3	6256.442	9222.548	-14.42109	0.592678	0.0011	0.2393
Ray 4	6256.297	9222.532	-14.42084	1.09902	0.0008	0.267

LA=4.75

	Time, sec	Range,km	Longitude	Depth	Error L	Error D
Ray 1	6255.593	9222.382	-14.41888	0.61118	0.0011	0.221
Ray 2	6255.393	9222.326	-14.41805	1.139497	0.0019	0.307

LA=5.0

	Time, sec	Range,km	Longitude	Depth	Error L	Error D
Ray 1	6254.874	9222.272	-14.41788	0.55961	0.0021	0.2724
Ray 2	6254.285	9222.427	-14.42019	0.580166	0.0002	0.2518
Ray 3	6254.951	9222.304	-14.41842	1.08	0.0016	0.248

LA=5.25

	Time, sec	Range,km	Longitude	Depth	Error L	Error D
Ray 1	6254.642	9222.281	-14.418	1.104011	0.002	0.272
Ray 2	6254.562	9222.159	-14.41618	1.07074	0.0038	0.238
Ray 3	6254.913	9222.703	-14.42427	0.78058	0.0057	0.0515
Ray 4	6254.773	9222.478	-14.42093	1.0377	0.0009	0.206
Ray 5	6254.726	9222.408	-14.41988	1.06278	0.0001	0.231
Ray 6	6254.837	9222.57	-14.4223	1.10143	0.0023	0.269
Ray 7	6254.614	9222.243	-14.41744	1.107318	0.0026	0.275
Ray 8	6254.345	9222.276	-14.41789	1.08102	0.0021	0.249
Ray 9	6254.913	9222.705	-14.4243	0.7351	0.0043	0.097

LA=5.5

	Time, sec	Range,km	Longitude	Depth	Error L	Error D
Ray 1	6254.196	9222.703	-14.42417	0.52629	0.0042	0.3057
Ray 2	6253.877	9222.713	-14.42433	1.02665	0.0043	0.195

LA=5.75

	Time, sec	Range,km	Longitude	Depth	Error L	Error D
Ray 1	6253.957	9222.536	-14.42137	0.5542	0.0014	0.2778
Ray 2	6253.664	9222.097	-14.41487	0.52161	0.0051	0.3104

LA=6

	Time, sec	Range,km	Longitude	Depth	Error L	Error D
Ray 1	6253.081	9222.339	-14.41889	0.80671	0.0011	0.0253
Ray 2	6253.337	9222.68	-14.42396	1.1262	0.004	0.2942
Ray 3	6253.519	9222.35	-14.41907	0.5876	0.0009	0.2444
Ray 4	6253.042	9222.183	-14.41658	0.48903	0.0034	0.343
Ray 5	6253.03	9222.226	-14.41723	1.21112	0.0028	0.379
Ray 6	6253.275	9222.637	-14.42331	0.724091	0.0033	0.108
Ray 7	6253.602	9222.521	-14.42162	1.149474	0.0016	0.318

LA=6.25

	Time, sec	Range,km	Longitude	Depth	Error L	Error D
Ray 1	6252.964	9222.616	-14.42282	0.5053	0.0028	0.3267
Ray 2	6252.887	9222.67	-14.42358	1.15308	0.0036	0.321
Ray 3	6252.896	9222.542	-14.42167	0.8374	0.0017	0.005
Ray 4	6252.709	9222.238	-14.41717	0.5074	0.0028	0.475
Ray 5	6252.679	9222.192	-14.41648	0.5059	0.0035	0.3261
Ray 6	6252.87	9222.581	-14.42224	0.6338	0.0022	0.1982
Ray 7	6252.84	9222.542	-14.42167	0.5433	0.0017	0.2887
Ray 8	6252.798	9222.546	-14.42174	1.21896	0.0017	0.387
Ray 9	6252.867	9222.511	-14.42119	0.9311	0.0012	0.099
Ray 10	6252.772	9222.507	-14.42116	1.24002	0.0012	0.408
Ray 11	6252.775	9222.509	-14.42119	1.2023	0.0012	0.37
Ray 12	6252.864	9222.511	-14.42122	1.002	0.0012	0.17
Ray 13	6252.784	9222.523	-14.4214	1.19422	0.0014	0.362
Ray 14	6252.734	9222.45	-14.42032	1.2588	0.0003	0.426
Ray 15	6252.744	9222.469	-14.42059	1.2552	0.0006	0.423

	Time, sec	Range,km	Longitude	Depth	Error L	Error D
Ray 16	6252.847	9222.6	-14.42254	0.97922	0.0025	0.147
Ray 17	6252.914	9222.562	-14.42197	0.7599	0.002	0.072
Ray 18	6252.643	9222.33	-14.41852	1.0008	0.0015	0.169
Ray 19	6252.688	9222.207	-14.4167	0.48022	0.0033	0.352
Ray 20	6252.881	9222.565	-14.42202	0.99737	0.002	0.165

LA=6.5

	Time, sec	Range,km	Longitude	Depth	Error L	Error D
Ray 1	6252.548	9222.518	-14.4214	1.12819	0.0014	0.296
Ray 2	6252.507	9222.262	-14.41753	0.8693	0.0025	0.037
Ray 3	6252.413	9222.315	-14.41839	1.0823	0.0016	0.25
Ray 4	6252.465	9222.385	-14.4194	1.0251	0.0006	0.193
Ray 5	6252.394	9222.291	-14.41805	1.14342	0.002	0.311
Ray 6	6252.749	9222.615	-14.42284	0.84029	0.0028	0.008
Ray 7	6252.526	9222.415	-14.4199	0.71432	0.0001	0.118
Ray 8	6252.388	9222.281	-14.41788	1.150145	0.0021	0.318
Ray 9	6252.413	9222.279	-14.4179	0.71312	0.0021	0.119
Ray 10	6252.886	9222.827	-14.42597	0.81557	0.006	0.016
Ray 11	6252.388	9222.281	-14.4179	1.1398	0.0021	0.3078
Ray 12	6252.737	9222.595	-14.42254	0.93785	0.0025	0.1059
Ray 13	6252.785	9222.669	-14.42363	0.8986	0.0036	0.067
Ray 14	6252.537	9222.498	-14.4211	1.13578	0.0011	0.304
Ray 15	6252.628	9222.527	-14.42154	1.21604	0.0015	0.384
Ray 16	6252.438	9222.21	-14.41683	0.76615	0.0032	0.0659
Ray 17	6252.423	9222.331	-14.41863	1.147514	0.0014	0.3155
Ray 18	6252.426	9222.168	-14.4162	0.4817	0.0038	0.35
Ray 19	6252.444	9222.198	-14.41666	0.48346	0.0033	0.349
Ray 20	6252.575	9222.556	-14.42196	1.13611	0.002	0.304
Ray 21	6252.361	9222.239	-14.4173	1.1558	0.0027	0.324
Ray 22	6252.328	9222.19	-14.41654	1.155	0.0035	0.323
Ray 23	6252.823	9222.75	-14.42482	0.621658	0.0048	0.21
Ray 24	6252.399	9222.255	-14.4175	0.69784	0.0025	0.135
Ray 25	6252.476	9222.243	-14.41732	0.4991	0.0027	0.3329

LA=6.75

	Time, sec	Range,km	Longitude	Depth	Error L	Error D
Ray 1	6251.375	9222.557	-14.42277	0.50002	0.0028	0.332
Ray 2	6251.428	9222.64	-14.42401	0.54858	0.004	0.284
Ray 3	6251.368	9222.69	-14.42473	0.7102	0.0047	0.122
Ray 4	6251.411	9222.084	-14.4156	1.27591	0.0044	0.444

LA=7.0

	Time, sec	Range,km	Longitude	Depth	Error L	Error D
Ray 1	6251.743	9222.486	-14.42115	0.50763	0.0012	0.324
Ray 2	6251.832	9222.561	-14.42223	1.2396	0.0022	0.408
Ray 3	6251.778	9222.489	-14.42117	1.08045	0.0012	0.248
Ray 4	6250.889	9222.18	-14.41653	1.28603	0.0035	0.454
Ray 5	6251.528	9222.16	-14.41628	0.61481	0.0037	0.218
Ray 6	6251.651	9222.334	-14.41887	0.716851	0.0011	0.115
Ray 7	6251.54	9222.167	-14.41639	0.7345	0.0036	0.097

LA=7.25

	Time, sec	Range,km	Longitude	Depth	Error L	Error D
Ray 1	None					

LA=7.5

	Time, sec	Range,km	Longitude	Depth	Error L	Error D
Ray 1	6249.89	9222.313	-14.41902	0.74816	0.001	0.084
Ray 2	6249.765	9222.122	-14.4162	0.747638	0.0038	0.085
Ray 3	6249.882	9222.68	-14.42448	1.32519	0.0045	0.493

LA=7.75

	Time, sec	Range,km	Longitude	Depth	Error L	Error D
Ray 1	6248.067	9222.077	-14.4166	1.3533	0.0034	0.521
Ray 2	6248.293	9222.409	-14.42157	1.375	0.0016	0.543
Ray 3	6248.37	9222.529	-14.42337	1.39542	0.0034	0.563
Ray 4	6248.164	9222.218	-14.41873	1.3583	0.0013	0.526
Ray 5	6248.136	9222.18	-14.41816	1.342	0.0018	0.510
Ray 6	6248.139	9222.179	-14.4182	1.3556	0.0018	0.523
Ray 7	6248.085	9222.106	-14.41708	1.3685	0.0029	0.537
Ray 8	6248.258	9222.363	-14.4209	1.3529	0.0009	0.521
Ray 9	6248.174	9222.235	-14.419	1.3452	0.001	0.513
Ray 10	6248.221	9222.306	-14.42	1.3432	0	0.511
Ray 11	6248.439	9222.629	-14.4249	1.403	0.0049	0.571
Ray 12	6248.463	9222.567	-14.42391	0.453485	0.0039	0.3786
Ray 13	6248.426	9222.517	-14.42316	0.3485	0.0032	0.4835
Ray 14	6248.084	9222.1	-14.41698	1.3683	0.003	0.5363

LA =8

	Time, sec	Range,km	Longitude	Depth	Error L	Error D

None

LA=8.25

	Time, sec	Range,km	Longitude	Depth	Error L	Error D
Ray 1	6246.175	9222.508	-14.42265	1.58583	0.0027	0.753
Ray 2	6245.862	9222.127	-14.41697	0.70018	0.003	0.617
Ray 3	6246.015	9222.266	-14.41904	1.622	0.001	0.790
Ray 4	6246.244	9222.604	-14.4241	1.43566	0.0041	0.603
Ray 5	6246.084	9222.369	-14.4206	1.55543	0.0006	0.723
Ray 6	6246.024	9222.277	-14.41923	1.5777	0.0008	0.746
Ray 7	6246.111	9222.412	-14.4212	1.5058	0.0012	0.674
Ray 8	6246.041	9222.308	-14.4197	1.6314	0.0003	0.799
Ray 9	6246.049	9222.317	-14.4198	1.57712	0.0002	0.745
Ray 10	6246.174	9222.502	-14.4226	1.45562	0.0026	0.624
Ray 11	6246.123	9222.426	-14.42143	1.51594	0.0014	0.683
Ray 12	6246.11	9222.412	-14.4212	1.5961	0.0012	0.764
Ray 13	6246.087	9222.373	-14.42063	1.53499	0.0006	0.703
Ray 14	6246.185	9222.519	-14.42281	1.4707	0.0028	0.139
Ray 15	6246.039	9222.414	-14.42125	0.4763	0.0013	0.356
Ray 16	6246.142	9222.457	-14.4219	1.541	0.0019	0.709
Ray 17	6246.047	9222.314	-14.4198	1.6017	0.0002	0.769
Ray 18	6246.144	9222.458	-14.4219	1.45795	0.0019	0.626
Ray 19	6246.042	9222.307	-14.4197	1.5738	0.0003	0.741
Ray 20	6246.028	9222.288	-14.4194	1.6417	0.0006	0.809
Ray 21	6245.885	9222.275	-14.41919	1.05125	0.0008	0.219
Ray 22	6246.066	9222.349	-14.42028	1.6324	0.0003	0.8
Ray 23	6246.113	9222.411	-14.42121	1.5148	0.0012	0.683
Ray 24	6246.03	9222.287	-14.41938	1.5868	0.0006	0.755
Ray 25	6246.072	9222.433	-14.4215	0.740505	0.0015	0.091
Ray 26	6246.071	9222.349	-14.4203	1.5857	0.0003	0.753
Ray 27	6246.146	9222.462	-14.422	1.4553	0.002	0.623
Ray 28	6246.168	9222.496	-14.4225	1.5754	0.0025	0.743

	Time, sec	Range,km	Longitude	Depth	Error L	Error D
Ray 29	6246.08	9222.364	-14.4205	1.4971	0.0005	0.665
Ray 30	6246.068	9222.348	-14.42027	1.61637	0.0003	0.784
Ray 31	6246.154	9222.473	-14.42214	1.46983	0.0021	0.638
Ray 32	6246.173	9222.503	-14.4226	1.4536	0.0026	0.622
Ray 33	6245.801	9222.18	-14.4178	1.322	0.0022	0.49
Ray 34	6245.738	9222.084	-14.4164	1.3297	0.0036	0.498

LA=8.5

	Time, sec	Range,km	Longitude	Depth	Error L	Error D
Ray 1	6244.726	9222.037	-14.41604	1.75247	0.004	0.920
Ray 2	6244.834	9222.196	-14.4184	1.74041	0.0016	0.908
Ray 3	6244.935	9222.349	-14.42069	1.7427	0.0007	0.911
Ray 4	6244.722	9222.031	-14.41596	1.73772	0.004	0.906
Ray 5	6244.828	9222.188	-14.4183	1.7366	0.0017	0.906
Ray 6	6245.037	9222.497	-14.4229	1.7429	0.0029	0.911
Ray 7	6244.82	9222.179	-14.41816	1.737	0.0018	0.905
Ray 8	6244.763	9222.093	-14.41688	1.73196	0.0031	0.9
Ray 9	6244.782	9222.118	-14.41726	1.7593	0.0027	0.928
Ray 10	6244.926	9222.336	-14.4205	1.74	0.0005	0.908
Ray 11	6245.005	9222.449	-14.42217	1.74205	0.0022	0.910
Ray 12	6244.86	9222.235	-14.419	1.73653	0.001	0.905
Ray 13	6244.763	9222.095	-14.4169	1.7399	0.0031	0.907
Ray 14	6244.774	9222.107	-14.41709	1.7518	0.0029	0.920
Ray 15	6244.794	9222.136	-14.41752	1.7382	0.0025	0.906
Ray 16	6244.774	9222.106	-14.41708	1.7362	0.0029	0.904
Ray 17	6244.947	9222.362	-14.4209	1.74075	0.0009	0.909
Ray 18	6244.99	9222.431	-14.42191	1.7452	0.0019	0.913
Ray 19	6244.981	9222.419	-14.42173	1.7433	0.0017	0.911
Ray 20	6244.771	9222.102	-14.417	1.7339	0.003	0.902
Ray 21	6244.804	9222.152	-14.4178	1.76324	0.0022	0.931
Ray 22	6244.77	9222.102	-14.41701	1.7416	0.003	0.910
Ray 23	6244.96	9222.384	-14.42121	1.7384	0.0012	0.906
Ray 24	6244.697	9221.988	-14.41532	1.7467	0.0047	0.915
Ray 25	6244.82	9222.175	-14.41811	1.7347	0.0019	0.903
Ray 26	6244.812	9222.164	-14.41795	1.7312	0.002	0.899
Ray 27	6244.877	9222.258	-14.41932	1.74013	0.0007	0.908
Ray 28	6244.724	9222.032	-14.41598	1.7353	0.004	0.903
Ray 29	6244.964	9222.389	-14.4213	1.74772	0.0013	0.916
Ray 30	6244.724	9222.032	-14.41598	1.7353	0.004	0.903

LA=8.75

	Time, sec	Range,km	Longitude	Depth	Error L	Error D
Ray 1	6244.073	9222.321	-14.42028	1.6431	0.0003	0.811
Ray 2	6244.079	9222.326	-14.42036	1.6312	0.0004	0.799
Ray 3	6244.072	9222.309	-14.4201	1.4702	0.0001	0.638
Ray 4	6244.064	9222.302	-14.41999	1.667	0	0.835

LA=9.0

	Time, sec	Range,km	Longitude	Depth	Error L	Error D
Ray 1	6244.828	9222.26	-14.41909	1.56	0.0009	0.728
Ray 2	6244.977	9222.455	-14.42205	1.602	0.002	0.770
Ray 3	6244.796	9222.191	-14.4181	1.56557	0.0019	0.734
Ray 4	6244.972	9222.453	-14.42201	1.59571	0.002	0.764
Ray 5	6244.899	9222.338	-14.4203	1.59307	0.0003	0.761
Ray 6	6244.973	9222.466	-14.4222	1.2741	0.0022	0.442

LA=9.25

	Time, sec	Range,km	Longitude	Depth	Error L	Error D
Ray 1	none					

LA=9.5

	Time, sec	Range,km	Longitude	Depth	Error L	Error D
Ray 1	6241.44	9222.008	-14.41572	1.25978	0.0043	0.428
Ray 2	6241.725	9222.445	-14.42222	1.43979	0.0022	0.608
Ray 3	6241.823	9222.59	-14.42438	1.389362	0.0044	0.557
Ray 4	6241.737	9222.46	-14.42243	1.3751	0.0024	0.543
Ray 5	6241.667	9222.352	-14.4208	1.3754	0.0008	0.543
Ray 6	6241.679	9222.377	-14.42119	1.4106	0.0012	0.579
Ray 7	6241.801	9222.551	-14.42381	1.3441	0.0038	0.512

LA=9.75

	Time, sec	Range,km	Longitude	Depth	Error L	Error D
Ray 1	6240.401	9222.261	-14.4199	0.7692	0.0001	0.063
Ray 2	6240.45	9222.283	-14.42025	0.42419	0.0003	0.408
Ray 3	6240.404	9222.283	-14.42026	0.8805	0.0003	0.048
Ray 4	6240.377	9222.249	-14.41975	0.9078	0.0002	0.076
Ray 5	6240.453	9222.292	-14.42037	0.3653	0.0004	0.467
Ray 6	6240.442	9222.293	-14.4204	0.5638	0.0004	0.268
Ray 7	6240.432	9222.278	-14.4202	0.5646	0.0002	0.268
Ray 8	6240.42	9222.304	-14.4206	0.8649	0.0006	0.033

LA=10

	Time, sec	Range,km	Longitude	Depth	Error L	Error D
Ray 1	6237.277	9222.271	-14.42022	1.7324	0.0002	0.900
Ray 2	6237.295	9222.113	-14.4179	0.3	0.0021	0.532
Ray 3	6237.255	9222.033	-14.4167	0.507	0.0033	0.325
Ray 4	6237.266	9222.271	-14.42022	1.9642	0.0002	1.132

LA=10.5

	Time, sec	Range,km	Longitude	Depth	Error L	Error D
Ray 1	6233.845	9221.917	-14.416	1.7913	0.004	0.959
Ray 2	6233.964	9222.085	-14.4185	1.9243	0.0015	1.092
Ray 3	6233.942	9222.048	-14.418	1.9368	0.002	1.105
Ray 4	6234.008	9222.157	-14.41963	1.9401	0.0004	1.108
Ray 5	6234.019	9222.173	-14.4199	1.9433	0.0001	1.111
Ray 6	6234.07	9222.248	-14.42099	1.9365	0.001	1.105
Ray 7	6233.836	9221.903	-14.4158	1.8368	0.0042	1.005
Ray 8	6234.129	9222.334	-14.4223	1.943	0.0023	1.111
Ray 9	6233.841	9221.909	-14.41593	1.8249	0.0041	0.993
Ray 10	6234.18	9222.409	-14.42338	1.98242	0.0034	1.150
Ray 11	6233.997	9222.138	-14.4193	1.8938	0.0007	1.062
Ray 12	6233.9	9221.994	-14.4172	1.8747	0.0028	1.043
Ray 13	6234.193	9222.425	-14.42363	2.0105	0.0036	1.179
Ray 14	6234.081	9222.261	-14.42118	1.96827	0.0012	1.136
Ray 15	6234.218	9222.464	-14.4242	1.9966	0.0042	1,165
Ray 16	6234.201	9222.439	-14.42384	1.9921	0.0038	1.16
Ray 17	6234.105	9222.3	-14.42176	1.9741	0.0018	1.142
Ray 18	6234.292	9222.571	-14.42578	2.0119	0.0058	1.180
Ray 19	6234.053	9222.219	-14.4205	1.9425	0.0005	1.11
Ray 20	6234.09	9222.272	-14.42135	1.9652	0.0014	1.133
Ray 21	6234.063	9222.234	-14.42078	1.9165	0.0008	1.084
Ray 22	6234.114	9222.307	-14.42186	1.9639	0.0019	1.132

	Time, sec	Range, km	Longitude	Depth	Error L	Error D
Ray 23	6233.962	9222.085	-14.41856	1.9067	0.0014	1.075
Ray 24	6233.853	9221.932	-14.41628	1.85032	0.0037	1.018

LA=11

	Time, sec	Range, km	Longitude	Depth	Error L	Error D
Ray 1	6233.935	9222.335	-14.4214	0.50716	0.0014	0.325
Ray 2	6233.763	9222.304	-14.4209	2.12911	0.0009	1.297
Ray 3	6234.186	9222.134	-14.4184	1.7626	0.0016	0.93
Ray 4	6234.174	9222.126	-14.4183	1.8266	0.0017	0.995
Ray 5	6233.623	9222.093	-14.4178	2.0576	0.0022	0.83
Ray 6	6233.575	9222.021	-14.4167	1.9942	0.0033	1.162
Ray 7	6234.252	9222.248	-14.4201	1.891	0.0001	1.059

VII. APPENDIX 3: LYAPUNOV EXPONENT DOES NOT QUANTIFY PREDICTABILITY

The main conclusion of Lorenz's paper [31] is that for some deterministic systems very long range forecasting is impossible. In his work, he also mentioned that "There remains the very important question as to how long is 'very long range'." To answer this question, Shaw [32] has computed an information parameter for Lorenz model. With this parameter, he made a prediction as to how long the information in a given initial condition will persist. His prediction was confirmed by an analog computer experiment. The information parameter he used is identical to Lyapunov exponent, as he mentioned in his paper. Therefore, Shaw's work implies that Lyapunov exponent quantifies the predictability of chaotic systems -- a very important concept.

This concept is accepted by many researchers,[33,34,35,36] and has been used to define a predictability horizon in ocean acoustics. However, there is not enough evidence to support this concept. In the published references 33,34,35,and 36 those researchers who believe that Lyapunov exponent quantifies predictability did not give any example to

show it in their specific cases. In fact, the only evidence we have found is the result of the analog computer experiment presented by Shaw [32].

Therefore, the objective of this appendix is to numerically test the correctness of that concept. Considering that Lyapunov exponent is an asymptotic value at very long range, but loss of predictability usually occurs at a short range, we have a question: Can Lyapunov exponent quantify predictability? In the following, we use Wolf et al.'s method [33] to compute Lyapunov exponents for Lorenz model. Then we use the Lyapunov exponents to make predictions as to how long the information in a given initial condition will persist. Finally, we conduct numerical experiments to test the correctness of this prediction.

We use Wolf et al.'s published computer code [33] to estimate Lyapunov exponents for the Lorenz model

$$
\begin{aligned}
\dot{X} &= \sigma(Y - X) \\
\dot{Y} &= X(R - Z) - Y. \\
\dot{Z} &= XY - bZ
\end{aligned}
\tag{25}
$$

We make a few revisions in this published FORTRAN program. First, we use FORTRAN's double precision. Second, we use Press et al.'s subroutine RK4 instead of the DEVERK in the published code. Third, we change the model parameters to what Lorenz and Shaw used.

In the following calculations, the model parameters are $\sigma = 10.0$, $R = 28.0$, $b = 8/3$, the same as that Lorenz[31] and Shaw[32] used. The initial conditions are $X(0) = 0.0$, $Y(0) = 1.0$, $Z(0) = 0.0$, according to Lorenz[31]. The step size is 0.001, the same as Shaw's, and 1,000,000 steps of integration are performed for each calculation. Numerical experiments are performed with a digit personal computer (486DX2, 66 MHz).

First we estimate Lyapunov exponents. With the method and parameters given in the previous paragraph, we get the largest Lyapunov exponent: $\lambda_1 = 1.30$ bits/sec.

Then let us make a prediction using the Lyapunov exponent. We perform two calculations. In the first calculation, we use initial conditions (0, 1, 0), and in the second calculation, we use (0.0001, 1, 0). The information value of $X(0)$ we set in this way is approximately 13 bits ($-\log_2 0.0001$). Thus, the time after which the initial data is lost, according to Shaw[32], is $t_p = 13$ bits/1.30 bits per second = 10 sec. Therefore, the prediction made with the Lyapunov exponent is: the system may become unpredictable at about 10 seconds. In the Lorenz model, time is dimensionless. We use "second" here as the unit of time to be in consistent with that used by Shaw.

Now, we depict the results of the two calculations in Fig. 23 to test the correctness of this prediction. In this figure, the solid line is the result of the first calculation, and the

dashed line represents the second calculation. If the prediction made with Lyapunov

exponent is correct, the two lines should diverge from each other at about 10 seconds, as

a result of losing 13 bits of initial data. However, the divergence did not occur until

about 29 seconds. This suggests that the relative error of the prediction made with the

Lyapunov exponent is (29-10)/29≈66%. It is too large to be accepted. Obviously,

Lyapunov exponent does not have predictive value and cannot be used to quantify

predictability.

Let us discuss why the Lyapunov exponent did not quantify the predictability in

this case. Fig. 24 gives the largest Lyapunov exponent we estimated for this particular

case. From this figure, we can see that at 29 seconds the value of the exponent is about

0.49 bits per second (Point A in Fig. 24). This means that before the system became

unpredictable the maximum rate of destroying information was actually 0.49 bits/sec.

However, the asymptotic value 1.30 bits/sec -- the Lyapunov exponent -- was used to

measure the predictability. This is why we could not make a correct prediction.

The objective of this appendix is to investigate whether Lyapunov exponent has

predictive value. This is done by performing numerical experiments with Lorenz model.

Our numerical results show clearly that Lyapunov exponent does not quantify the

predictability of a chaotic system.

paths should be stable, if the motion of the source ship can be ignored. When the acoustic signals were transmitted from the source ship, acoustic energy propagated to Ascension Island through these stable eigenray paths. Therefore, the received signals had phase stability.

As long as the source illuminated the eigenray paths, the signals received at Ascension Island have phase stability. This could always happen, because a source can transmit energy through a wide range of angles so that the launch angles of the eigenrays, although need to be specified with very high accuracy due to chaos, can always be satisfied. However, the source should have a transmitting directivity – it transmits the acoustic energy at different intensity in different directions. Therefore, a very slight motion of the source can cause significant amplitude variation of the received signals. Since the source was deployed in a vertical array through a ship[16], we can expect that during the transmissions the source moved slightly and stochastically due to the ocean wave. Therefore, the intensity of the energy transmitted through the eigenray paths might fluctuate stochastically during the transmissions. This in turn caused the amplitude variation of the received signals. This phenomenon might exhibit even if ray paths are not chaotic. However, chaos might enhance the amplitude variability. The reason is as follows. Chaotic ray paths are very sensitive to launch angles. Therefore, in the presence of chaos even a very small fluctuation in the axial direction of the source may cause large amplitude variation of received signals.

A main conclusion is: Lyapunov exponent is an asymptotic value at very long range, while initial data is lost at the early stage of the system's evolution. At the early stage, the actual rate at which a system destroys information may substantially differ from the value of the largest Lyapunov exponent. This is why Lyapunov exponent cannot be used to quantify predictability.

Recently, there have been some publications emphasizing Lyapunov exponent's role in quantifying predictability and this situation may continue. Therefore, it is necessary to present an illustrative counterexample in this paper, showing that Lyapunov exponent does not quantify predictability.

REFERENCES

[1] Moon, F. C., *Chaotic Vibrations, An Introduction for Scientists and Engineers* (Wiley, New York, 1987), p.4.

[2] Palmer, D. R., Brown, M. G., Tappert, F. D., and Bezdek, H. F., "Classical chaos in nonseparable wave propagation problems," *Geophys. Res. Lett.* **15**, 569-572 (1988).

[3] Abdullaev, S. S., and Zaslavskii. G. M., "Fractals and ray dynamics in a longitudinally inhomogeneous medium," **34**, 334-336 (1989).

[4] Tappert, F. D., Brown, M. G., and Goni, G., "Weak chaos in an area-preserving mapping for sound ray propagation," *Phys. Lett.* **A 153**, 181-185 (1991).

[5] Brown, M. G., Tappert, F. D., and Goni, G., "An investigation of sound ray dynamics in the ocean volume using an area preserve mapping," *Wave Motion* **14**, 93-99 (1991).

[6] Brown, M. G., Tappert, F. D., Goni, G., and Smith, K. B., "Chaos in underwater acoustics," in *Ocean Variability and Acoustic Propagation,* edited by J. Potter and A. Warn-Varnas (Kluwer Academic, Dordrecht), pp. 139-160 (1991).

[7] Smith, K. B., Brown, M. G., and Tappert, F. D., "Ray chaos in underwater acoustics," *J. Acoust. Soc. Am.* **91**, 1939-1949 (1992).

[8] Smith, K. B., Brown, M. G., and Tappert, F. D., "Acoustic ray chaos induced by mesoscale ocean structure," *J. Acoust. Soc. Am.* **91**, 1950-1959 (1992).

[9] Yan, J., "Ray chaos in underwater acoustics in view of local instability," *J. Acoust. Soc. Am.* **94**, 2739-2745 (1993).

[10] M. D. Collins, and W. A. Kuperman, "Overcoming ray chaos," J. Acoust. Soc. Am. **95**, 3167-3170 (1994).

[11] Tappert, F. D., and Tang, X., "Ray chaos and eigenrays," *J. Acoust. Soc. Am.* **99**, 185-195 (1996).

[12] Yan, J., and Yen, K. K., "A derivation of three-dimensional ray equations in ellipsoidal coordinates," *J. Acoust. Soc. Am.* **97**, 1538-1544 (1995).

[13] Munk, W. H., O'Reilly, W. C., and Reid, J. L., "Australia-Bermuda sound transmission experiment (1960) revisited," *J. Phys. Oceanogr.* **18**, 1876-1898 (1988).

[14] Yan, J., and Yen, K. K., "Chaos of underwater sound in long-range propagation," *Proceedings of the third conference on nonlinear dynamics (Chaos) and full spectrum processing,* July 10-14, 1995, Mystic, CT (In press).

[15] Baggeroer, A., and Munk, W., "The Heard Island feasibility test," *Physics Today* **Sept.**, 22-30 (1992).

[16] Munk, W. H., Spinder, R. C., Baggeroer, A., Birdsall, T. G., "Heard Island feasibility test," *J. Acoust. Soc. Am.* **96**, 2330-2342 (1994).

[17] Palmer, D. R., Georges, T. M., Wilson, J. J., Weiner, L. D., Paisley, J. A., Mathiesen, R., Pleshek, R. R., and Mabe, R. R., "Reception at Ascension of the Heard Island Feasibility Test transmissions," *J. Acoust. Soc. Am.* **96**, 2432-2440 (1994).

[18] Bomford, G., Geodesy (Oxford University Press, London, 1971), pp. 107-112, pp. 562-566.

[19] Press, W. H., Flannery, B. P., Teukolsky, S. A., and Vetterling, W. T., Numerical Recipes, The Art of Scientific Computing (Cambridge University Press, New York, 1988), pp. 226-228.

[20] Carnahan, B., Applied Numerical Methods (Wiley, New York, 1969), pp. 405-408.

[21] Wolf, A., Swift, J. B., Swinney, H. L., and Vastano, J. A., "Determining Lyapunov exponents from a time series," *Physica D* **16**, 285-317 (1985).

[22] Private communications with Peter Worcester at The Scripps Institution of Oceanography, University of California at San Diego.

[23] R. Shaw, "Strange attractors, chaotic behavior, and information flow," Z. Naturforsch, **36 a**, 80-112 (1981).

[24] Tappert, F., "The parabolic approximation method," *Lecture Notes in Physics, Vol. 70, Wave Propagation and Underwater Acoustics,* edited by J. B. Keller and J. S. Papadakis (Springer-Verlag, New York, 1977), pp. 224-287.

[25] Boylesm, C. A., *Acoustic Waveguides, Application to Oceanic Science* (Wiley, New York, 1984), pp. 263-269.

[26] Lee, O. S., *J. Acoust. Soc. Am.* **33**, 677-681 (1961).

[27]Baxter, L., and Orr, M. H., *J. Acoust. Soc. Am.* **71**, 61-65 (1982).

[28]Flatte, S. M., Dashen, R., Munk, W. H., Watson, K. M., Zachariasen, F., Sound Transmission through a fluctuating ocean (Cambridge University Press, Cambridge, 1979), pp. 44-47.

[29]Munk, W. H., Worcester, P., Wunsch, C., Ocean Acoustic Tomography, Cambridge University Press, New York, ch. 4, pp. 154-157.

[30]Robinson A. R., and Lee, D., *Oceanography and Acoustics, Prediction and Propagation Models*, AIP Press, New York, 1994, ch. 2, pp. 26-27.

[31]E. N. Lorenz, Deterministic nonperiodic flow, Journal of the Atmospheric Sciences **20**, 130 (1963).

[32]R. Shaw, Z. Naturforsch **36A**, 80 (1981).

[33]A. Wolf, J. B. Swift, H. L. Swinney, and J. A. Vastano, Physica D **16**, 285 (1985).

[34]K. B. Smith, M. G. Brown, and F. D. Tappert, J. Acoust. Soc. Am. **91**, 1939 (1992).

[35]K. B. Smith, M. G. Brown, and F. D. Tappert, J. Acoust. Soc. Am. **91**, 1950 (1992).

[36] L. A. Anosov, O. Ya. Butkovskii, Yu. A. Kravtsov, edited by R. A. Katz, Chaotic, Fractal, and Nonlinear Signal Processing (American Institute of Physics Press, New York, 1996) p. 71.

Graz=0.5

Graz=0.500000005
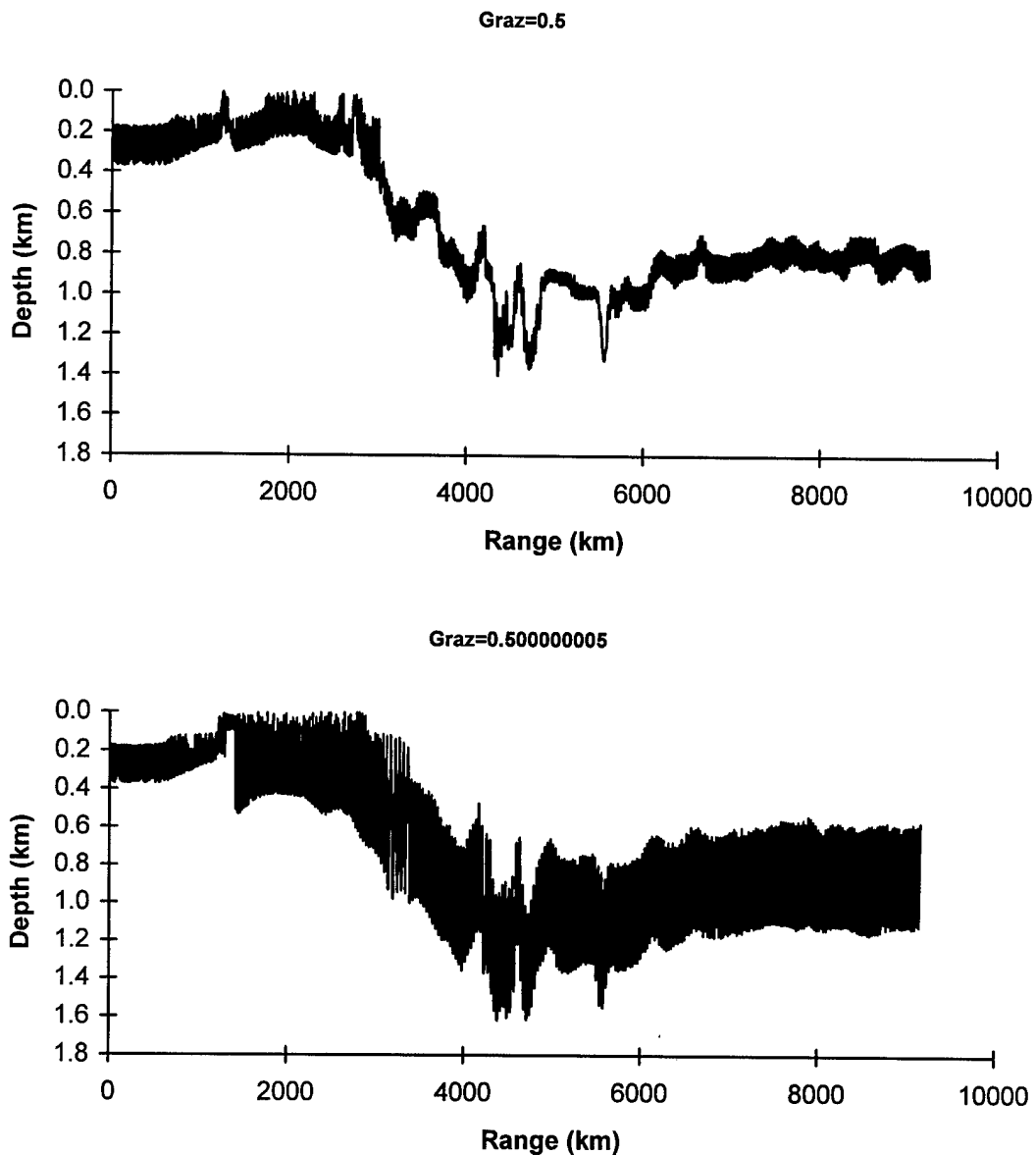
Fig.1 Extreme sensitive dependence on initial conditions
Upper: the vertical ray path of eigenray 1 with launch angles
$\alpha(0)=266.7258936017752°$ and $\theta(0)=0.5°$
Lower: the vertical ray path constructed using the same $\alpha(0)$
but $\theta(0)$ is perturbed by $0.000000005°$.
Such a small difference in $\theta(0)$ caused the ray path to change substantially.
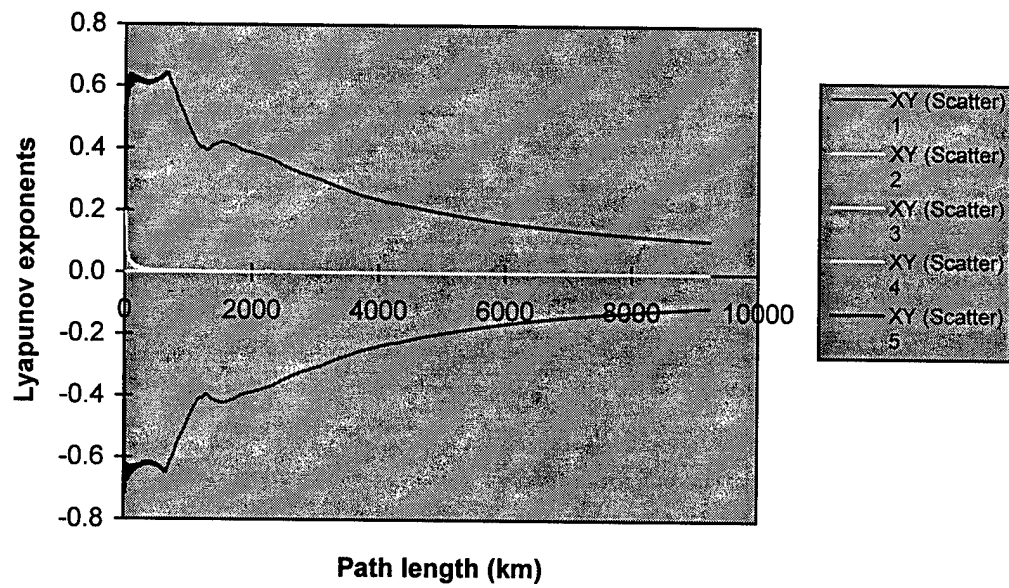
Fig.2 The Lyapunov exponents for eigenray 1.
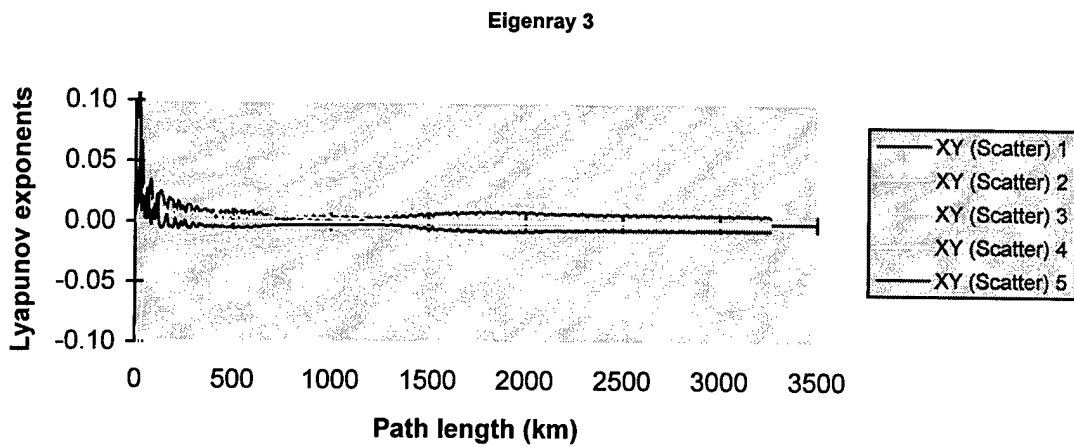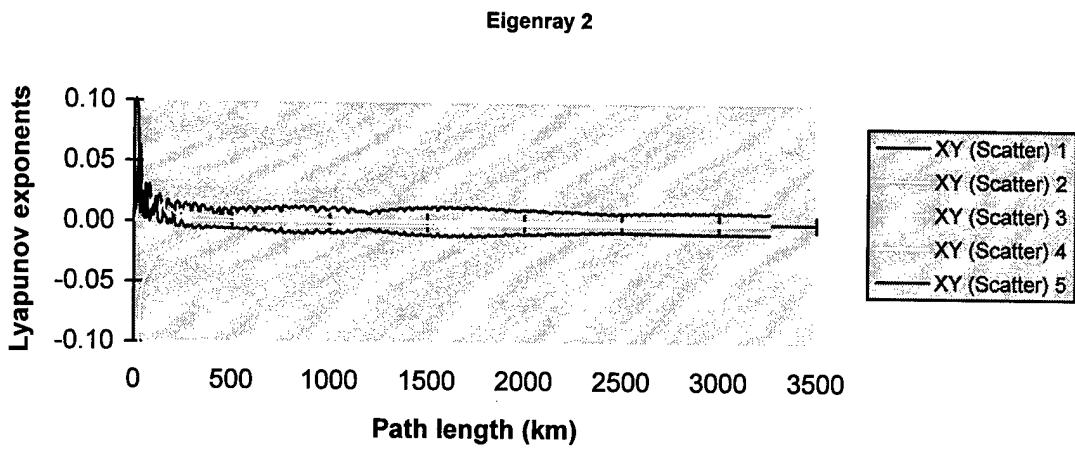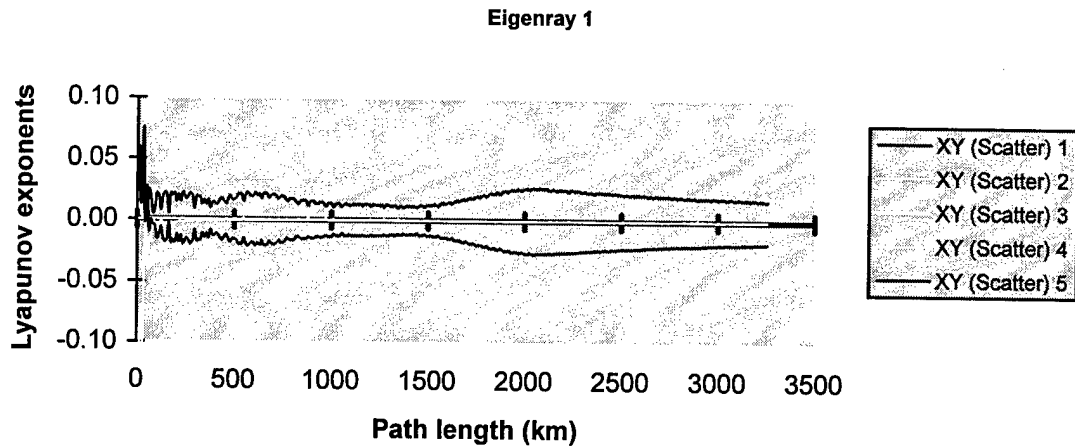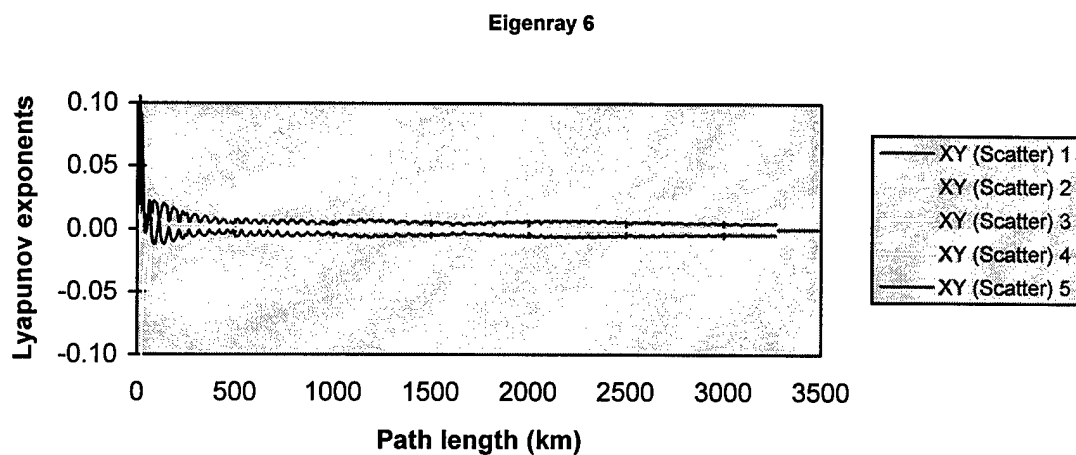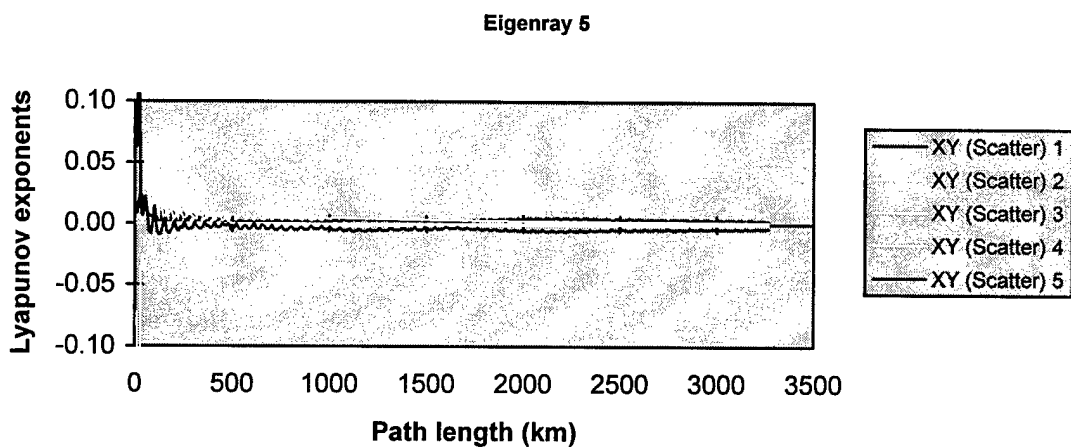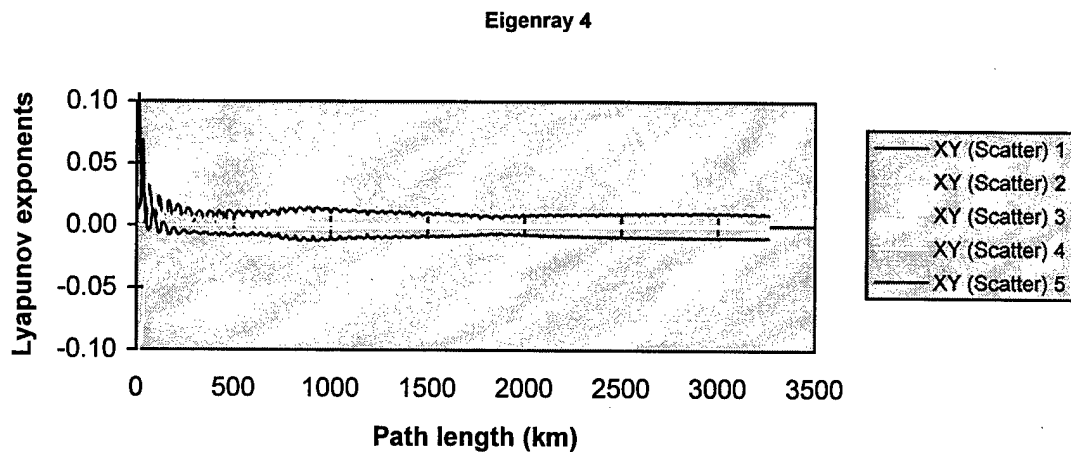
Eigenray 1

Eigenray 2

Eigenray 3

Fig. 3   Lyapunov exponents of eigenrays between California and Hawaii

Eigenray 4

Eigenray 5

Eigenray 6

Fig. 3   Lyapunov exponents of eigenrays between California and Hawaii (continue)

Eigenray 7

Eigenray 8

Eigenray 9

Fig. 3   Lyapunov exponents of eigenrays between California and Hawaii (continue)
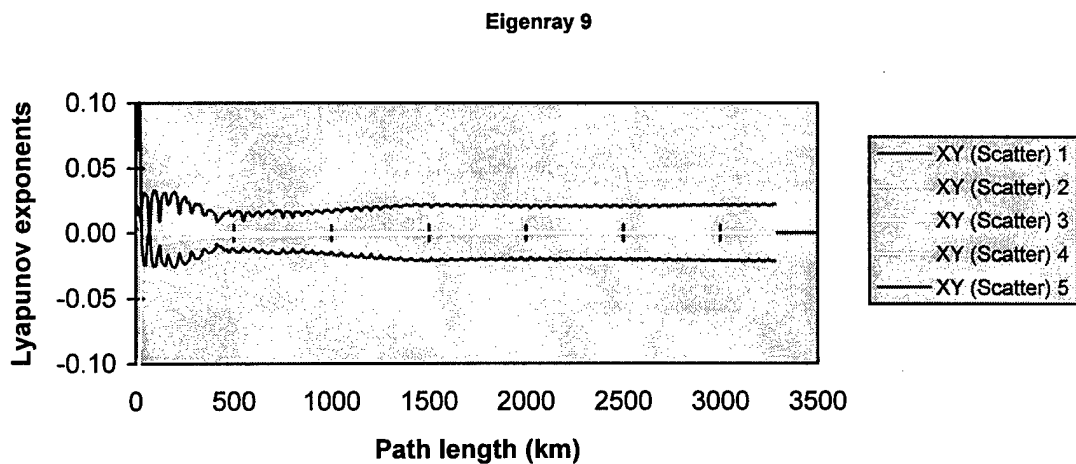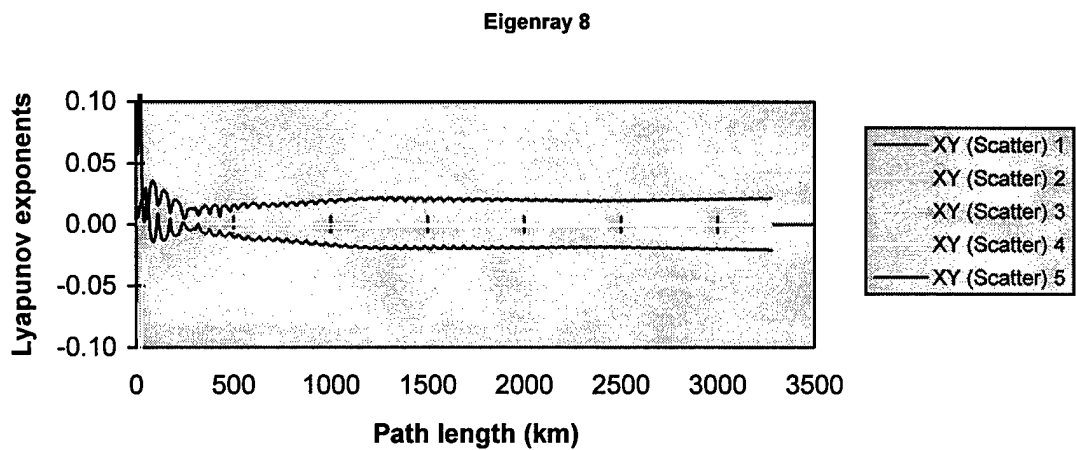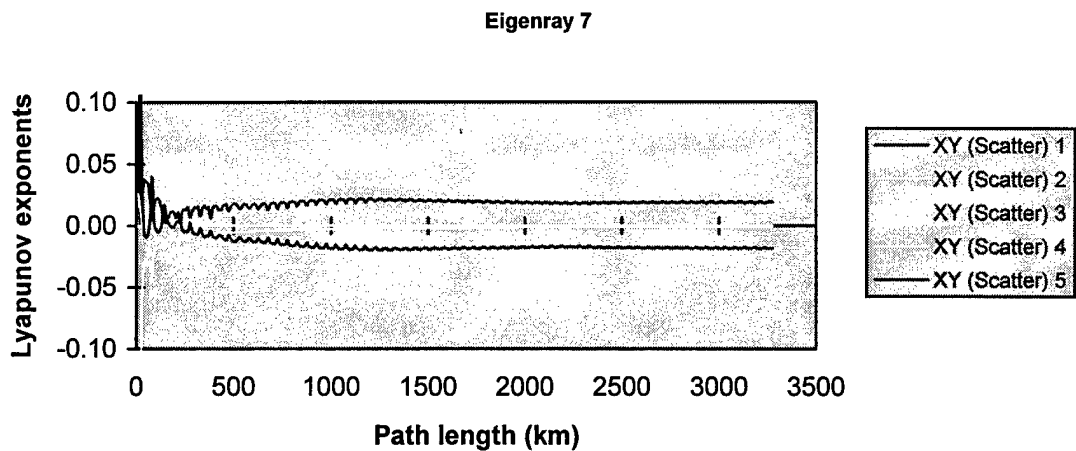
Power spectra of eigenray 1

Power spectra of eigenray 2

Power spectra of eigenray 3
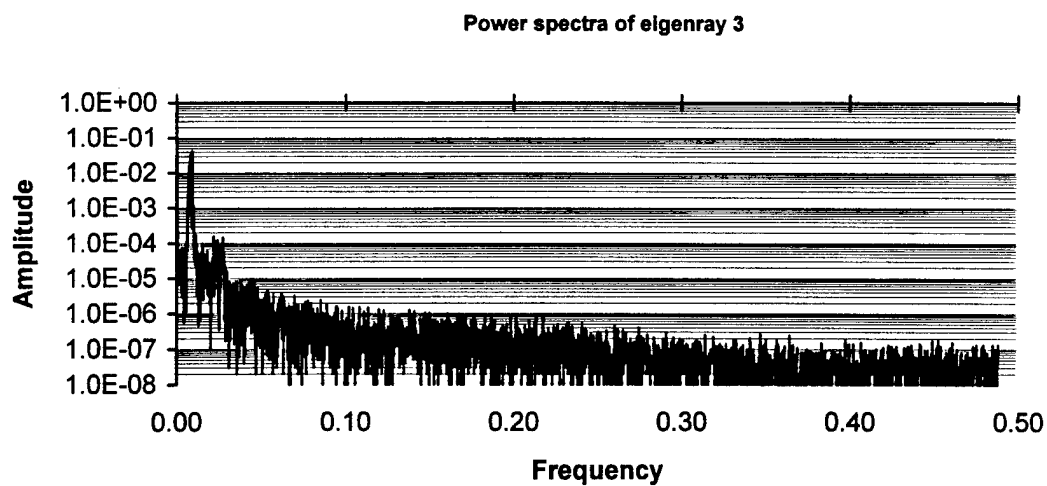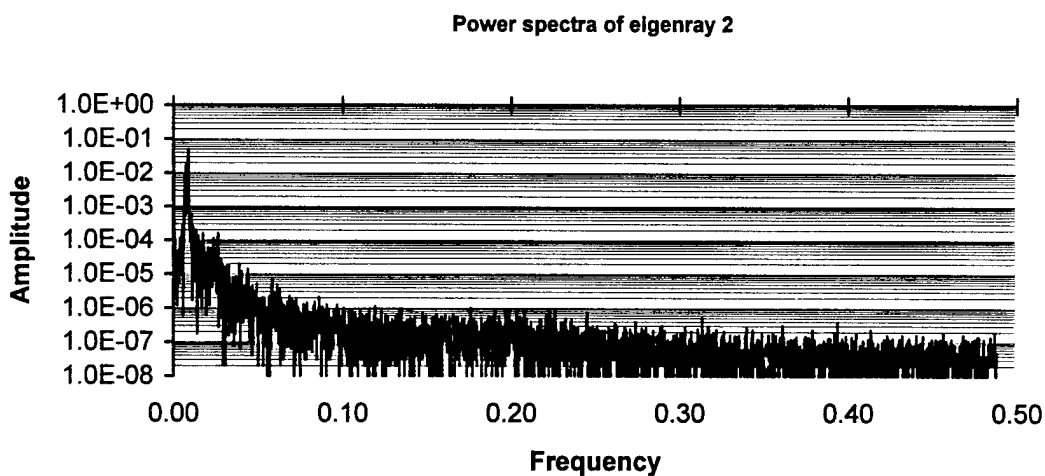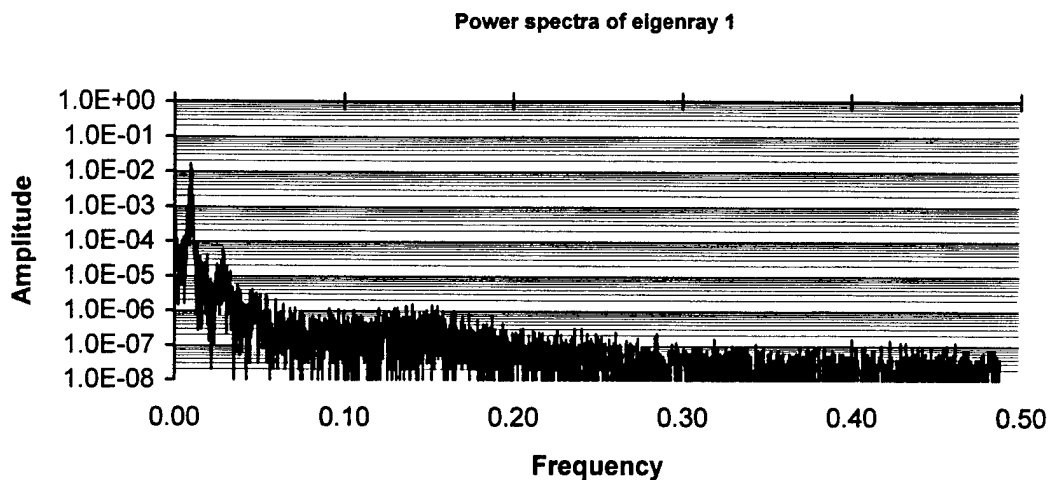
Fig. 4   Power spectra of eigenrays between California and Hawaii

Power spectra of eigenray 4
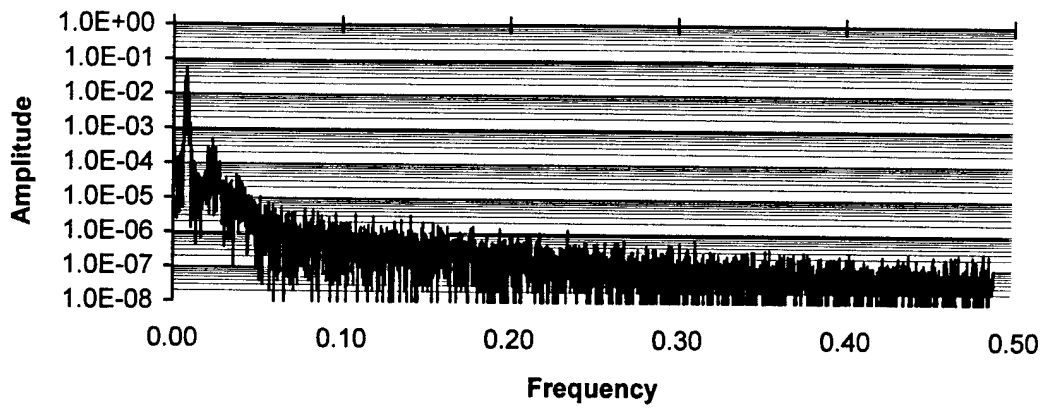
Power spectra of eigenray 5
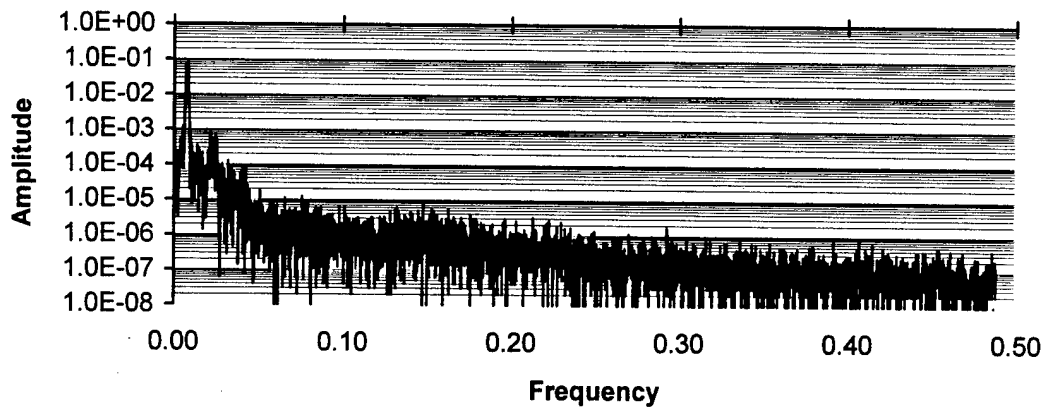
Power spectra of eigenray 6
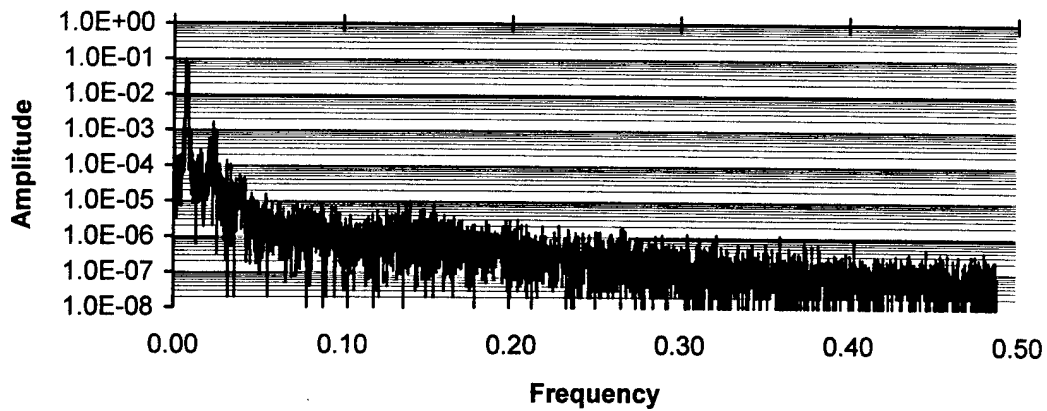
Fig. 4   Power spectra of eigenrays between California and Hawaii (Continue)

Power spectra of eigenray 7
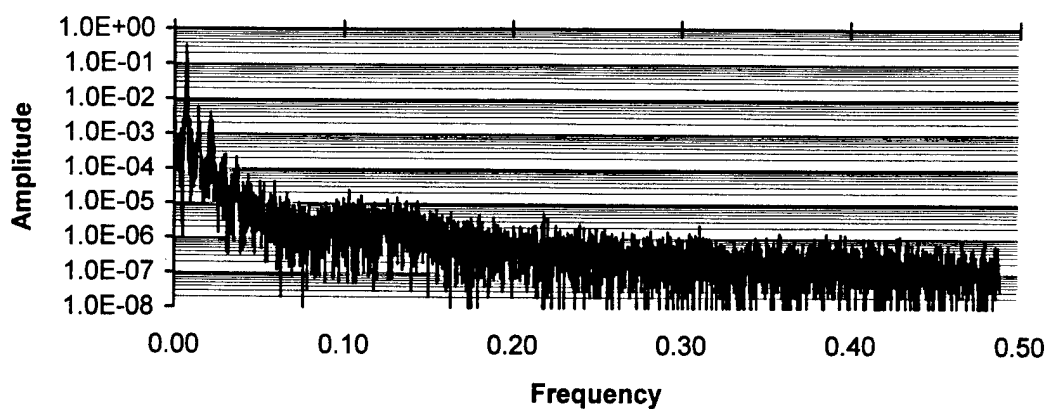
Power spectra of eigenray 8
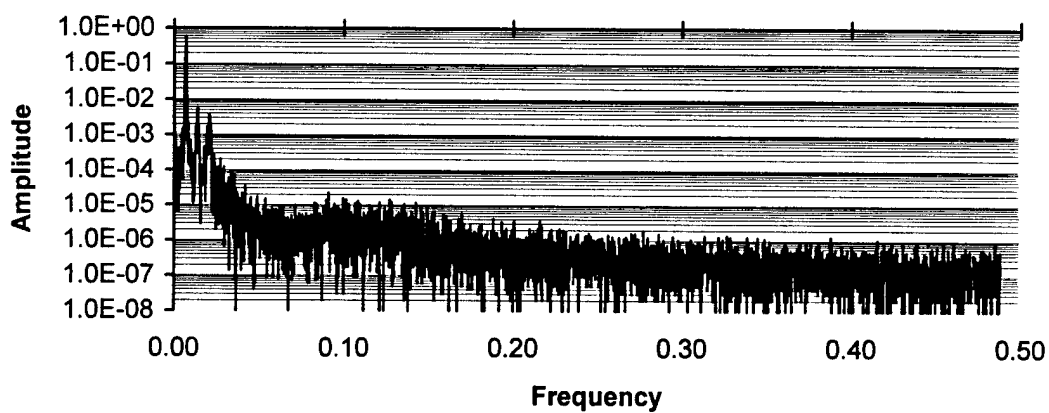
Power spectra of eigenray 9
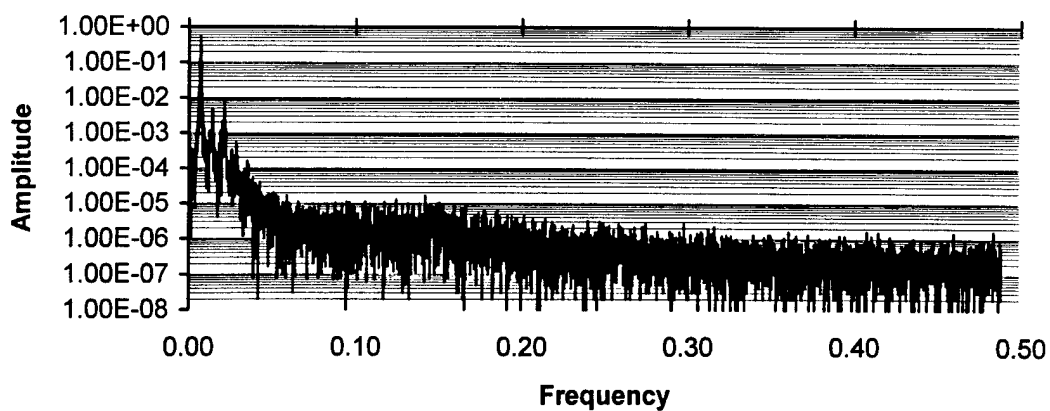
Fig. 4   Power spectra of eigenrays between California and Hawaii (Continue)
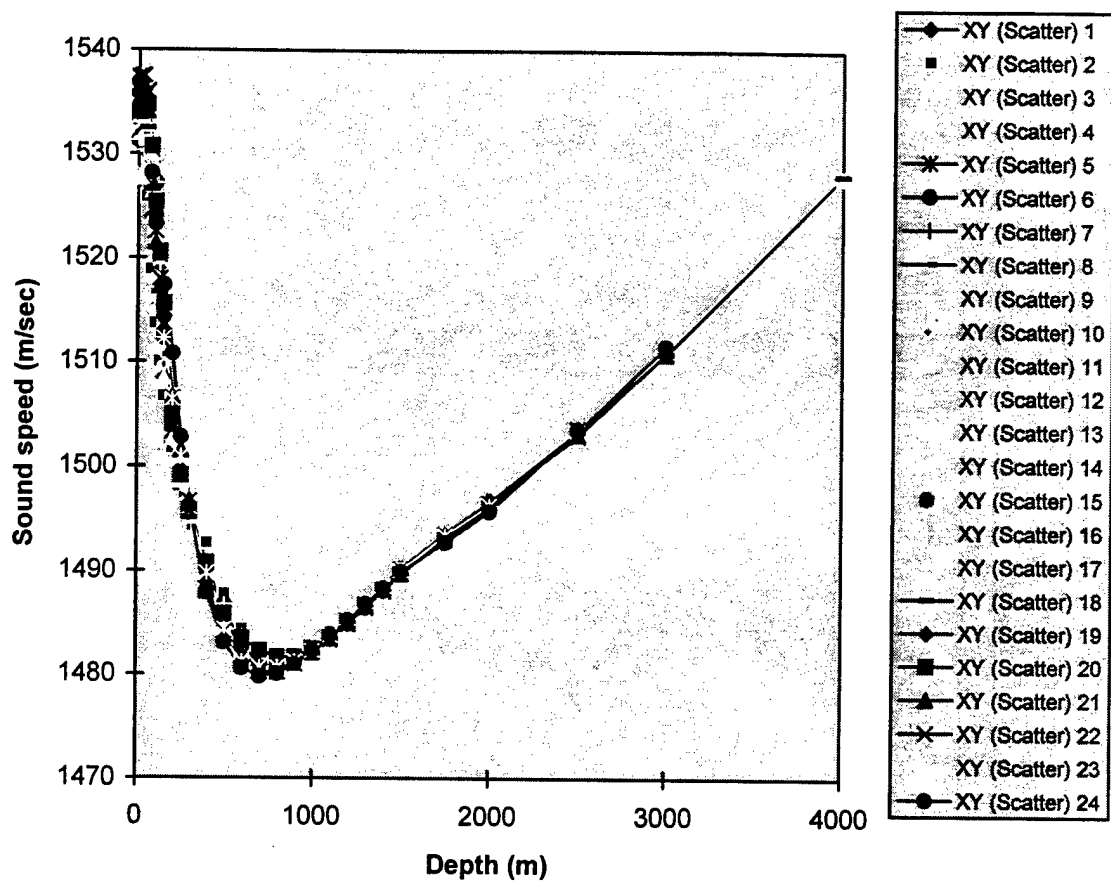
Fig. 5 NODC sound speed profiles of the Atlantic Ocean (Latitude 15 °S, Longitude from 3 °W to 13 °W). The sound speed fluctuates significantly at the upper ocean, but they are similar in shape.
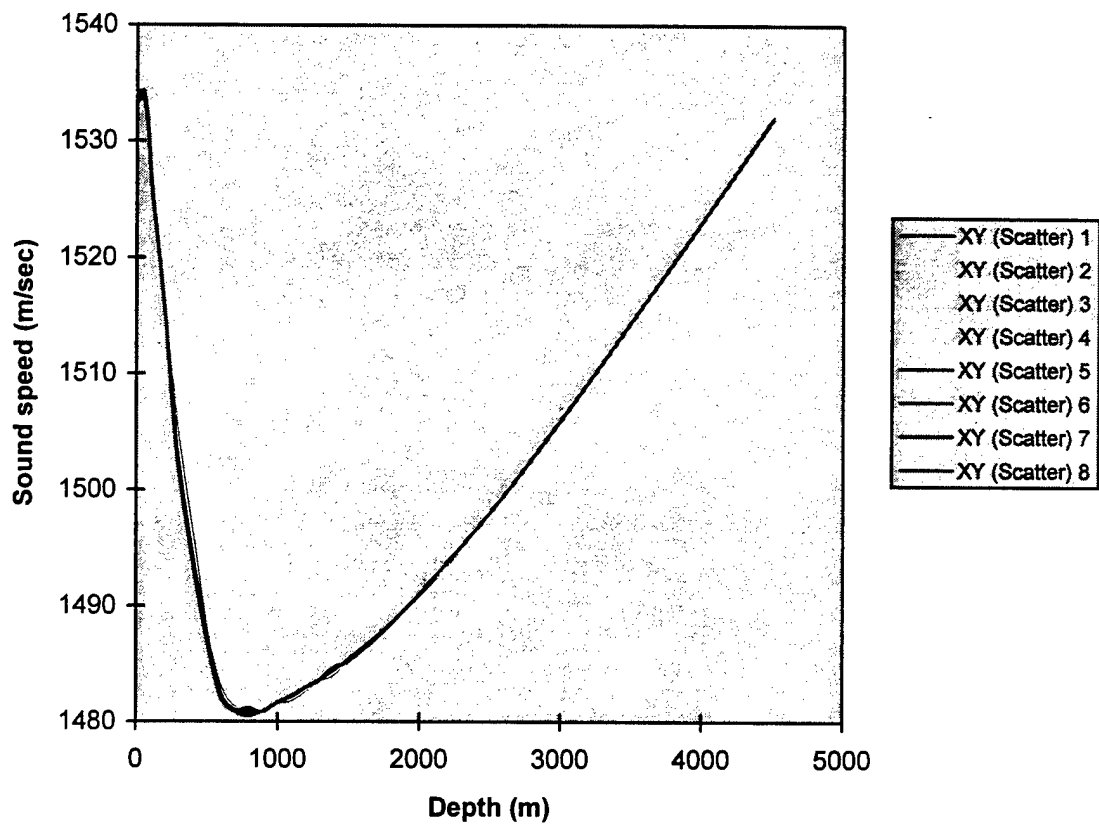
Fig. 6 Levitus sound speed profiles of Pacific Ocean (Latitude 25.5 °N, Longitude from 159.5 °W to 120.5 °W). These profiles are smooth compared with the NODC data in Fig. 5.
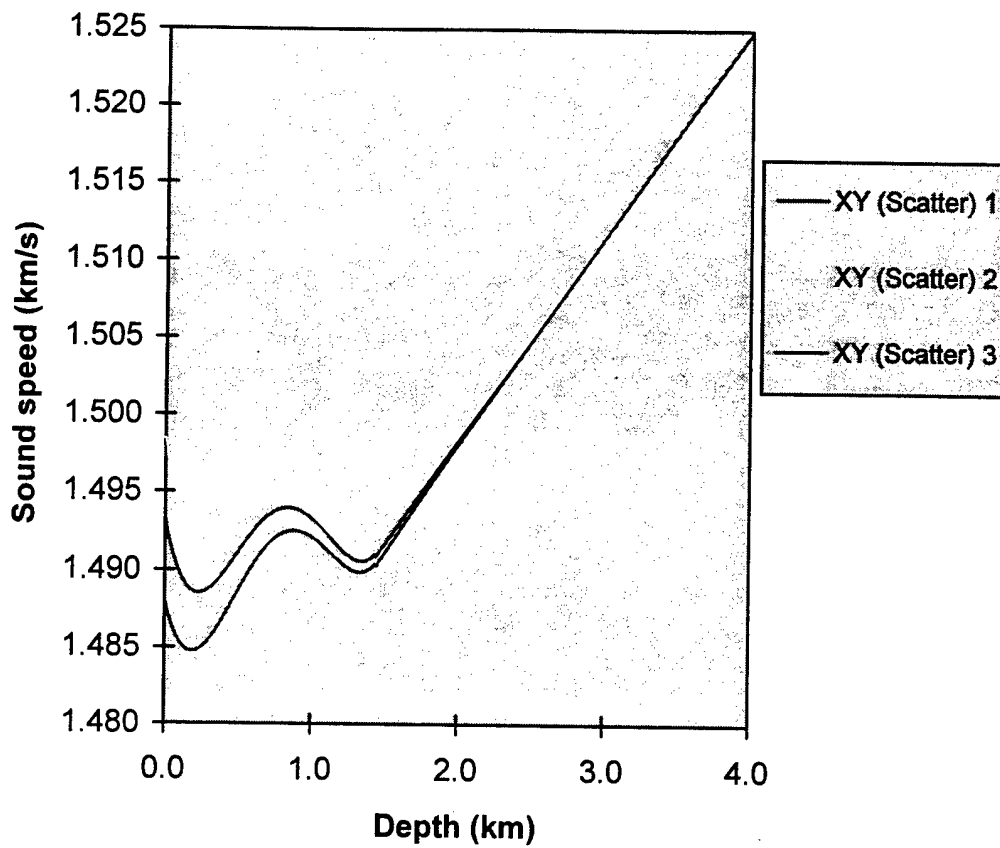
Fig. 7   Double-channel North Atlantic profile used in this study.
XY (Scatter) 1 is the profile without perturbation, depicted using Eq. (20).
XY (Scatter) 2, and 3 are the profiles with the maximum and minimum perturbations,
respectively.   The perturbations are calculated using Eq. (21).

A=0.0025,R=5 km, Zs=0.231 km
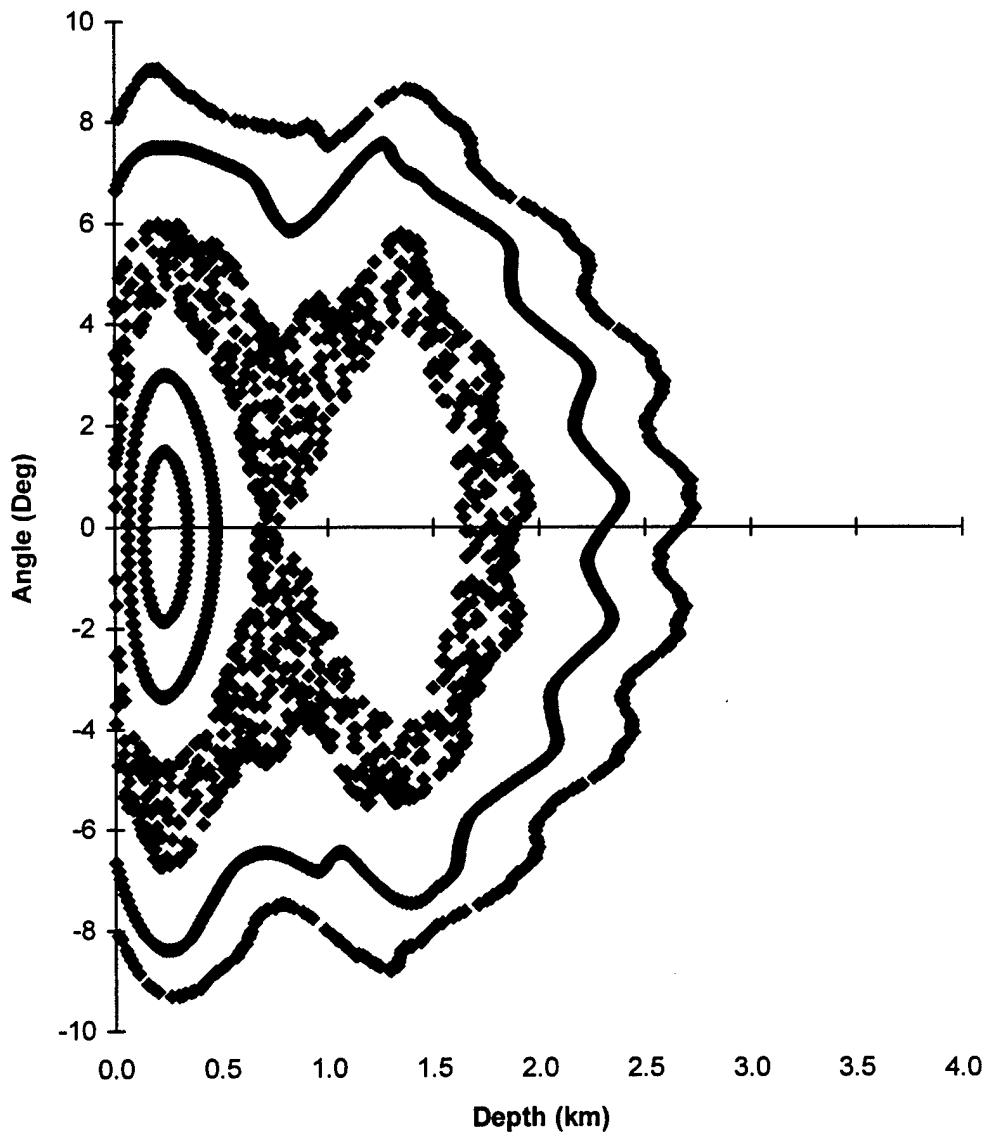
Fig. 8   Poincare section.   From inner to outer, launch angles are 1.5°, 3.0°, 4.5°, 6.0°, 7.5°, and 9.0°, respectively.   Source is at upper channel axis.

A=0.0025, R=10 km, Zs=0.231 km
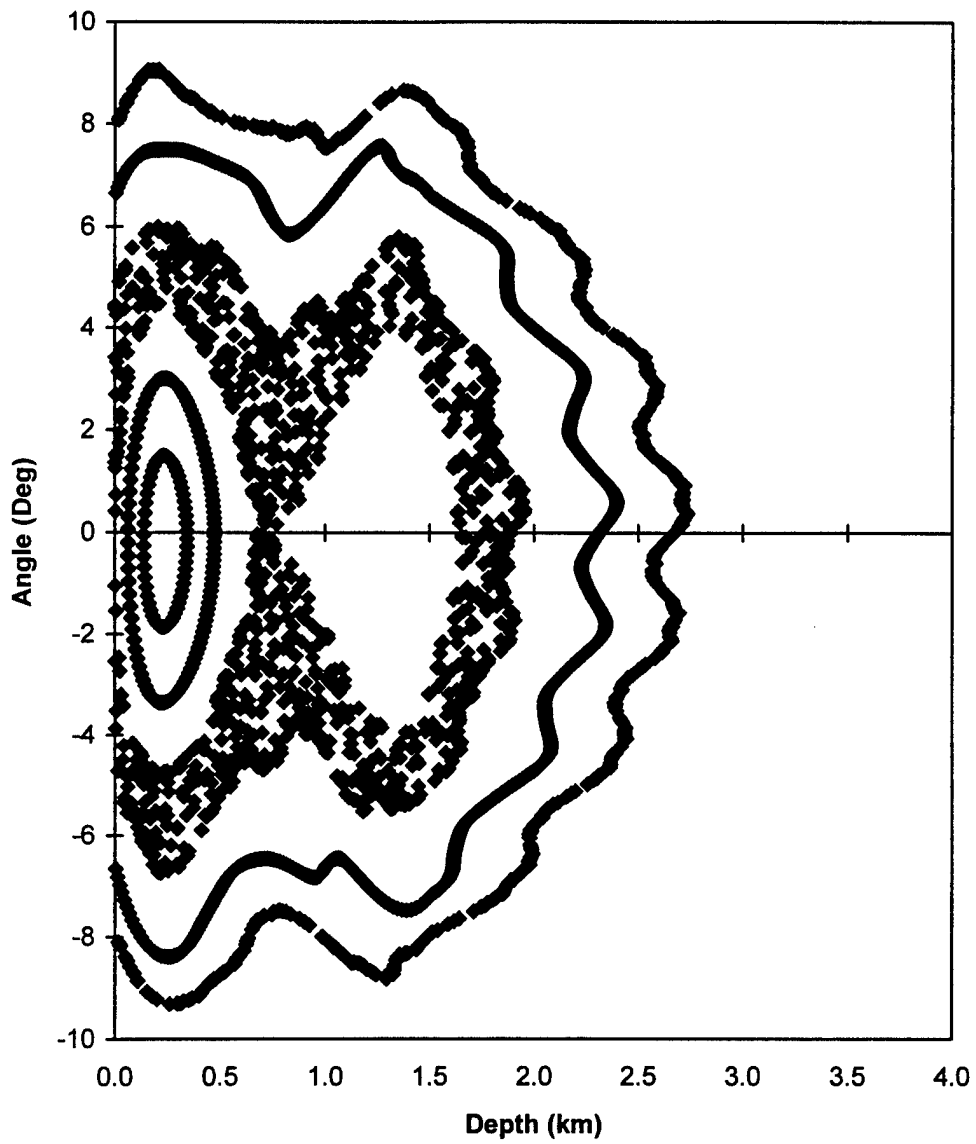
Fig. 9   Poincare section. From inner to outer, launch angles are 1.5°, 3.0°, 4.5°, 6.0°, 7.5°, and 9.0°, respectively. Source is at upper channel axis.

A=0.0025, R=15, Zs=0.231
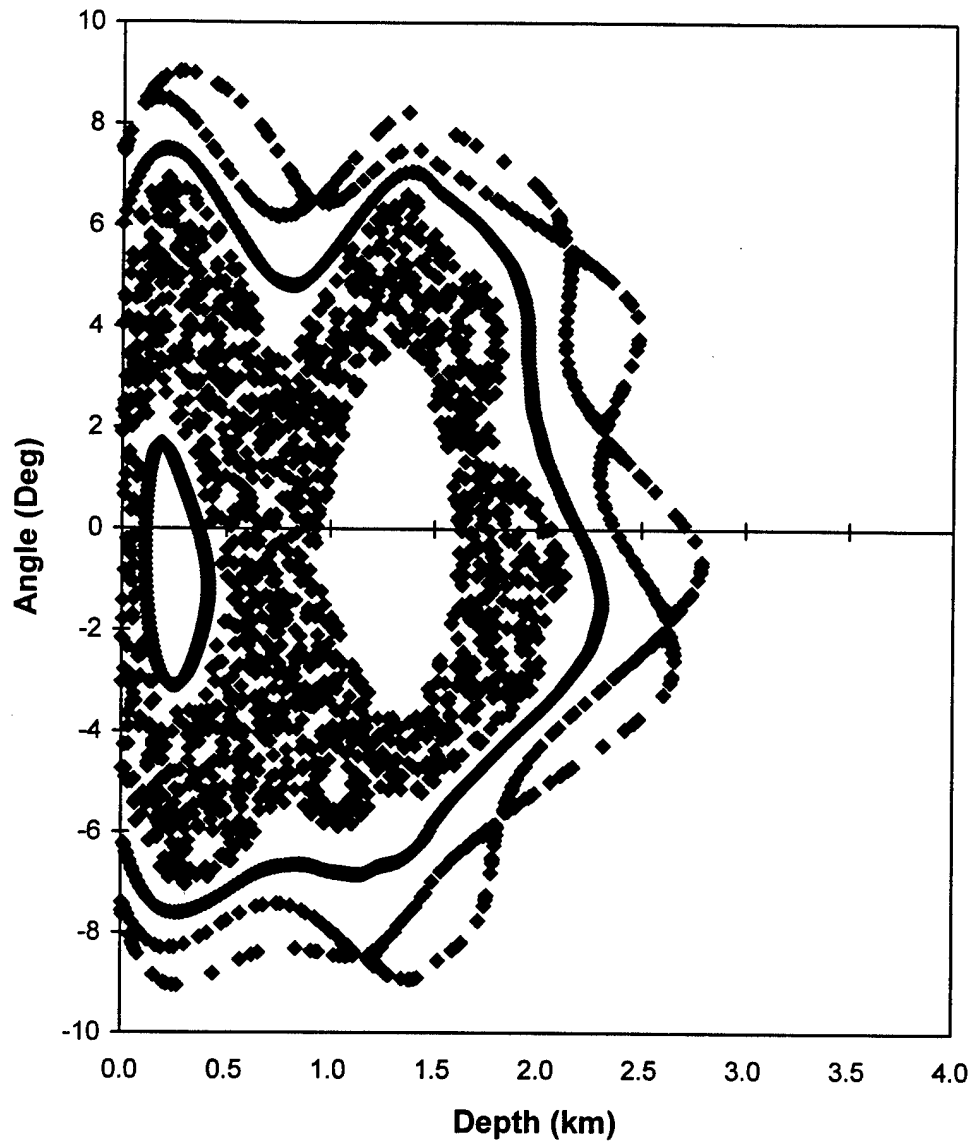
Fig. 10   Poincare section.   From inner to outer, launch angles are 1.5°, 3.0°, 4.5°, 6.0°, 7.5°, and 9.0°, respectively.   Source is at upper channel axis.

A=0.0025, R=5, Zs=1.345
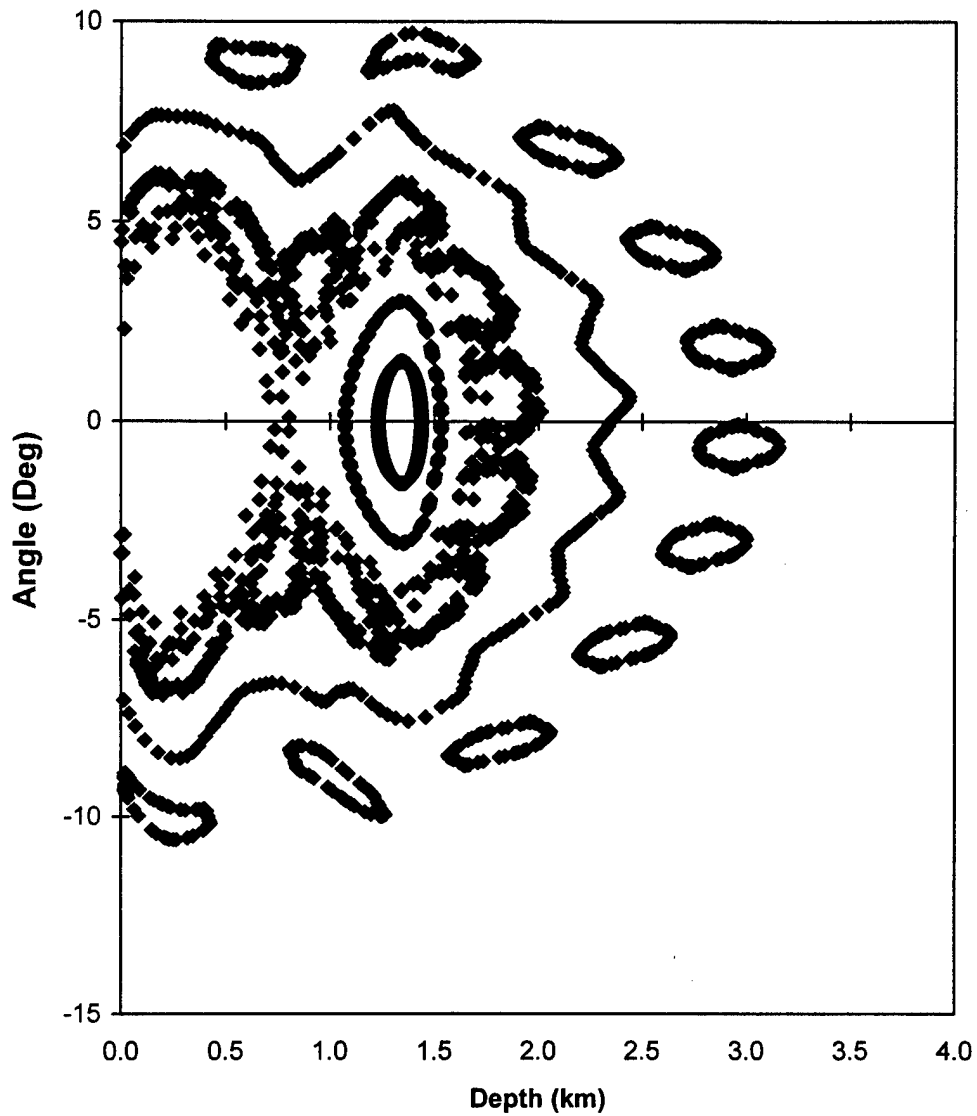
Fig. 11   Poincare section.   From inner to outer, launch angles are 1.5°, 3.0°, 4.5°, 6.0°, 7.5°, and 9.0°, respectively.   Source is at lower channel axis.

A=0.0025, R=10 km, Zs=1.345 km
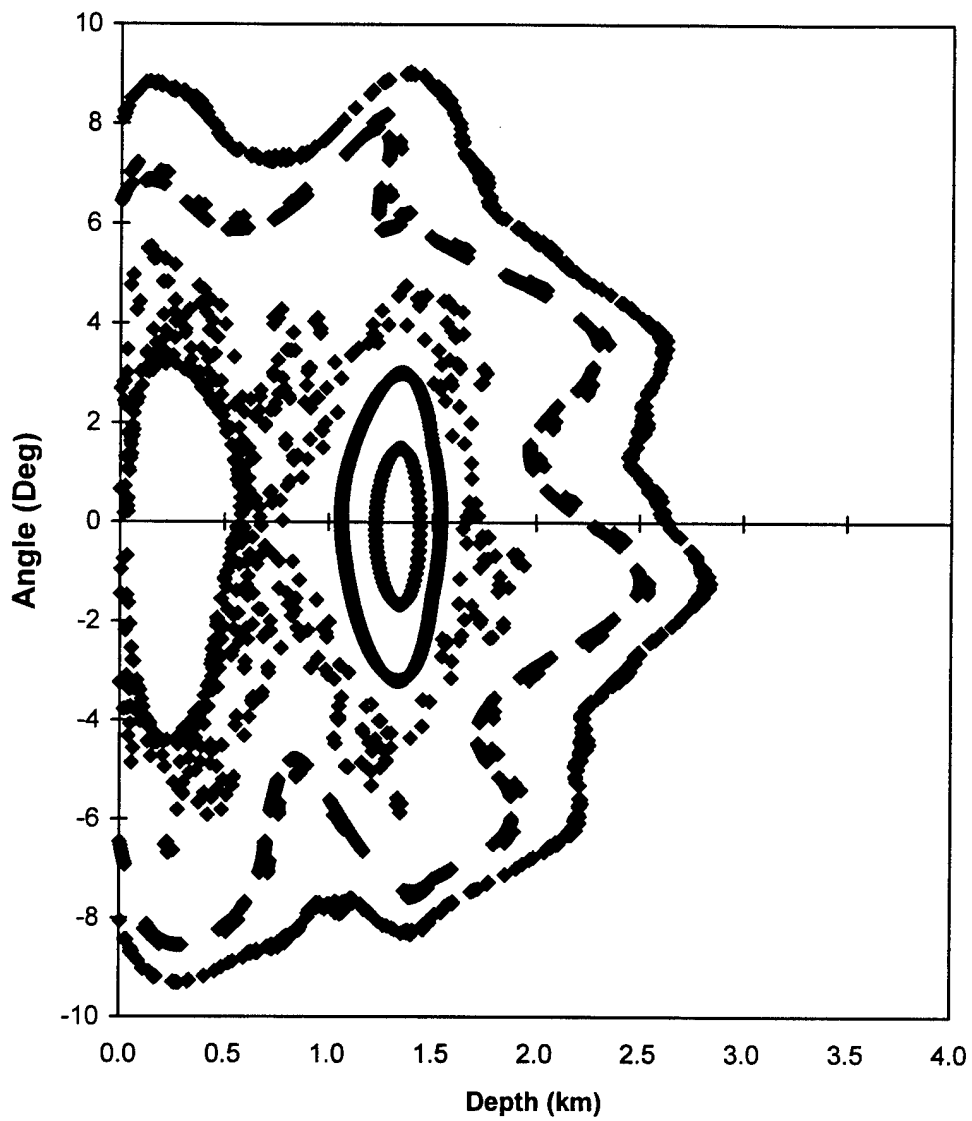
Fig. 12   Poincare section.   From inner to outer, launch angles are 1.5°, 3.0°, 4.5°, 6.0°, 7.5°, and 9.0°, respectively.   Source is at lower channel axis.

A=0.0025, R=15 km, Zs=1.345 km
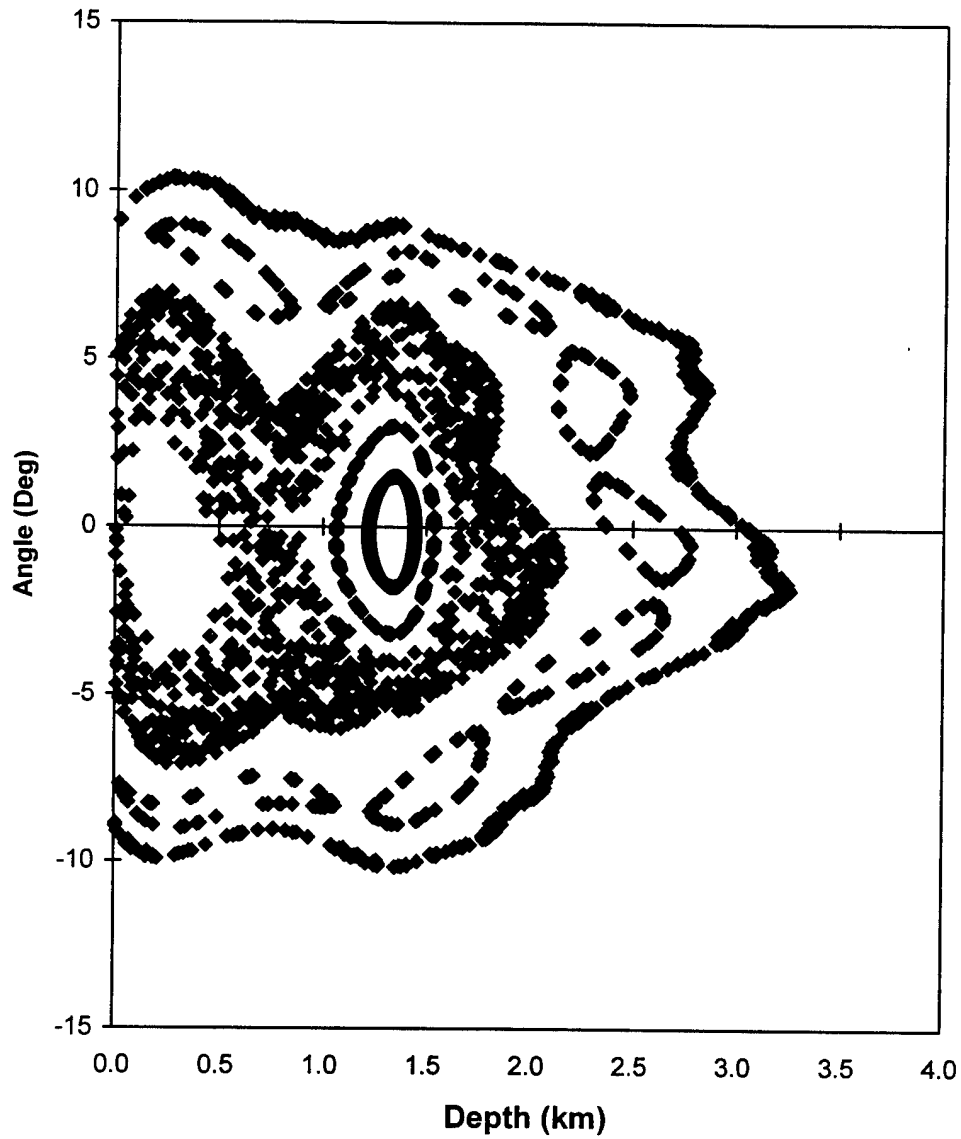
Fig. 13   Poincare section.   From inner to outer, launch angles are 1.5°, 3.0°, 4.5°, 6.0°, 7.5°, and 9.0°, respectively.   Source is at lower channel axis.

A=0.001, R=5 km, Zs=0.231 km
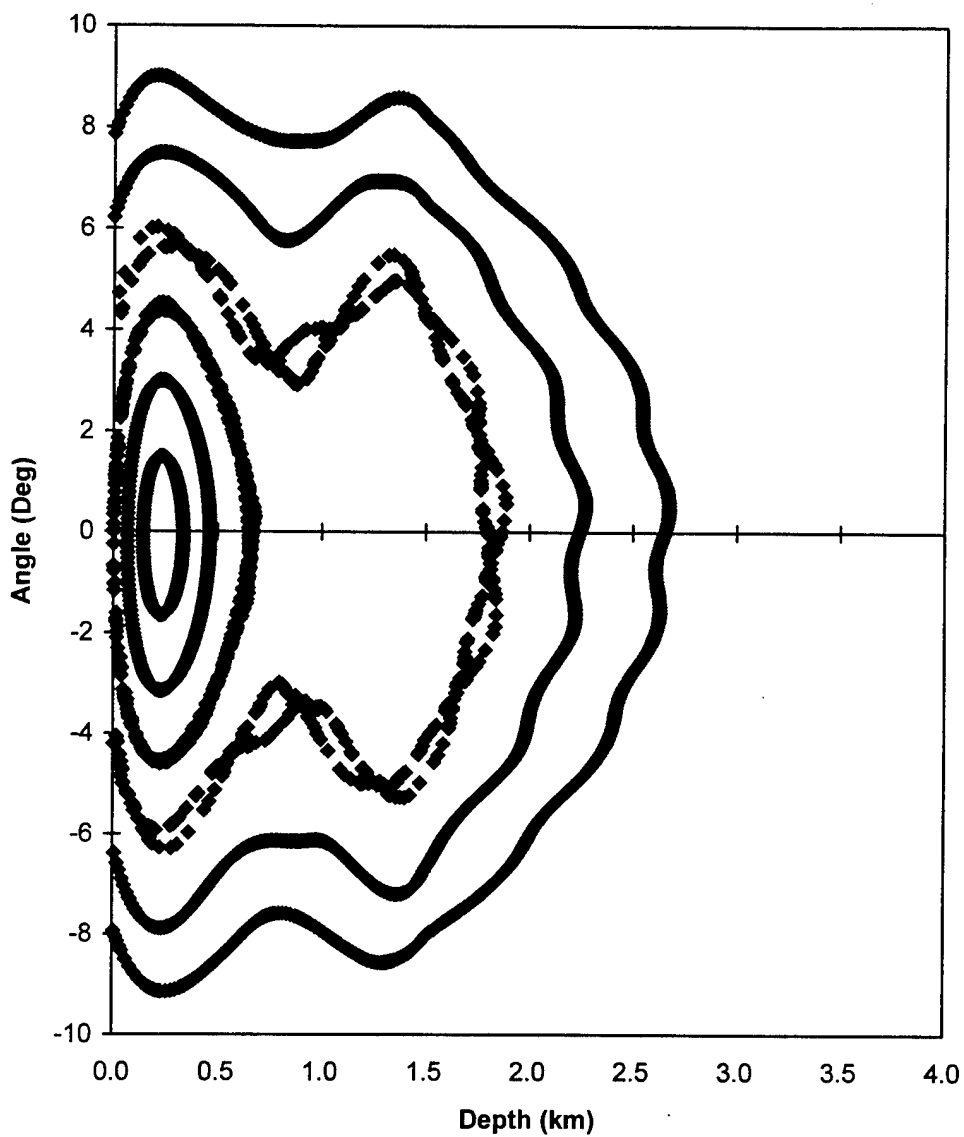
Fig. 14   Poincare section. From inner to outer, launch angles are 1.5°, 3.0°, 4.5°, 6.0°, 7.5°, and 9.0°, respectively. Source is at upper channel axis.

A=0.001, R=10 km, Zs=0.231 km
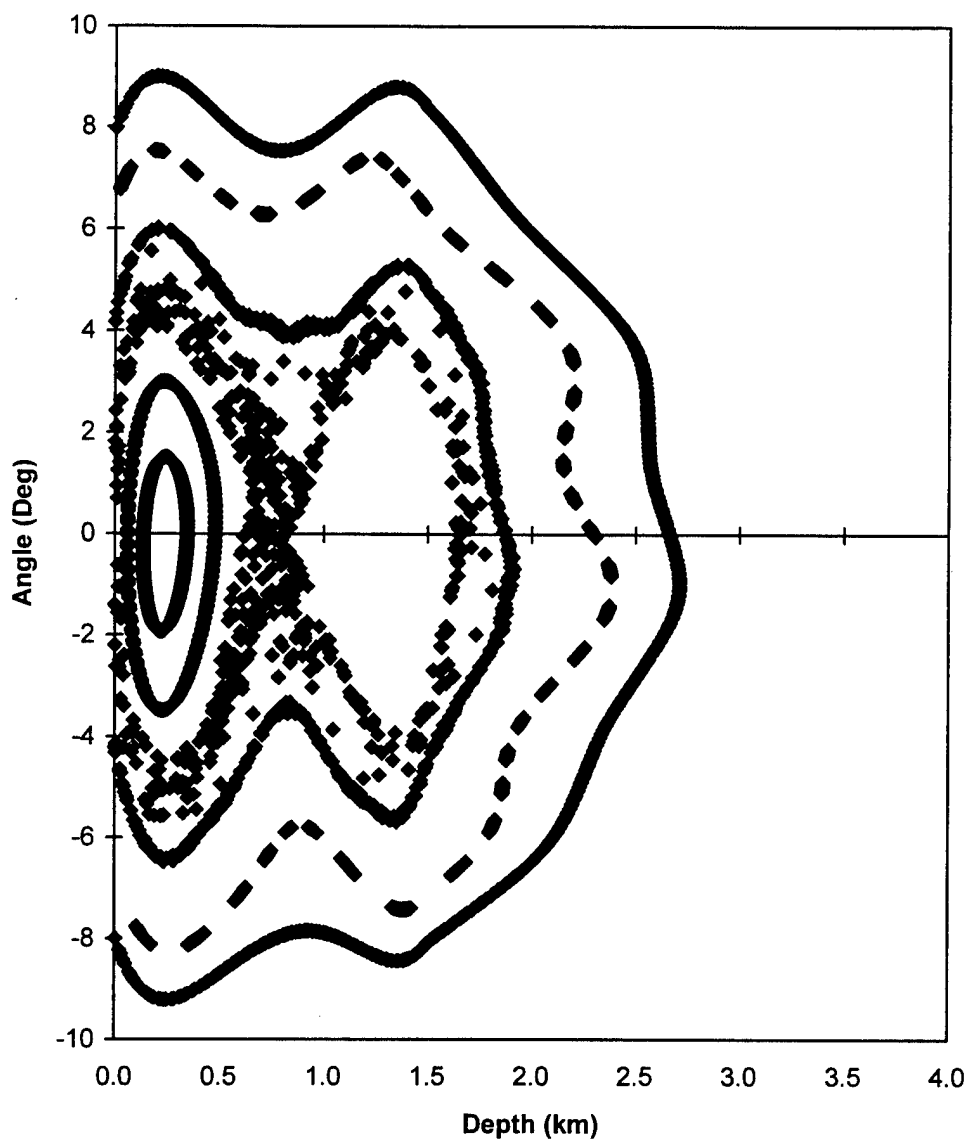
Fig. 15 Poincare section. From inner to outer, launch angles are 1.5°, 3.0°, 4.5°, 6.0°, 7.5°, and 9.0°, respectively. Source is at upper channel axis.

A=0.001, R=15 km, Zs=0.231 km
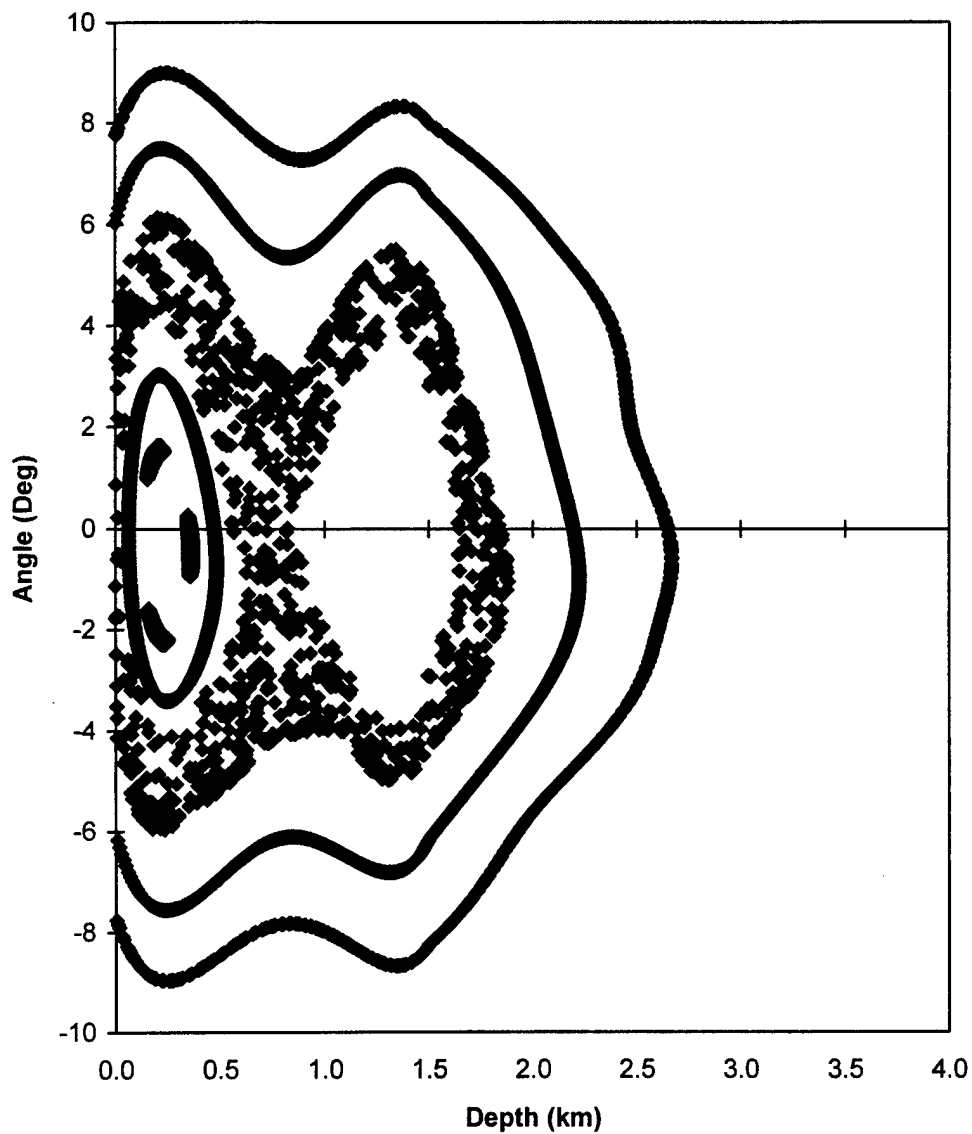
Fig. 16   Poincare section.   From inner to outer, launch angles are 1.5°, 3.0°, 4.5°, 6.0°, 7.5°, and 9.0°, respectively.   Source is at upper channel axis.

A=0.001, R=5 km, Zs=1.345 km
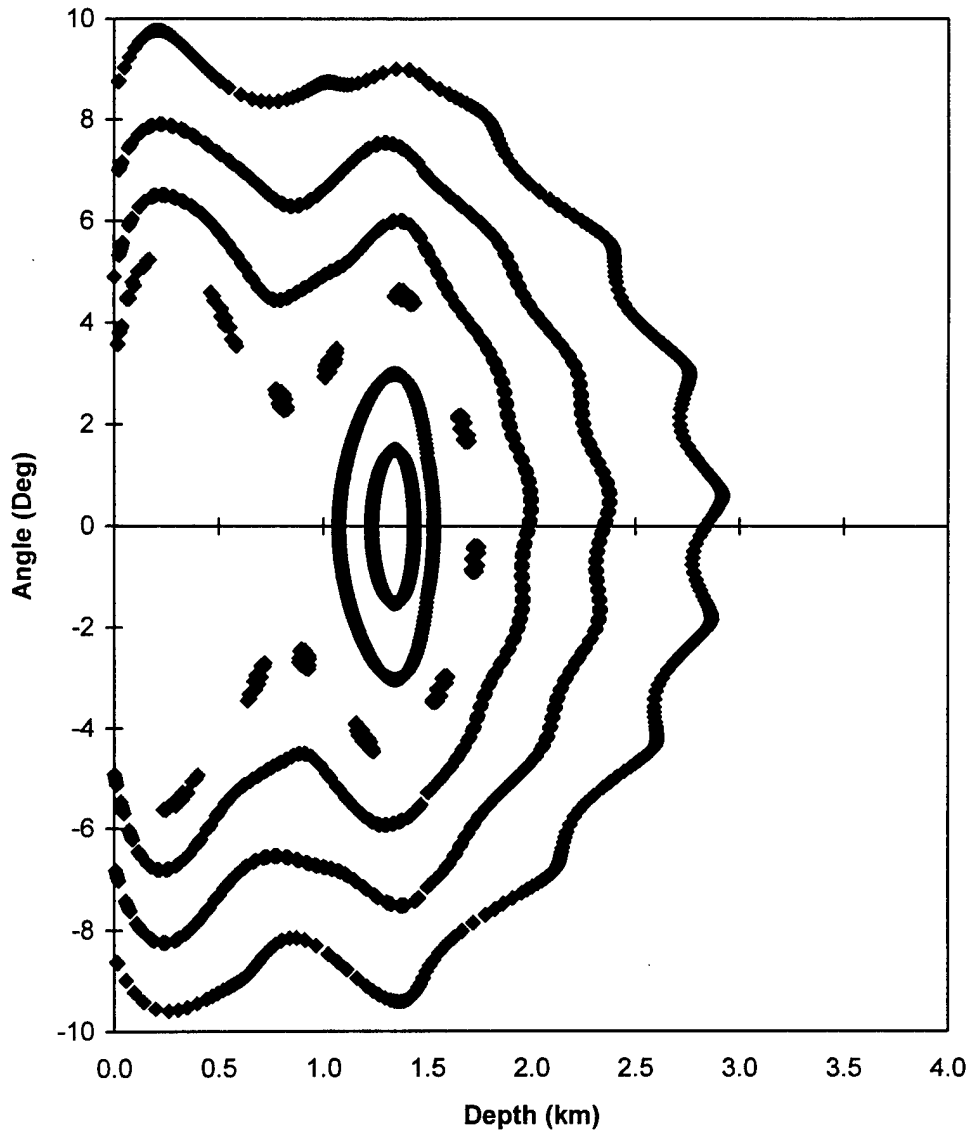
Fig. 17   Poincare section.   From inner to outer, launch angles are 1.5°, 3.0°, 4.5°, 6.0°, 7.5°, and 9.0°, respectively.   Source is at lower channel axis.

A=0.001, R=10 km, Zs=1.345 km
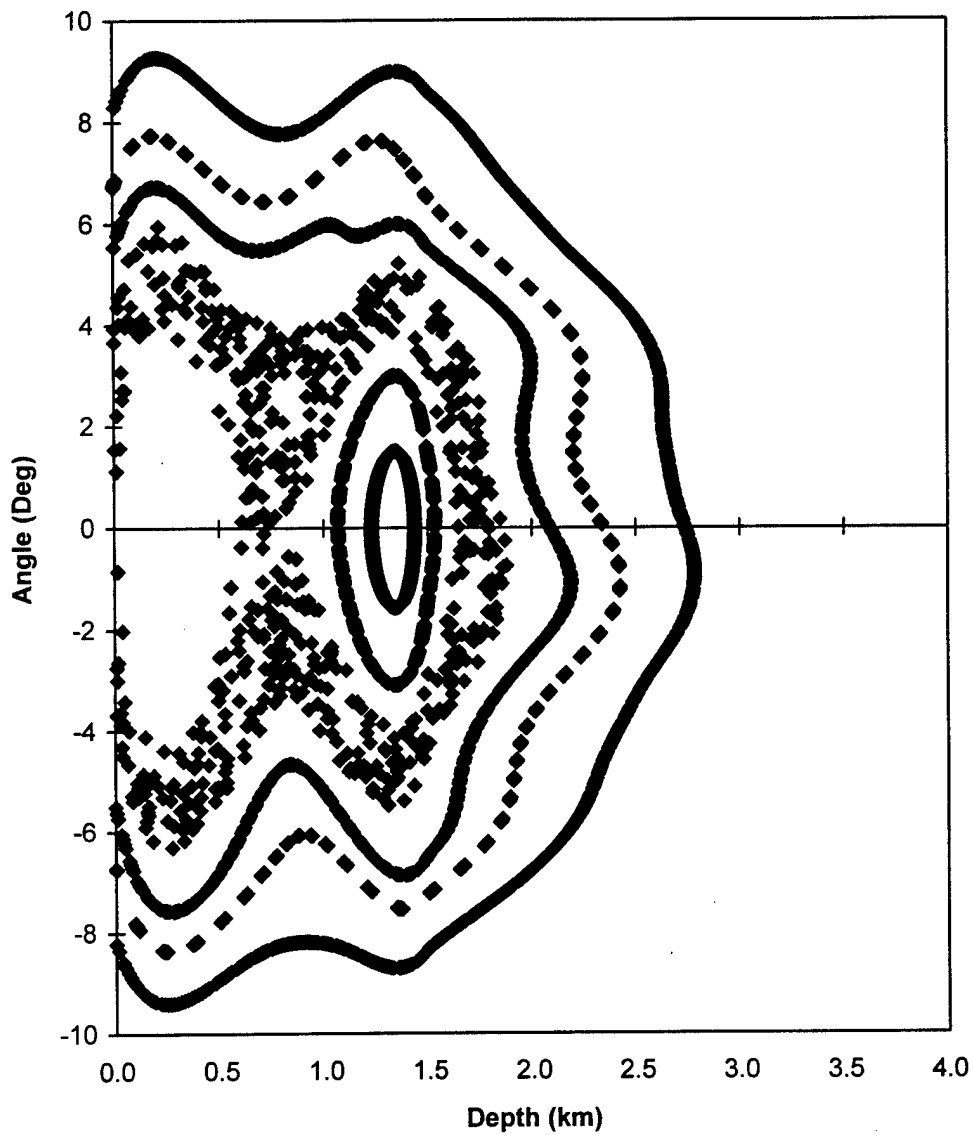
Fig. 18   Poincare section.   From inner to outer, launch angles are 1.5°, 3.0°, 4.5°, 6.0°, 7.5°, and 9.0°, respectively.   Source is at lower channel axis.

A=0.001, R=15 km, Zs=1.345 km
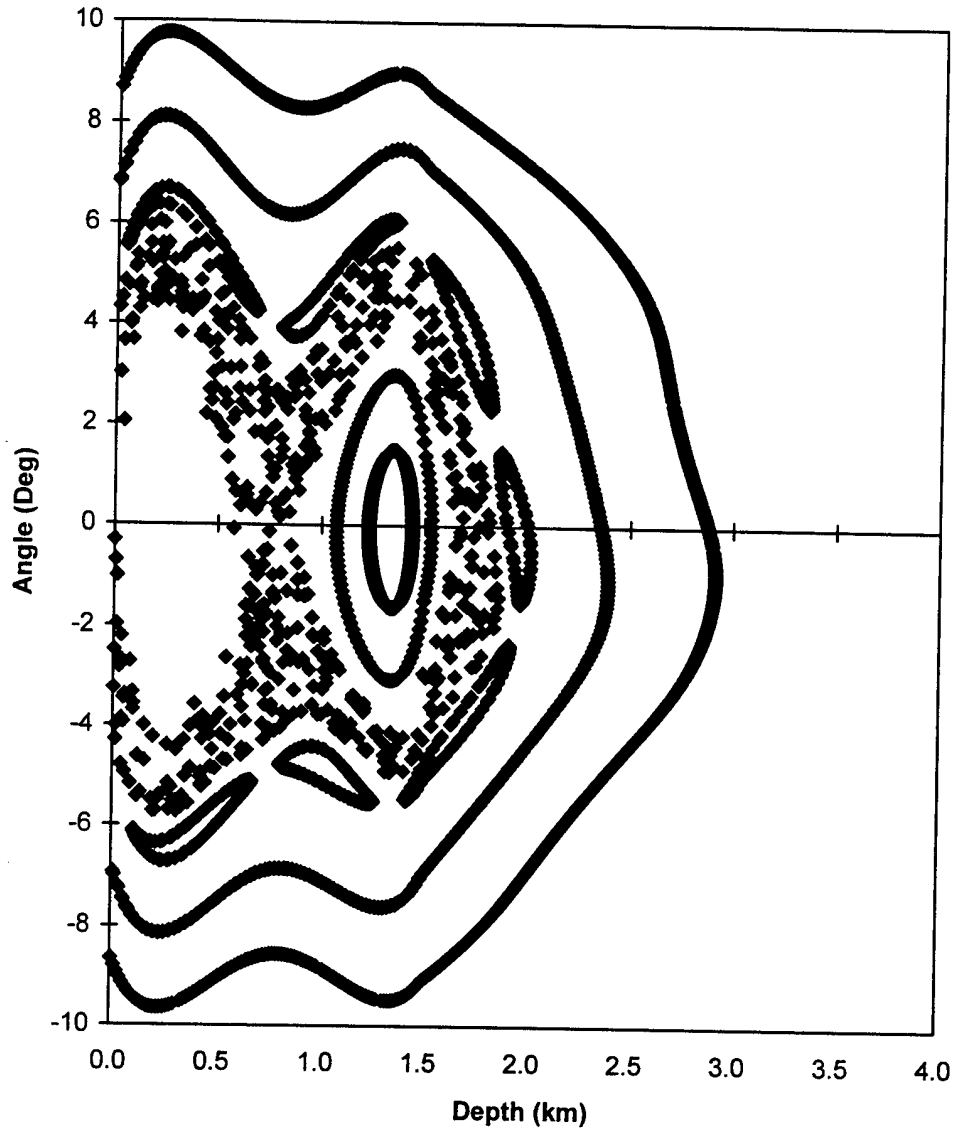
Fig. 19   Poincare section.   From inner to outer, launch angles are 1.5°, 3.0°, 4.5°, 6.0°, 7.5°, and 9.0°, respectively.   Source is at lower channel axis.
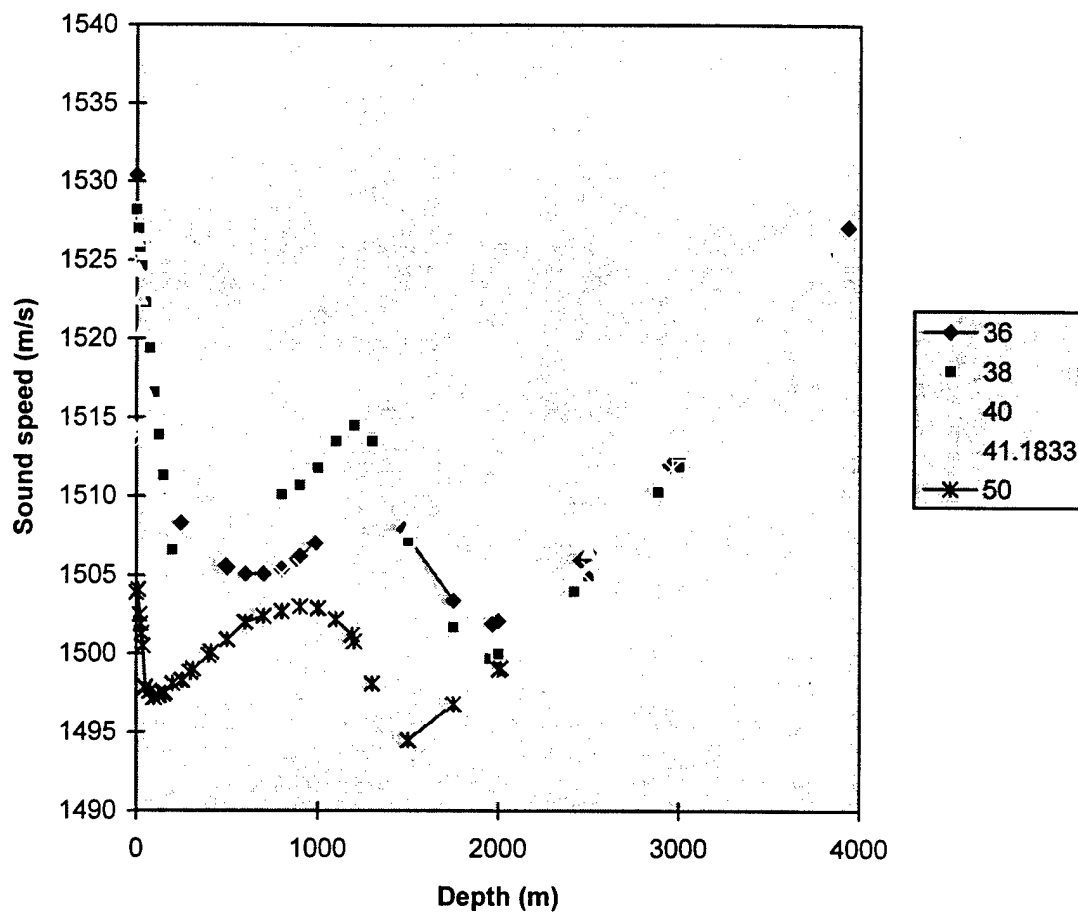
Fig. 20   NODC double-channel profiles used in ray tracing
(Longitude: 14 °E, Latitude: listed in the legends.)

Source depth: 0.4 km, Launch grazing angle=0
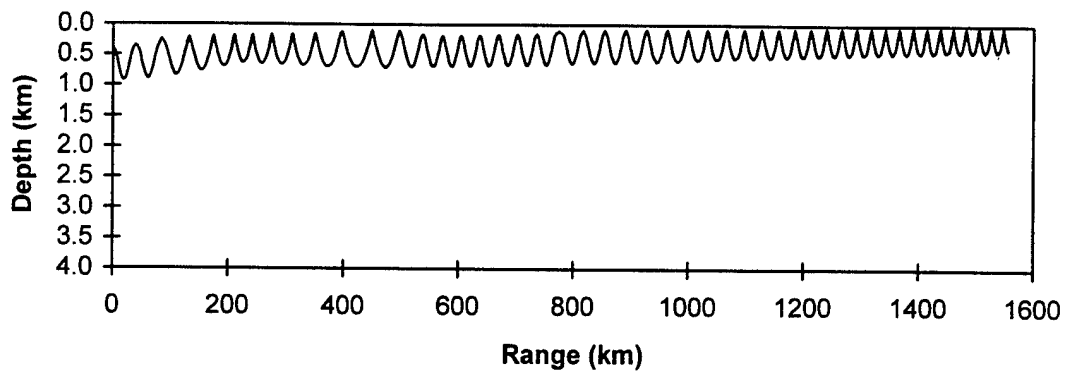
Source depth: 0.4 km, Launch grazing angle: 1 Deg.
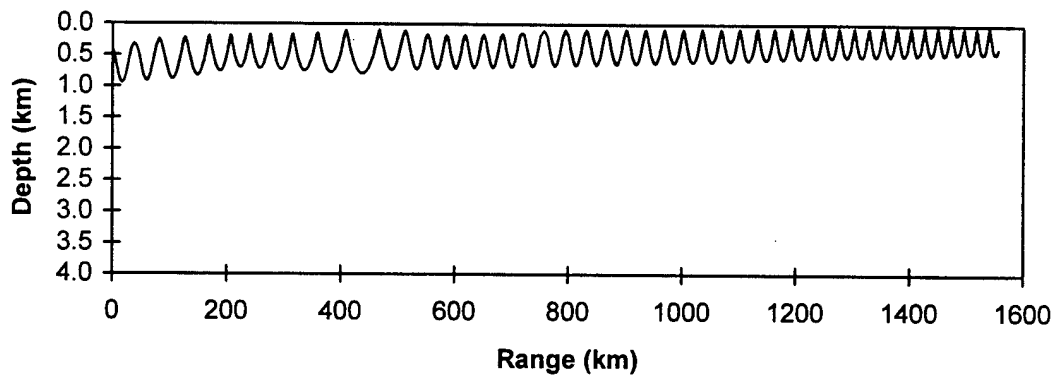
Source depth: 0.4 km, Launch grazing angle: 2 Deg.

Fig. 21   Ray paths in the double-channel

78
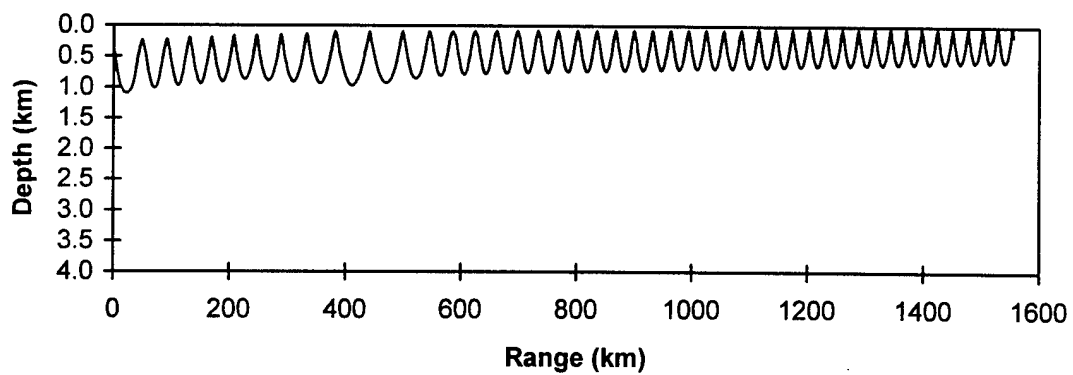
Source depth: 0.4 km, Launch grazing angle: 3 Deg.
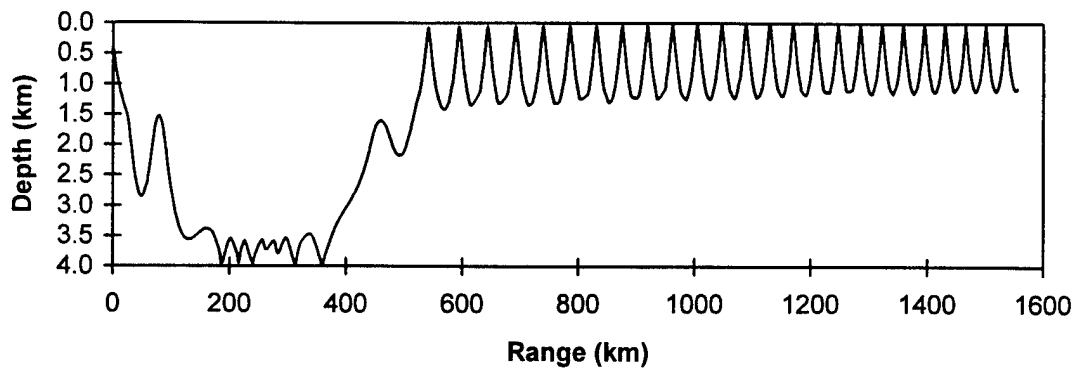
Source depth: 0.4 km, launch grazing angle: 4 Deg.
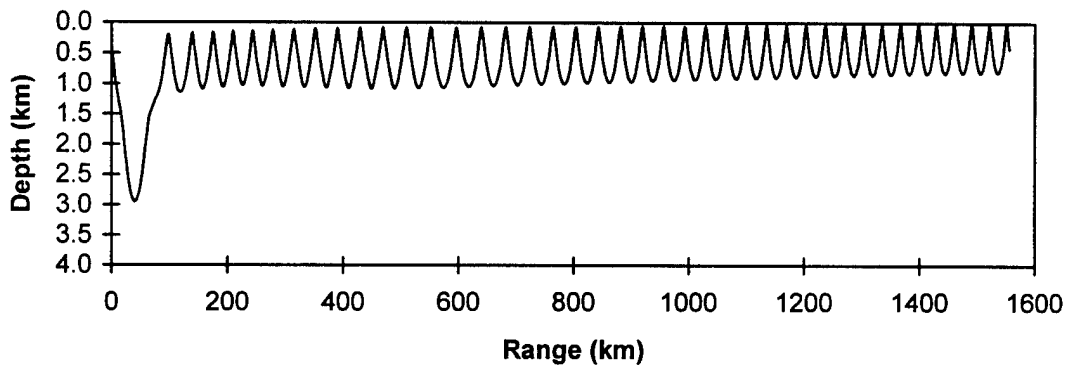
Source depth: 0.4 km, launch grazing angle: 5 Deg.
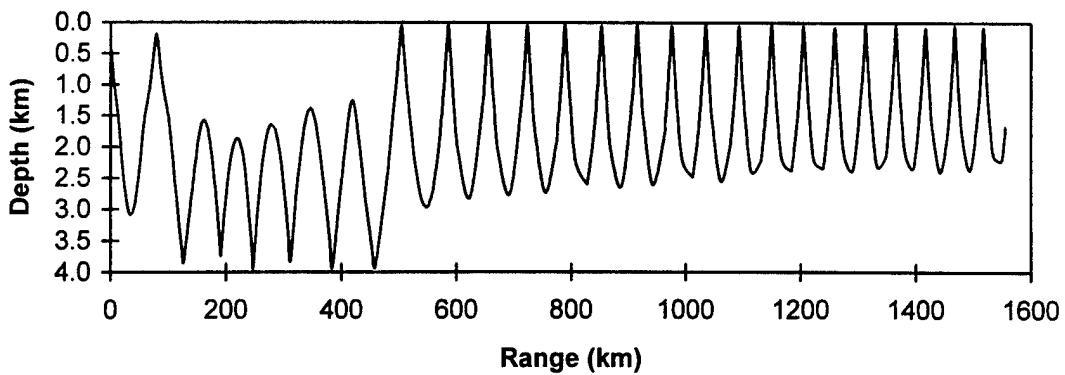
Fig. 21   Ray paths in the double-channel (continue)

Source depth: 0.4 km, launch grazing angle: 6 Deg.
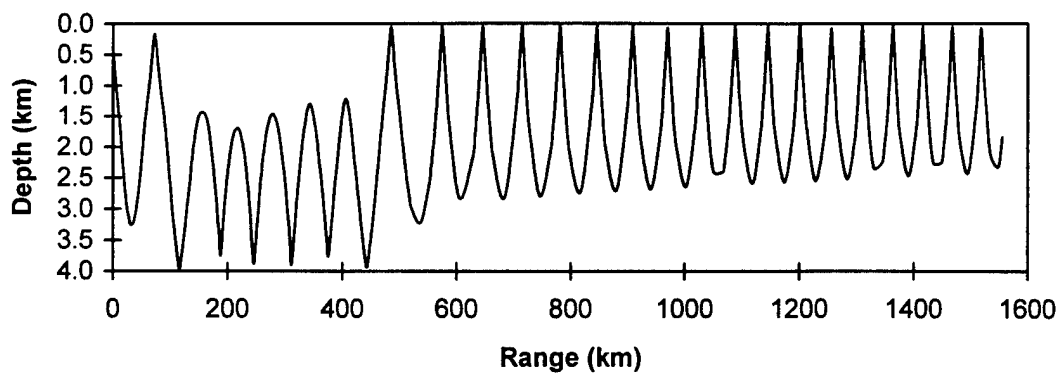
Source depth: 0.4 km, launch grazing angle: 7 Deg.
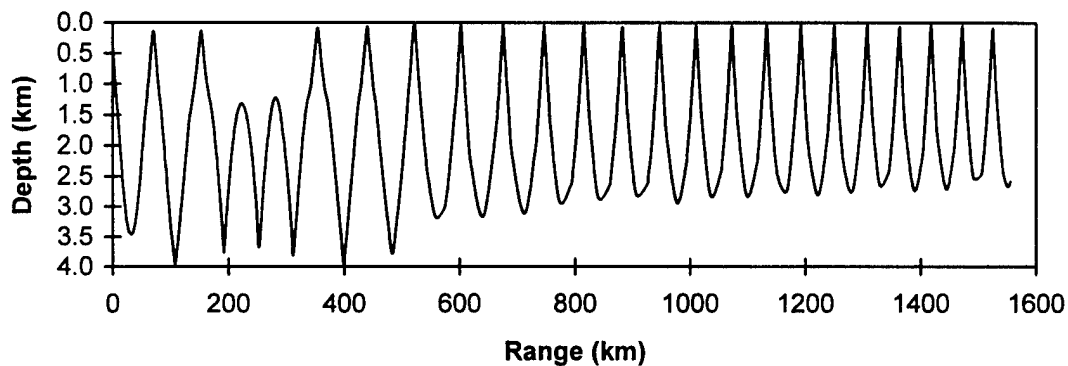
Source depth: 0.4 km, launch grazing angle: 8 Deg.
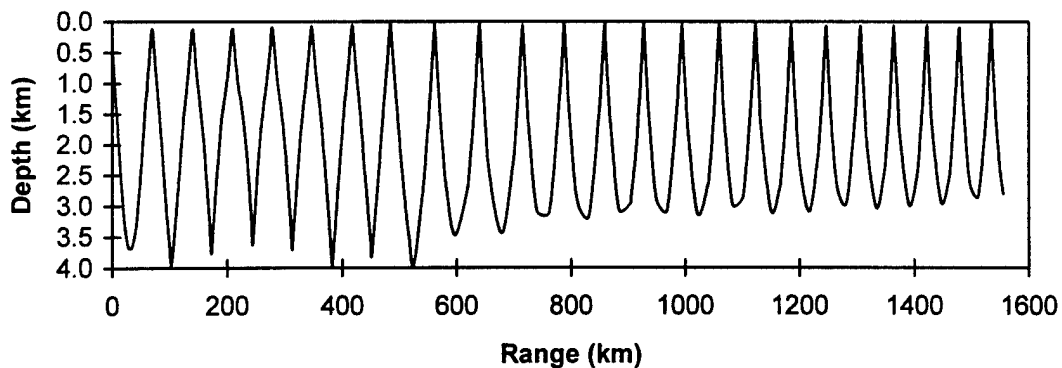
Fig. 21   Ray paths in the double-channel (Continue)

Source depth: 0.4 km, launch grazing angle: 9 Deg.
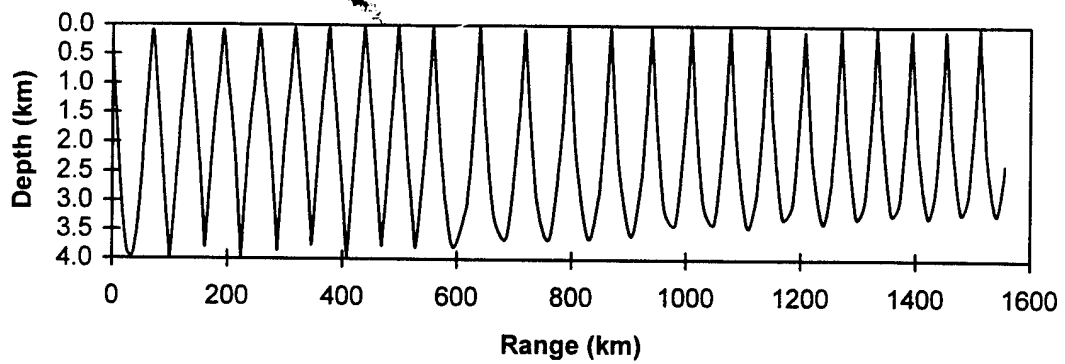
Source depth: 0.4 km, launch grazing angle: 10 Deg.

Fig. 21   Ray paths in the double-channel (continue)

81

Zs= 0.4 km, Grazing angle= 0 Deg.
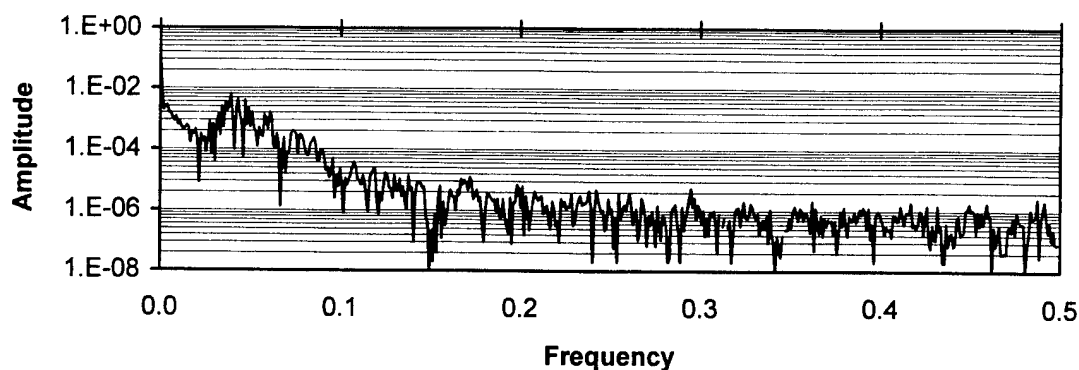
Zs = 0.4 km, Grazing angle = 1 Deg.
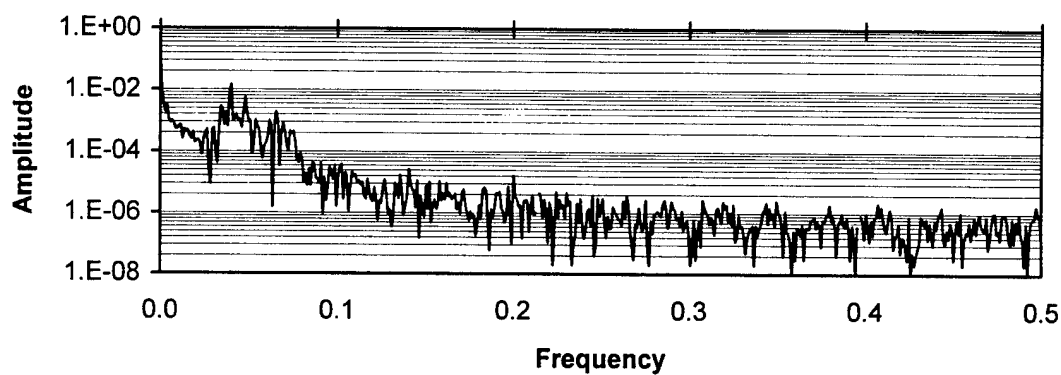
Zs = 0.4 km, Grazing angle = 2 Deg.
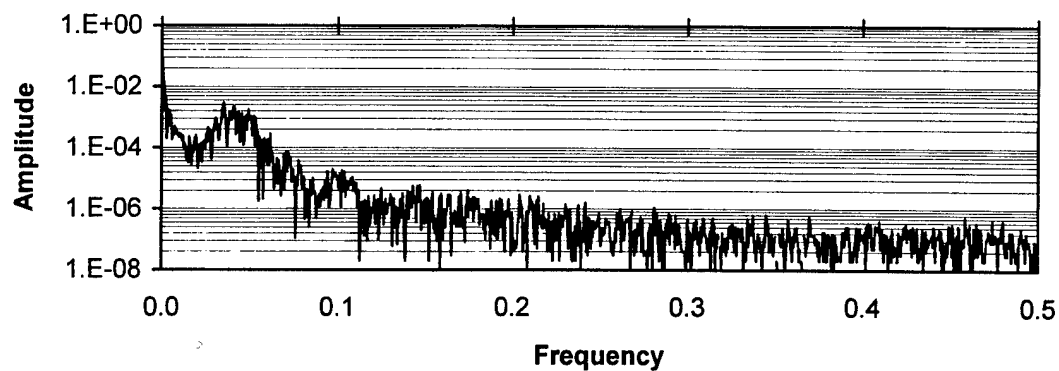
Fig. 22   Power spectra for the ten rays in figure 21

Zs= 0.4 km, Grazing angle = 3 Deg.
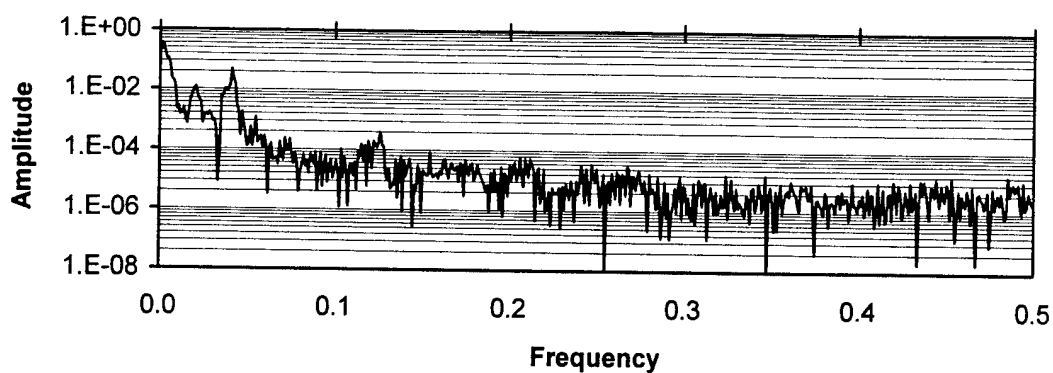
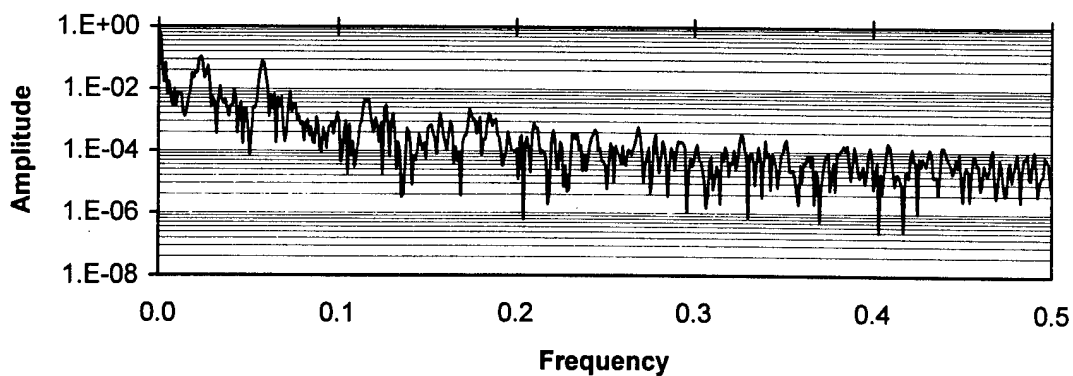Zs = 0.4 km, Grazing angle = 4 Deg.
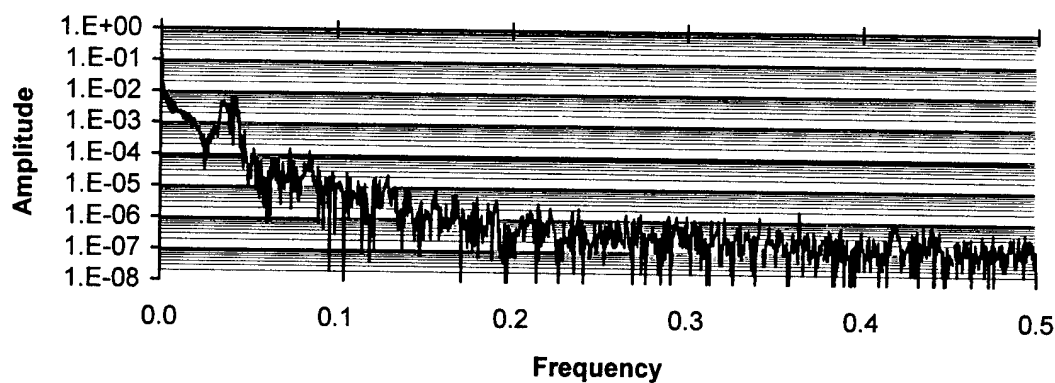
Zs = 0.4 km, Grazing angle = 5 Deg.
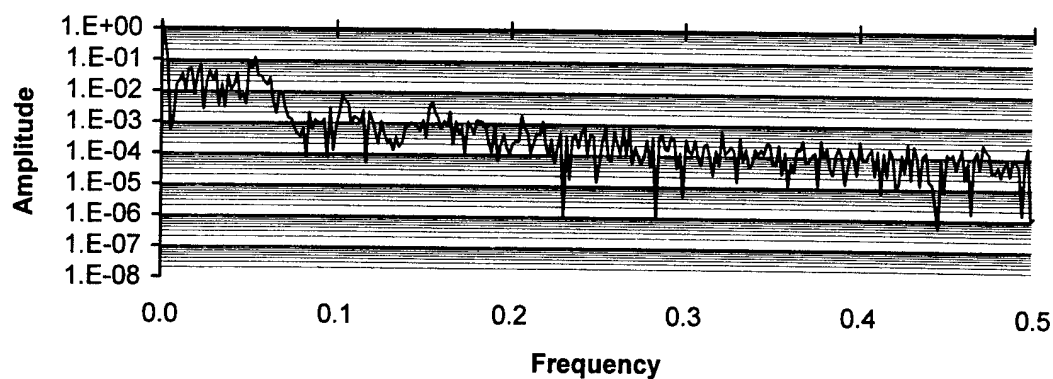
Fig. 22   Power spectra for the eleven rays in figure 21 (continue)

Zs = 0.4 km, Grazing angle = 6 Deg.
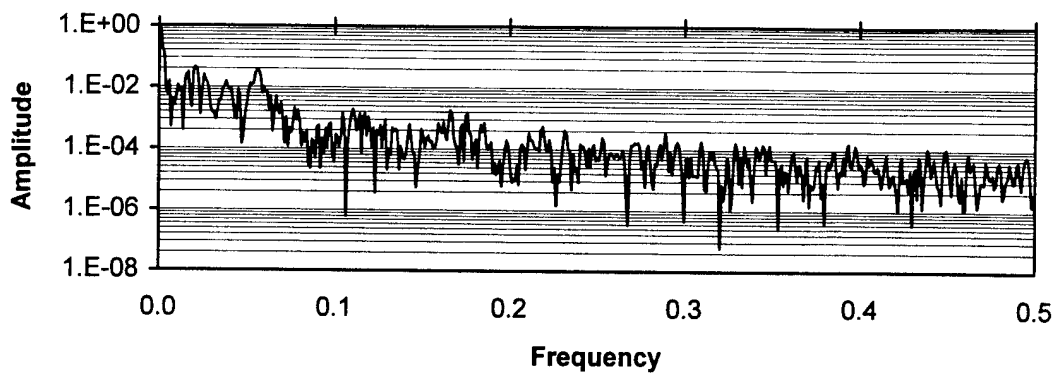
Zs = 0.4 km, Grazing angle = 7 Deg.
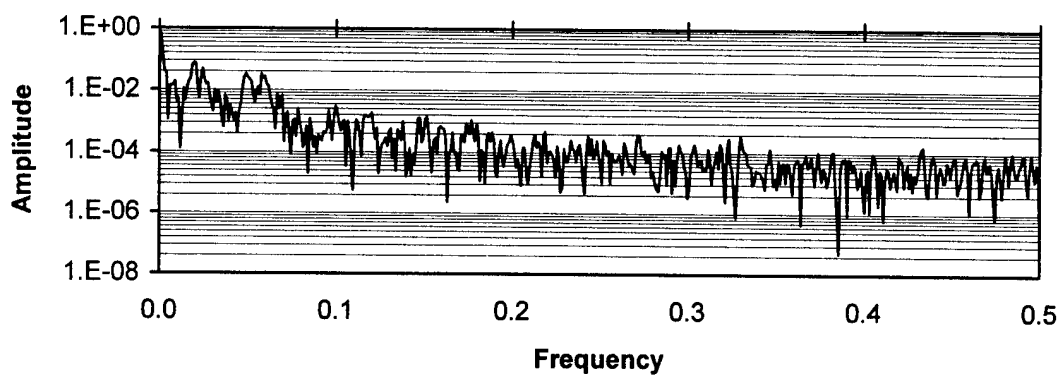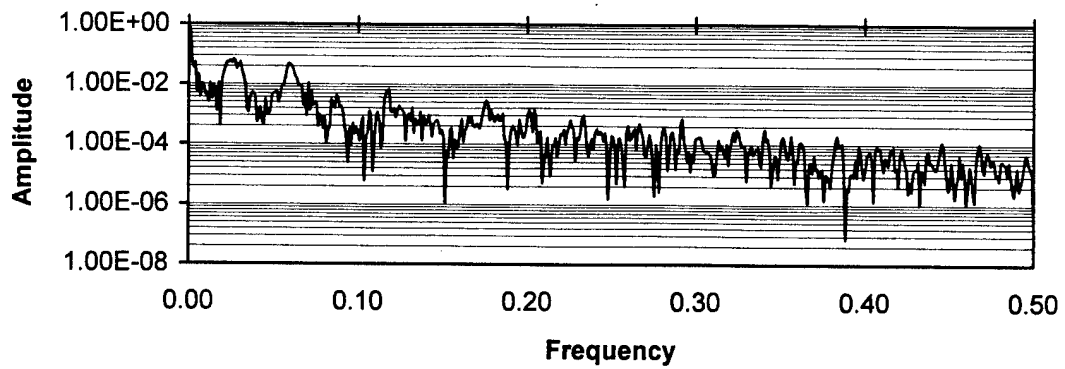

Zs = 0.4 km, Grazing angle = 8 Deg.

Fig. 22   Power spectra for the eleven rays in figure 21 (continue)

Zs = 0.4 km, Launch angle = 9 Deg.
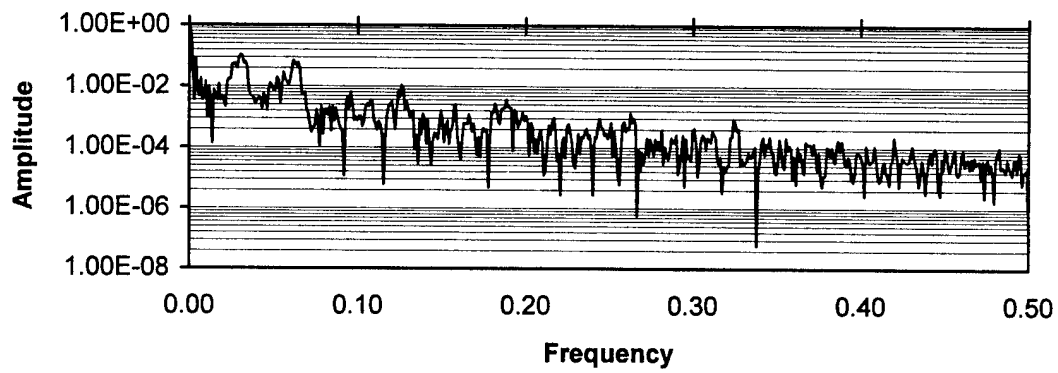

Zs = 0.4 km, Launch angle = 10 Deg.

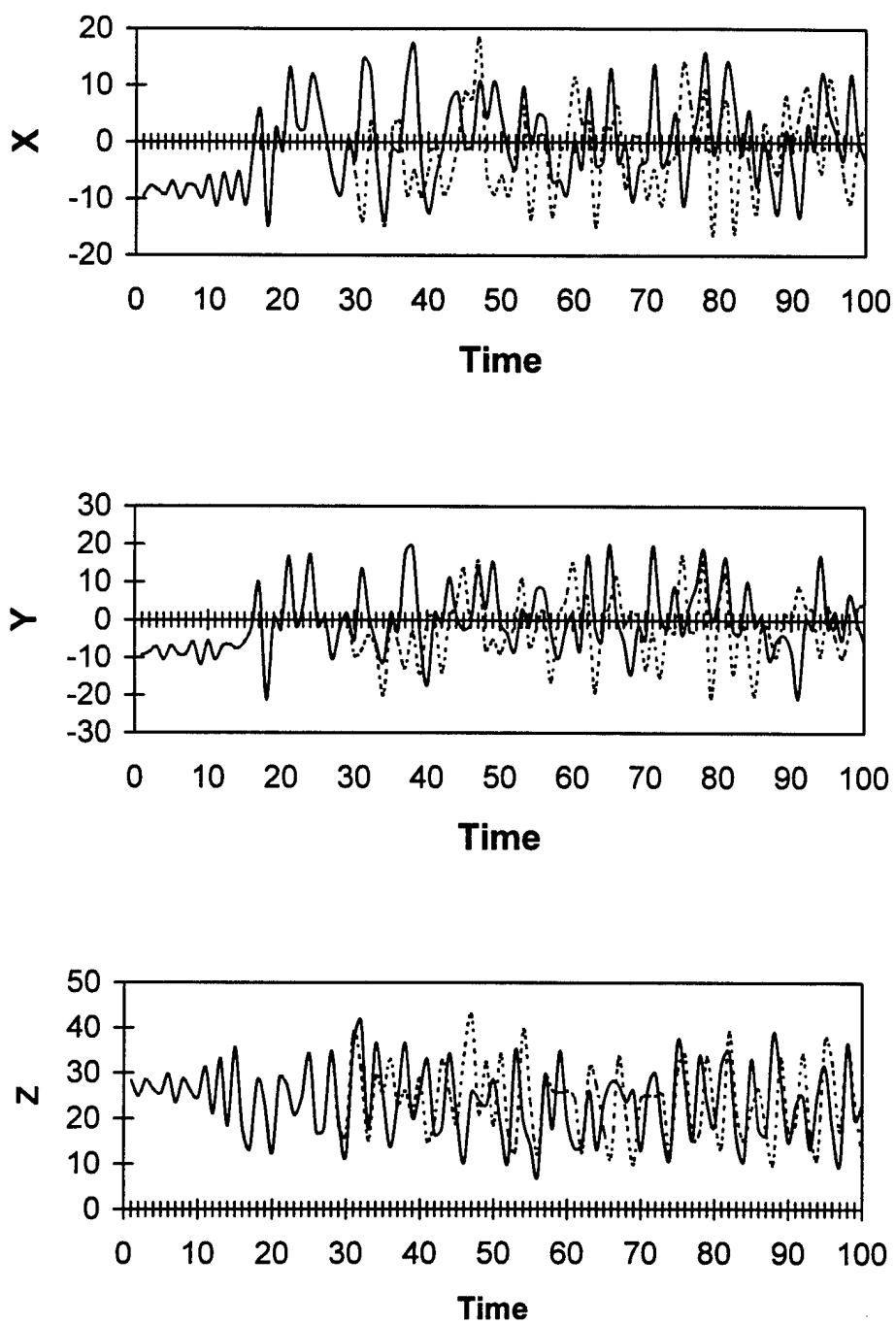*Fig. 22   Power spectra for the eleven rays in figure 21 (continue)*

Fig. 23   Time (dimensionless) evolution of X in Lorenz model with parameters
σ=10.0, R=28.0,
b=8/3. The solid line corresponds to the initial state of (0,1,0),
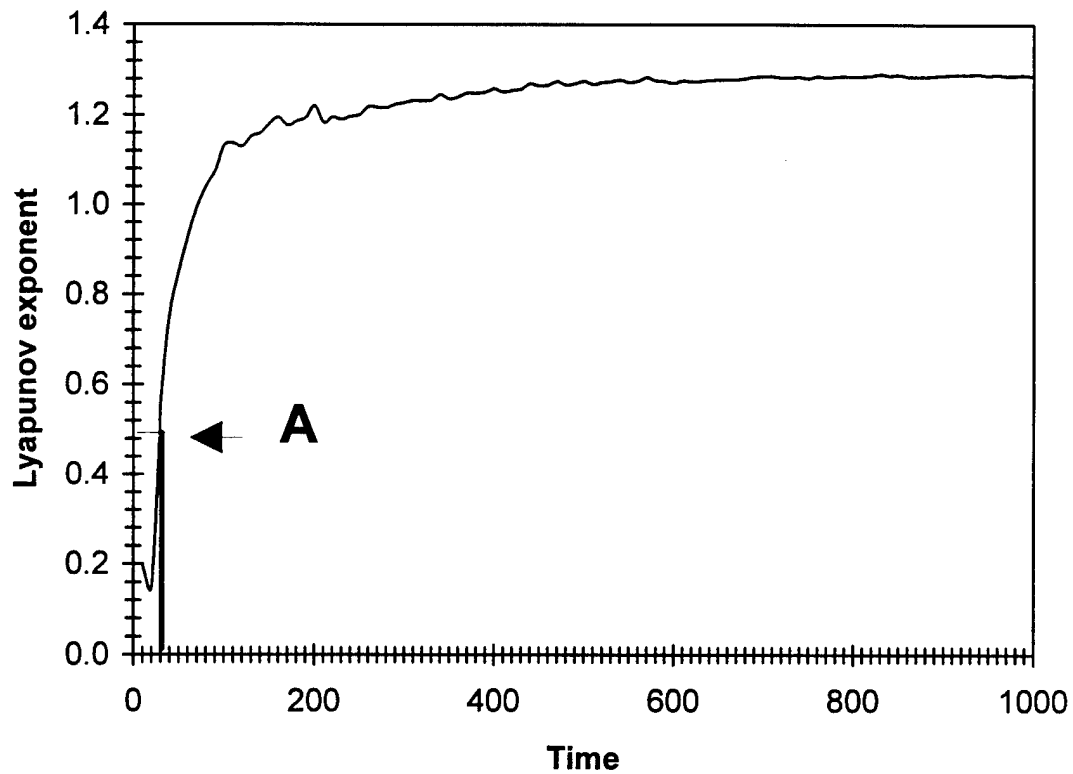*and the dashed line corresponds to the initial state of (0.0001,1,0).*

Fig. 24   Calculation of the largest Lyapunov exponent for Lorenz model

with parameters: σ=10.0, R=28.0, b=8/3, and initial state of (0,1,0).

Point A corresponds to the local value of the exponent at the time

after which the future behavior of the system could not be predicted.